



Search for heavy, long-lived, charged particles with large ionisation energy loss in pp collisions at $\sqrt{s} = 13$ TeV using the ATLAS experiment and the full Run 2 dataset

The ATLAS Collaboration

This paper presents a search for hypothetical massive, charged, long-lived particles with the ATLAS detector at the LHC using an integrated luminosity of 139 fb^{-1} of proton–proton collisions at $\sqrt{s} = 13$ TeV. These particles are expected to move significantly slower than the speed of light and should be identifiable by their high transverse momenta and anomalously large specific ionisation losses, dE/dx . Trajectories reconstructed solely by the inner tracking system and a dE/dx measurement in the pixel detector layers provide sensitivity to particles with lifetimes down to $\mathcal{O}(1)$ ns with a mass, measured using the Bethe–Bloch relation, ranging from 100 GeV to 3 TeV. Interpretations for pair-production of R -hadrons, charginos and staus in scenarios of supersymmetry compatible with these particles being long-lived are presented, with mass limits extending considerably beyond those from previous searches in broad ranges of lifetime.

1 Introduction

A large number of physics models that extend the Standard Model (SM) predict the existence of new, massive, long-lived particles (LLPs) which have a decay length long enough to be observed using particle detectors. These particles appear in proposed solutions to the gauge hierarchy problem, including supersymmetric (SUSY) models [1–7] that either conserve or violate R -parity.¹ Within SUSY models, supersymmetric particles (sparticles) may have lifetimes that depend on the mass-hierarchy parameters or on the size of any R -parity-violating coupling.

SUSY models are theoretical extensions of the SM which relate fermions and bosons. They postulate that each SM particle has a SUSY partner (a sparticle) that is a boson if the corresponding particle is a fermion, and vice-versa. The sparticles are named so as to recall their SM partner: the gluino, stau, wino and higgsino are the SUSY partners of the gluon, τ -lepton, W boson and Higgs boson. The chargino is a linear combination of the charged wino and the charged higgsinos, while the neutralino is a linear combination of the bino, the neutral wino and the neutral higgsino, where the bino is the SUSY partner of the SM $U(1)$ weak hypercharge gauge field.

This study is sensitive to SUSY along with many other models of new physics beyond the Standard Model (BSM physics models), particularly those that predict the production of massive particles with lifetimes exceeding $\mathcal{O}(1)$ ns at LHC energies. In this paper, the results of the search are interpreted in the context of pair production, from proton–proton (pp) collisions at $\sqrt{s} = 13$ TeV, of several different long-lived sparticles of charge $|q| = 1$. Within the SUSY framework, several different processes yielding LLPs are present, and the production diagrams of the processes covered by this search are shown in Figure 1. Gluinos (\tilde{g}) can be long-lived if R -parity is conserved and the squark mass scale is very high, as proposed by mini-split SUSY scenarios [8, 9]. Although the gluino itself is neutral, a long-lived gluino is predicted to hadronise, involving SM quarks or gluons with its QCD interaction and forming a colour-neutral state referred to as an R -hadron [10], which can be electrically charged. Charginos ($\tilde{\chi}_1^\pm$) can be long-lived when they and the counterpart neutralino ($\tilde{\chi}_1^0$) are almost mass-degenerate, for instance in anomaly-mediated SUSY-breaking (AMSB) models predicting a ‘pure wino’ scenario [11, 12]. Staus ($\tilde{\tau}$) can also be long-lived when a quasi-massless gravitino (\tilde{G}) is assumed as the lightest neutral sparticle and the coupling between the stau and gravitino is very weak [13–15].

Extensive searches for charged or neutral LLPs have been carried out in the ATLAS and CMS experiments. Limits on gluino R -hadrons have been set by various complementary search techniques, including an explicit requirement of decay-vertex or displaced jet reconstruction [16–18], and time-of-flight (ToF) and its optional combination with pixel dE/dx [19–21]. Very long-lived R -hadrons, eventually trapped within the calorimeters, were searched for by looking for decays during empty beam bunch-crossings [22, 23]. The search presented here is agnostic with regard to decay activity, and is therefore also sensitive when the mass difference between the gluino and the neutralino is small, a situation in which displaced decay detection becomes more challenging.

Limits on long-lived charginos, for pure-wino (AMSB, [11, 12]) as well as pure-higgsino [24] scenarios, have also been set using a disappearing-track signature [25–29] and using the ToF technique [19, 20]. Masses up to 660 (210) GeV are excluded in scenarios where the chargino is a pure wino (higgsino) for theoretically preferred lifetimes of each, and the largest excluded mass is 860 (720) GeV at lifetimes of 1–1.3 ns [30]. For a stable chargino, masses up to 1.09 TeV are excluded using the ToF technique [19].

¹ R -parity is a quantum number defined as $(-1)^{3(B-L)+2S}$ where S is the particle spin and L and B are, respectively, its lepton and baryon number.

Long-lived sleptons in the context of gauge-mediated SUSY-breaking (GMSB) [13–15] were searched for by a dedicated displaced-leptons search for stau ($\tilde{\tau}$), smuon ($\tilde{\mu}$) and selectron (\tilde{e}) cases separately, and masses up to 340 GeV, 680 GeV and 720 GeV, respectively, are excluded for lifetimes of 0.1 ns [30]. For a stable $\tilde{\tau}$, masses up to 430 GeV are excluded using the ToF technique [19, 21]. The search presented in this paper is more sensitive than previous ATLAS searches for most of the lifetime range of $\tau \gtrsim 1$ ns and is complementary to the other search strategies mentioned above.

A charged particle produced by a collision propagates outwards in space until its decay, and specific ionisation losses (dE/dx) along its path produce hit records on the detector layers. Appropriate fitting of these hits reconstructs the trajectory of the particle, referred to as a track. Charged LLPs with masses greater than $\mathcal{O}(100)$ GeV produced at the LHC are expected to be significantly slower than the speed of light, and therefore should have dE/dx significantly higher than any SM particle of the same momentum, following the Bethe–Bloch relation. The pixel detector [31–33] at the core of the ATLAS detector² [34] is able to measure dE/dx within a radius of about 13 cm from the pp collisions, and therefore can be used to identify LLPs with lifetime in excess of $\mathcal{O}(1)$ ns. To a good approximation, this identification method does not depend on the way the LLP interacts in the ATLAS calorimeters [35, 36] or on the LLP decay mode. Consequently, this search can capture a broad range of possible signals in BSM models predicting charged LLPs, without heavily depending on the specific features of these models.

This analysis uses the full Run 2 dataset, corresponding to an integrated luminosity of 139 fb^{-1} , and is an update of previous ATLAS searches performed in both Run 1 and Run 2 [37–40]. Similar searches were performed by the CMS experiment [21, 41]. In the last ATLAS search targeting the same signature, with 36 fb^{-1} of Run 2 data, no significant deviation from SM background expectations was observed. Results were interpreted assuming the pair production of R -hadrons. R -hadrons with lifetimes above 1 ns were excluded at the 95% confidence level (CL) of the CL_s prescription [42], with lower limits on the gluino mass ranging between 1.29 TeV and 2.06 TeV. In the case of R -hadrons stable enough to leave the detector (detector-stable), the lower limit on the gluino mass at the 95% CL is 1.89 TeV. In the previous ATLAS search [40], a mild excess of data events over the background prediction was observed with a local significance of 2.4σ in the mass range between 500 GeV and 800 GeV for the stable-particle selection. This has motivated an effort to improve the analysis sensitivity over a wide mass range from around several hundred GeV to a few TeV, as explained further in Section 3. Accordingly, this search aims to cover a wide range of production cross-sections, including both electroweak and strong production of charged LLPs.

This paper is organised as follows. Section 2 describes the ATLAS experiment and, in more detail, its pixel detector. Section 3 presents the search strategy and emphasises the model-independence of the method used. Section 4 describes the dataset used in the analysis and the simulation models used in interpreting the results. Section 5 explains the various corrections and calibrations applied to the pixel dE/dx measurement in order to make optimal use of this variable. It also explains and characterises the mass reconstruction obtained through the Bethe–Bloch relation. Section 6 describes the selection criteria applied to the events and candidate LLP tracks in this search, and the studies to optimise these criteria. Section 7 focuses on the data-driven background estimation, while Section 8 examines systematic uncertainties in the background estimation and signal efficiency. Finally, Section 9 discusses the combined signal significance and its interpretation, and Section 10 summarises the most important results of this search.

² ATLAS uses a right-handed coordinate system with its origin at the nominal interaction point in the centre of the detector and the z -axis coinciding with the axis of the beam pipe. The x -axis points from the interaction point to the centre of the LHC ring, and the y -axis points upward. Cylindrical coordinates (r, ϕ) are used in the transverse plane, ϕ being the azimuthal angle around the z -axis. The pseudorapidity is defined in terms of the polar angle θ as $\eta = -\ln \tan(\theta/2)$.

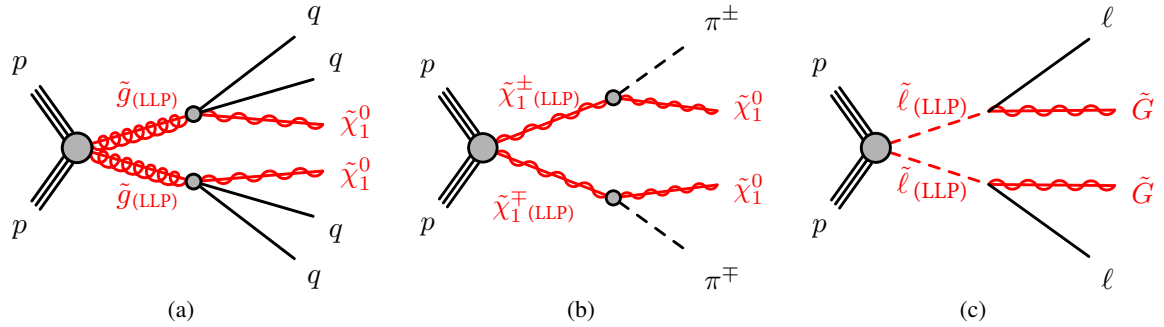


Figure 1: Production diagrams for (a) pair-produced gluinos which form R -hadrons, (b) pair-produced charginos, and (c) pair-produced sleptons.

2 ATLAS detector and dE/dx measurement

The ATLAS detector is a general-purpose detector with a forward-backward-symmetric cylindrical layout covering nearly 4π in solid angle [34]. It consists of an inner detector (ID) tracking system, to measure the trajectories of charged particles, surrounded by a 2 T solenoid, followed by calorimeters to measure the energy of particles that interact electromagnetically or hadronically, and a muon spectrometer (MS) inside toroidal magnets to provide additional tracking for muons. The detector is hermetic within its η acceptance and can therefore measure the missing transverse momentum (\vec{p}_T^{miss} , with magnitude E_T^{miss}) associated with each event. A two-level trigger system is used to select events [43]. The first-level trigger selects events from a bunch crossing (the LHC bunch crossings have a separation of 25 ns), is implemented in hardware and uses a subset of the detector information. This is followed by a software-based high-level trigger, which runs calibration and prompt reconstruction algorithms, reducing the event recording rate to about 1 kHz. An extensive software suite [44] is used in the reconstruction and analysis of real and simulated data, in detector operations, and in the trigger and data acquisition systems of the experiment.

The ID is made of three detector systems organised in concentric regions covering $|\eta| < 2.5$. The outermost system (TRT) [45] is made of densely packed 4-mm-diameter cylindrical drift tubes covering $|\eta| < 2$. The TRT covers the radial region from 60 cm to 100 cm and provides many (>30) measurements with 0.13 mm ($r-\phi$) accuracy, thus contributing to momentum measurement accuracy and robustness. The radial region from 30 cm to 60 cm is equipped with silicon microstrip detectors (SCT), providing at least four layers of double-sided strip modules with a 40 mrad stereo angle along trajectories within $|\eta| < 2.5$ [46]. The innermost region is covered by a silicon pixel detector [31–33], which, being crucial for this measurement, is described below in some detail.

The pixel detector provides, on average, four precision measurements for each track in the region $|\eta| < 2.5$ at radial distances of 3.4 cm to 13 cm from the LHC beam line. Compared to the other layers, the innermost pixel layer (IBL) [32, 33] has smaller-area pixels, reduced thickness, faster electronics, and provides charge measurements with lower resolution and dynamic range. At normal incidence and without any radiation damage, the average charge released by a minimum-ionising particle (MIP) in a pixel sensor is approximately $20\,000 e^-$ ($16\,000 e^-$ for the IBL) and the charge threshold (i.e. the minimum value for a charge to be recorded) is typically set to $3500 \pm 40 e^-$ ($2500 \pm 40 e^-$ for the IBL). If the charge released in a pixel exceeds the IBL dynamic range (which is set at approximately $30\,000 e^-$) an overflow bit (OF_{IBL}) is set. The overflow mechanism is not present in the outer pixel layers, and hits exceeding the

dynamic range ($\sim 200\,000\ e^-$) are lost. The presence of an IBL overflow bit ($\text{OF}_{\text{IBL}} = 1$) indicates that a high specific-ionisation charge was deposited locally in the IBL and this is much more likely to happen for a heavy, charged-LLP track than for a SM particle track. Tracks with an IBL overflow bit undergo a dedicated analysis treatment, as described in Section 5.

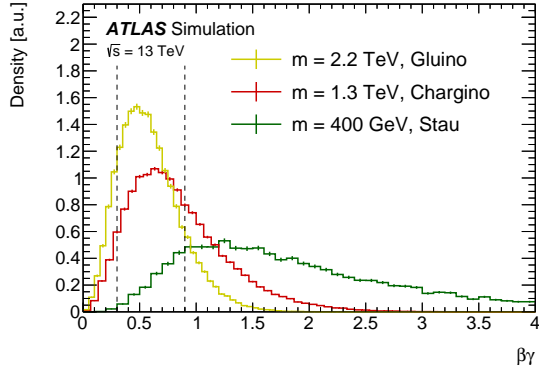
The time-over-threshold (ToT), i.e. the time interval with the signal above a preset threshold, is digitised and recorded to 8 bits (4 bits for the IBL). The ToT is approximately proportional to the ionisation charge [47] and allows the specific ionisation of a track to be calculated, as explained below. The charge released by a track crossing the pixel detector is rarely contained within just one pixel; neighbouring pixels registering hits are joined together using a connected component analysis [48] to form clusters. The charge of a cluster is calculated by summing the charges of all pixels belonging to the cluster after calibration corrections. The dE/dx measurement assigned to each track is then calculated by averaging the ionisation measurements (charge collected in the cluster per unit track length in the sensor) of its individual clusters. The specific ionisation follows a Landau distribution, and to reduce the effect of the tails of this distribution a truncated average ($\langle dE/dx \rangle_{\text{trunc}}$) is evaluated after removing the highest dE/dx cluster, or the two highest dE/dx clusters in the rare case of more than four pixel clusters on a track. Clusters including pixels at the sensor edges are dropped, as part of the charge may escape detection. The $\text{OF}_{\text{IBL}} = 1$ clusters are never used to calculate the $\langle dE/dx \rangle_{\text{trunc}}$, as their dE/dx is only known to be above a given value. A track is considered for this analysis if the $\langle dE/dx \rangle_{\text{trunc}}$ is calculated using at least two clusters after removal of those meeting the criteria defined above. The average number of clusters used for $\langle dE/dx \rangle_{\text{trunc}}$ calculation is ≈ 2.7 per track.

Finally, the $\langle dE/dx \rangle_{\text{trunc}}$ is corrected for variations of the pixel detector conditions during the data-taking period (e.g. charge losses due to radiation damage) and for the residual η -dependence, as described in detail in Section 5. The output is referred to as ‘corrected dE/dx ’ ($\langle dE/dx \rangle_{\text{corr}}$) and is the variable used in the signal selection for the search. This variable, like the *restricted energy loss* [49], has no logarithmic rise at high values of $\beta\gamma$ and no sensitivity to radiative effects.

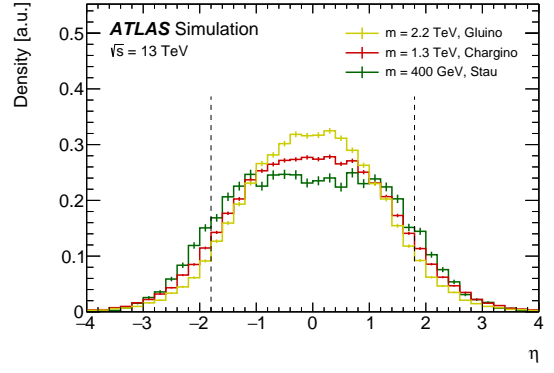
The $\beta\gamma$ of a particle can be calculated from the $\langle dE/dx \rangle_{\text{corr}}$ of its track using the Bethe–Bloch relation. A meaningful $\beta\gamma$ value can only be estimated in the range $0.3 \lesssim \beta\gamma \lesssim 0.9$ using the pixel detector. The lower limit is a consequence of the ToT dynamic range, while the upper limit is due to the proximity of the MIP regime which begins at $\beta\gamma \approx 3$ and where $\langle dE/dx \rangle_{\text{corr}}$ becomes quasi-independent of $\beta\gamma$.

3 Analysis overview

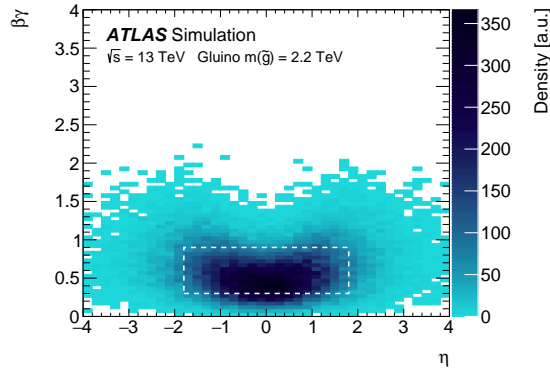
The search strategy consists of looking for isolated tracks with high transverse momentum, p_T , and large specific ionisation. The reconstructed mass is then calculated for each track using a parameterisation of the Bethe–Bloch relation and depends on its momentum and $\langle dE/dx \rangle_{\text{corr}}$. It is noteworthy that the effective $\beta\gamma$ range of $0.3 \lesssim \beta\gamma \lesssim 0.9$ matches that of pair-produced heavy charged LLPs over wide mass ranges, as illustrated in Figure 2(a). The $\beta\gamma$ distribution reflects the opening of relativistic phase space near the mass threshold, and the distribution peaks at lower values for larger LLP masses. This is a common feature of pair-production kinematics from an off-shell propagator, including the pair production of SM particles such as top quarks, and hence is not strongly dependent on the BSM dynamics of the LLP. Only tracks produced centrally ($|\eta| < 1.8$) are selected. This removes background tracks at high $|\eta|$ while retaining the acceptance for LLPs as shown in Figure 2, and also limits the pixel layers used in the dE/dx calculation to those within the barrel region, thereby simplifying the measurement.



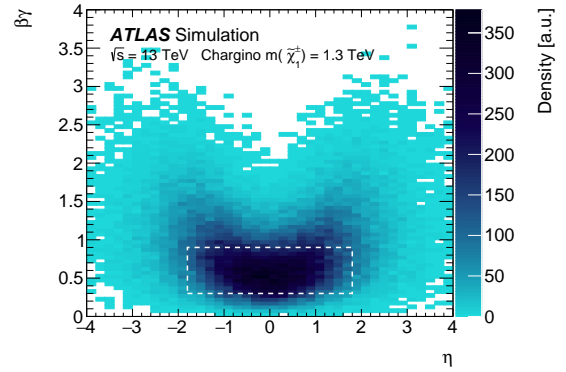
(a)



(b)



(c)



(d)

Figure 2: (a) $\beta\gamma$ distribution and (b) η distribution of various benchmark signal particles at the generator level, with the density displayed in arbitrary units. Preselections are not applied. The ranges $0.3 < \beta\gamma < 0.9$ of (a) and $|\eta| < 1.8$ of (b) indicated by vertical dashed lines approximately correspond to the acceptance of this search from the dE/dx and η requirements respectively. Panels (c) and (d) illustrate the distribution in the η - $\beta\gamma$ plane for the gluino and chargino samples respectively. The area within the dashed lines corresponds to the approximate acceptance of the search. The correlation between $\beta\gamma$ and $|\eta|$ loosely reflects the relation $\beta\gamma = p/m = p_T \cosh(\eta)/m$.

Events are selected using the lowest-threshold unrescaled calorimetric E_T^{miss} trigger, which is based on the magnitude of the negative of the vectorial energy sum measured in the calorimeters corrected to take into account the multiple pp interactions in each event [50]. In events with metastable LLPs (i.e. LLPs which decay inside the ATLAS detector), the measured E_T^{miss} originates mainly from neutralinos or gravitinos which carry away unmeasured momentum. In events where the LLPs are detector-stable and decay outside ATLAS, the LLPs leave only modest energy depositions in the calorimeters, even in the R -hadron case, and only a fraction of them are reconstructed as a muon owing to their late arrival time in the muon spectrometer. Therefore, most of the momentum of each LLP is not accounted for in the measurement of E_T^{miss} , and only QCD initial-state radiation (ISR) provides a visible contribution that results in a measured imbalance of transverse momentum. Due to the presence of neutralinos or gravitinos, the E_T^{miss} trigger efficiency is higher for metastable LLPs than for detector-stable LLPs. On the other hand, the track reconstruction efficiency is higher for detector-stable LLPs and penalises particles with lifetimes shorter than 10 ns, which may not have crossed enough detector layers. Further selections are applied to triggered events and candidate tracks as detailed in Section 6.

The signal can form a peak in the reconstructed mass distribution and thus be observed as an excess of events over the expected background. The search takes into account the mass resolution for the signal processes. Full-length ID tracks have a relative $1/p_T$ resolution of approximately 4% (40%) at $p_T = 100$ GeV (1 TeV) for $|\eta| < 0.5$. This resolution is approximately proportional to p_T in this high-momentum range and is dominated by the intrinsic position resolution and residual misalignment of the tracker [51]. Low-lifetime LLPs have shorter tracks, resulting in larger momentum uncertainties and larger mass uncertainties. Reflecting this momentum resolution and the dE/dx dispersion, the reconstructed mass distribution has a considerable width. For a predefined set of target mass-value hypotheses, the corresponding set of mass windows is defined so that each window captures approximately 70% of the expected signal at the given target mass, but differs slightly between lifetimes less than or equal to 1 ns and greater than 1 ns. Here, the choice of mass windows for lifetimes shorter than 1 ns accounts for the poorer mass resolution due to the shorter LLP tracks. The mass windows are common to sleptons, charginos and R -hadrons of the same mass and are defined as explained in Section 6.4.

The background is mostly due to SM processes generating high- p_T tracks with a large dE/dx that is randomly produced according to the Landau distribution of MIPs. The background yield and its distribution in the reconstructed mass spectrum is estimated in a fully data-driven approach, as described in Section 7. Data control samples are used to parameterise the momentum and dE/dx distributions and their interdependence, and then to generate pseudo-data which predict the background distribution. Potential signal contamination is minimised in these background samples by inverting some of the selection criteria.

4 Data and simulation samples

The analysis is conducted with 139 fb^{-1} of pp collision data which satisfy the ATLAS data quality requirements [52]. The dataset was taken during Run 2 of the LHC from 2015 to 2018, at a centre-of-mass energy of 13 TeV. The average number of collisions per bunch-crossing (pile-up, $\langle \mu \rangle$) is approximately 34. A dedicated 21 pb^{-1} low-pile-up dataset with $\langle \mu \rangle \sim 0.4$ taken in 2017 is used for the dE/dx -to- $\beta\gamma$ calibration. In this dataset, tracks are reconstructed if they have $p_T > 100$ MeV, while the minimum p_T requirement in the standard dataset is 500 MeV.

To optimise the analysis selection, Monte Carlo (MC) samples were produced to simulate events containing long-lived gluinos, charginos, and staus, corresponding to the production diagrams shown in Figure 1.

These three signal models are complementary in this study. The gluino samples have large production cross-sections and are suited to probing the high-mass frontier beyond 2 TeV. The slepton samples have production cross-sections that are several orders of magnitude smaller than for gluinos of the same mass, and are suited to probing the mass range from a few to several hundred GeV. The chargino sample cross-sections have intermediate values and are useful in probing the mass range from 500 GeV to 1.3 TeV.

Gluino pair production was simulated for gluino masses ranging from 400 GeV to 3 TeV and lifetimes ranging from 1 ns to stable within a simplified model inspired by a split-SUSY scenario [8, 9]. The events were generated by MADGRAPH5_AMC@NLO 2.6.2 with up to two additional partons at leading order, and interfaced to PYTHIA 8.240 [53] using the A14 set of tuned parameters (‘tune’) [54] and the NNPDF2.3LO parton distribution function (PDF) set for parton showering and hadronisation, with decays of bottom and charm hadrons performed by EVTGEN 1.6.0 [55]. The CKKW-L merging scheme [56, 57] was applied to combine the matrix element with the parton shower. The long-lived gluino, which carries colour charge, hadronises to form a colourless composite particle called an R -hadron. The details of the R -hadron simulation are given in Ref. [58]. The nominal cross-section values were calculated at next-to-leading order (NLO) with resummation of next-to-leading logarithms (NLL) and their uncertainty were taken from an envelope of predictions using different PDF sets and factorisation and renormalisation scales [59]. Each gluino decays into a neutralino and two quarks via a virtual squark at a very high mass scale. To probe decays with different kinematics, two sets of samples were produced: one with a fixed neutralino mass of $m(\tilde{\chi}_1^0) = 100$ GeV, and the other one having a compressed spectrum with a fixed mass-splitting of $\Delta m(\tilde{g}, \tilde{\chi}_1^0) = 30$ GeV. These two series of mass parameters are complementary and illustrate the breadth of the search, reflecting the fact that it does not require explicit decay properties of the charged LLP.

Samples with a combination of chargino–neutralino ($\tilde{\chi}_1^\pm \tilde{\chi}_1^0$) and chargino–chargino ($\tilde{\chi}_1^+ \tilde{\chi}_1^-$) events were generated with nearly degenerate chargino and neutralino masses, motivated by the ‘pure wino’ AMSB scenario [11, 12]. Each long-lived chargino decays into a neutralino and a pion, where the mass-splitting between the chargino and neutralino is set to approximately 160 MeV, with $\tan \beta = 5$ and a positive sign of the higgsino mass parameter. Although the AMSB model has a specific preference for the chargino’s lifetime ($\mathcal{O}(0.2)$ ns) and mass relation via the loop dynamics, this theoretical constraint was artificially loosened for experimental benchmarking, and lifetimes ranging from 1 ns to stable and chargino masses ranging from 400 GeV to 1.6 TeV were examined. Samples were produced using MADGRAPH5_AMC@NLO 2.6.2 with up to two additional partons at leading order in the matrix element, and interfaced to PYTHIA 8.230 using the A14 tune and the NNPDF2.3LO PDF set for parton showering and hadronisation, with decays of bottom and charm hadrons performed by EVTGEN 1.6.0. The CKKW-L merging scheme [56, 57] was applied to combine the matrix element with the parton shower. A 100% branching ratio for $\tilde{\chi}_1^\pm \rightarrow \pi^\pm \tilde{\chi}_1^0$ is assumed. The cross-sections for the electroweak and strong production models are calculated at NLO in the strong coupling constant α_s using Prospino2 [60].

Events with pair-produced staus, each of which decays into a τ -lepton and a gravitino, were produced in the GMSB scenario [13–15]. The stau masses range from 100 GeV to 1 TeV and the gravitino is massless. Samples with stau lifetimes ranging from 1 ns to stable were produced. Events were simulated with up to two additional partons at leading order using MADGRAPH5_AMC@NLO 2.6.1 with the NNPDF2.3LO PDF set, and interfaced to PYTHIA 8.230 using the A14 tune. The mixed states $\tilde{\tau}_{1,2}$ of the left- and right-handed staus ($\tilde{\tau}_{L,R}$) were generated with a mixing angle $\sin \theta_{\tilde{\tau}} = 0.95$. Signal cross-sections were calculated at next-to-leading order in α_s , with soft-gluon emission effects added at next-to-leading-logarithm accuracy [61–65].

Inelastic pp interactions were generated using PYTHIA 8.186 and EVTGEN 1.6.0 with the NNPDF2.3LO

PDF set and the A3 tune [66]. The inelastic collisions were overlaid onto the hard-scattering process to simulate the effect of multiple pp interactions. MC samples were reweighted to match the distribution of the average number of interactions per bunch crossing observed in data.

The MC events were passed through a full detector simulation [67] based on GEANT4 [68]. The propagation and decays of charginos and staus were simulated within GEANT4, taking into account ionisation loss and interactions with detector material. The propagation of R -hadrons and their interactions were handled by GEANT4 until their decay, at which point the decay chains and subsequent hadronisation were simulated by PYTHIA 8, and then information about the outgoing particles was transferred back to GEANT4.

The dE/dx response of the pixel detector is also simulated in the GEANT4 framework. It is based on a realistic charge-deposition model [69], but due to the sensitivity of the dE/dx measurement to detector conditions, including radiation damage, the simulated track dE/dx and especially the probability that a track has a hit in the IBL overflow do not follow the data accurately enough for this analysis. Hence, the dE/dx response for simulated events was customised in this analysis by replacing it with values from a data-driven template which was derived from a study described in the following section.

5 dE/dx corrections and mass calibration

The most probable value (MPV) of the track $\langle dE/dx \rangle_{\text{trunc}}$ as a function of delivered integrated luminosity is shown in Figure 3 for $p > 10$ GeV tracks, with and without a hit in the IBL overflow. As expected, the charge collection efficiency decreases with increasing integrated luminosity because of the damage induced in the silicon by the particle flux, and a decrease in the measured $\langle dE/dx \rangle_{\text{trunc}}$ is therefore visible across the dataset. Large occasional jumps in the trend (e.g. at around 92 fb^{-1}) indicate changes to the pixel detector’s charge calibration scheme, while smaller fluctuations correspond to regular updates of the charge and threshold calibrations during machine development periods or technical shutdowns. The effect of the radiation damage can be seen to depend on $|\eta|$, reflecting differences in the fluence over $|\eta|$. In addition, the fluence is higher in pixel sensors at smaller radii. However, the analysis does not compensate for the effect in each pixel sensor, since the $\langle dE/dx \rangle_{\text{trunc}}$ of a track is calculated before such compensation can be made, and each pixel cluster’s information is practically inaccessible in the data flow of the analysis. Corrections are therefore applied only to $\langle dE/dx \rangle_{\text{trunc}}$ in this analysis.

To minimise these dependences, run-dependent corrections are calculated and applied. The run-dependent corrections are calculated separately for tracks in bins of $|\eta|$ and OF_{IBL} . In each run with sufficient data, an estimate of the $\langle dE/dx \rangle_{\text{trunc}}$ peak for each $(|\eta|, \text{OF}_{\text{IBL}})$ bin is used to normalise the most probable $\langle dE/dx \rangle_{\text{trunc}}$ to that of a reference run.³ If a run does not have sufficient data, the correction from the closest run with sufficient data is applied. After the run-dependent corrections are applied, $|\eta|$ -dependent corrections are applied separately in bins of OF_{IBL} so that the MPV for MIPs is equalised over $|\eta|$. The resulting corrected dE/dx measurement is referred to as $\langle dE/dx \rangle_{\text{corr}}$ and is normalised for MIP-like tracks to peak at $\sim 1 \text{ MeV g}^{-1} \text{ cm}^2$, the value for unirradiated silicon of the thickness used in the ATLAS pixel detector. Hereafter, the symbol ‘ dE/dx ’ stands for $\langle dE/dx \rangle_{\text{corr}}$.

The dE/dx measurement provides a measurement of the particle $\beta\gamma$ through a calibrated relation between dE/dx and $\beta\gamma$. The calibration is performed in the range $0.3 < \beta\gamma < 5$, using a special low-pile-up dataset in which it is feasible to reconstruct tracks with p_T as low as 100 MeV (see Section 4). In a narrow low

³ the reference run has been chosen in the middle of total integrated luminosity and close to the low luminosity run used for the calibration of $\langle dE/dx \rangle_{\text{trunc}}$ into $\beta\gamma$

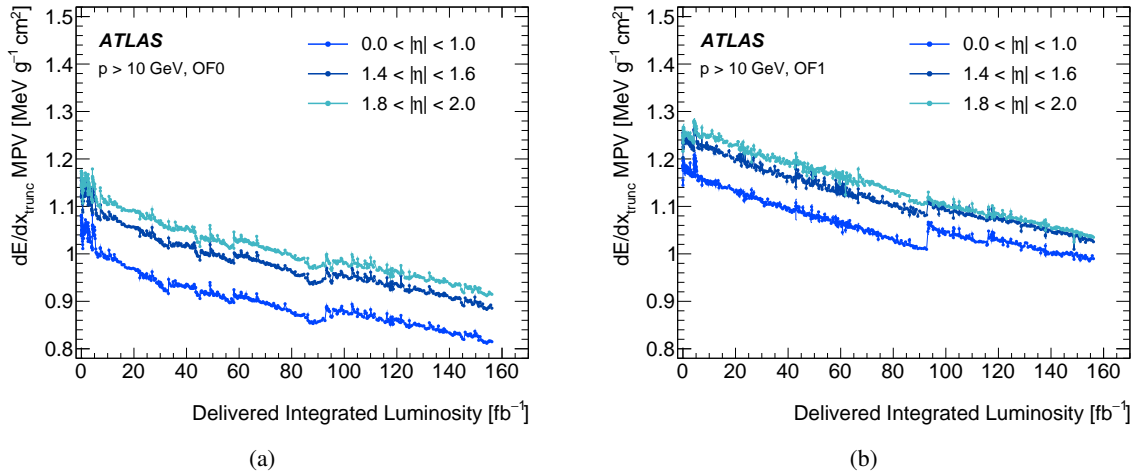


Figure 3: The drift of MIP-MPV $\langle dE/dx \rangle_{\text{trunc}}$ as a function of the delivered integrated luminosity in Run 2, divided into different pseudorapidity ranges, for MIP tracks of $p > 10$ GeV (a) without an IBL overflow (OF0) or (b) with an IBL overflow (OF1). The lower $\langle dE/dx \rangle_{\text{trunc}}$ in (a) is due to the contribution of the IBL clusters which are restricted by the overflow to be under ≈ 2 MIPs.

momentum slice, the contributions to the dE/dx spectrum from individual particle species can be resolved, as shown in Figure 4(a). The dE/dx distribution of the tracks in the special dataset, sliced into bins of momentum, $|\eta|$, and OF_{IBL} , is fitted with a superposition of Crystal Ball functions [70, 71] modified to have double-sided Gaussian cores to extract the most probable value of dE/dx for pions, kaons, and protons. These values trace out the dE/dx - $\beta\gamma$ relationship, as shown in Figure 4(b). In the ID, charged particles are assumed to be charged pions by default, and the reconstructed momentum is unbiased for charged pions. For other particle species, however, the reconstructed momentum at the low- p_T end below 300 MeV is biased. This momentum bias was derived using the same low- p_T track reconstruction for a minimum-bias Monte Carlo simulation sample and removed by applying a correction. This correction is already included in Figure 4(b). The fitted peaks as a function of $\beta\gamma$ are then fitted with the following empirical function inspired by the original Bethe–Bloch formula

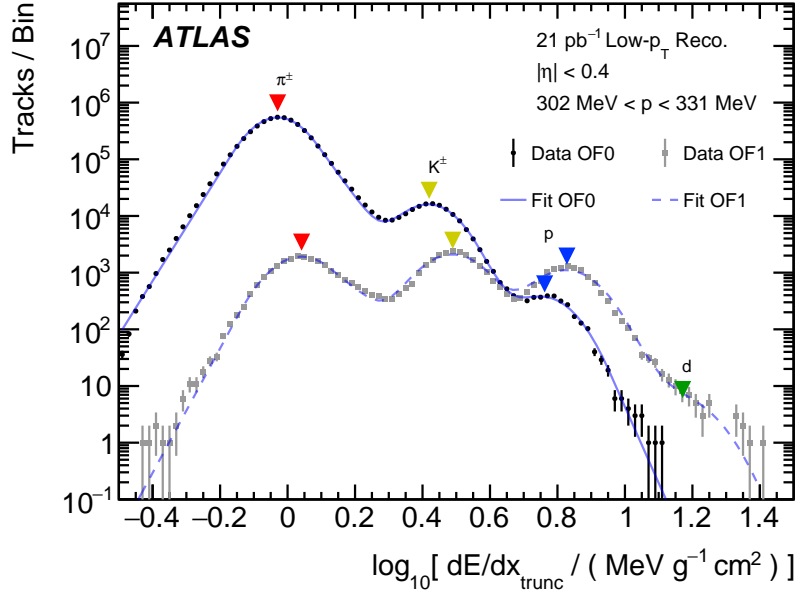
$$\text{MPV}_{dE/dx}(\beta\gamma) = \frac{1 + (\beta\gamma)^2}{(\beta\gamma)^2} \left(c_0 + c_1 \log_{10}(\beta\gamma) + c_2 [\log_{10}(\beta\gamma)]^2 \right) \quad (1)$$

where c_0 , c_1 , and c_2 are free parameters of the fit. Inversion of the above function provides an estimate of the charged-particle $\beta\gamma$ from the measured dE/dx . Combined with the momentum measurement, the mass of the particle associated with the track can be calculated as $m_{dE/dx} \equiv p_{\text{reco}}/\beta\gamma(\langle dE/dx \rangle_{\text{corr}})$. This reconstructed mass is hereafter simply denoted by ‘ m ’.

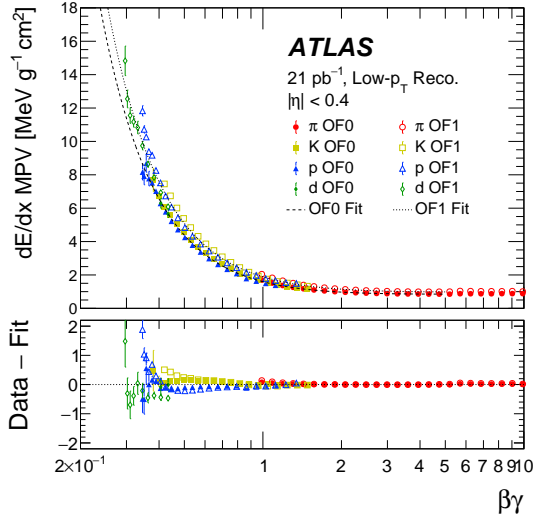
The fraction of $\text{OF}_{\text{IBL}} = 1$ tracks as a function of $\beta\gamma$, shown in Figure 4(c) for $|\eta| < 0.4$, is also monitored in the same low-pile-up dataset. Here, the power of OF_{IBL} as a key discriminant of the search is clearly illustrated: the fraction of MIP tracks with an IBL overflow is highly suppressed by more than two orders of magnitude, but a substantial fraction of tracks with smaller $\beta\gamma$ have an IBL overflow. The dE/dx - $\beta\gamma$ calibration and the fraction of $\text{OF}_{\text{IBL}} = 1$ tracks versus track $\beta\gamma$ form the basis of the data-driven template used to replace the simulated dE/dx and OF_{IBL} values in Monte Carlo samples: when the track associated with the signal particle is reconstructed, first the label OF_{IBL} is reassigned according to a

binomial probability depending on the particle ($\beta\gamma, |\eta|$), and then the $\langle dE/dx \rangle_{\text{corr}}$ value is determined from the probability density distribution template corresponding to the OF_{IBL} label of the ($\beta\gamma, |\eta|$) slice.

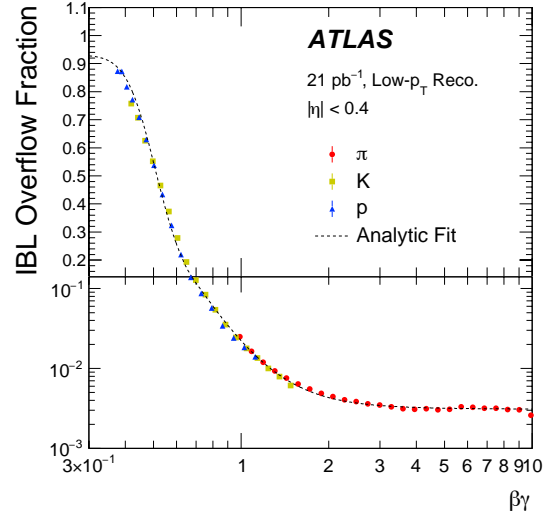
It is worth mentioning that the $|\eta|$ -dependence of $\langle dE/dx \rangle_{\text{trunc}}$ is not uniform over $\beta\gamma$, as illustrated in Figure 5. Even after the equalisation of the MPV over $|\eta|$ described above, the $\langle dE/dx \rangle_{\text{trunc}}$ response requires different mass calibration functions depending on $|\eta|$. This is because not only the MPV but also the shape of the Landau distribution depends on $|\eta|$ (the Landau tails are reduced increasing the traversed silicon thickness). The ionisation loss response is therefore treated by slicing in $|\eta|$ throughout this analysis.



(a)



(b)



(c)

Figure 4: (a) An example of a $\log_{10} [\langle dE/dx \rangle_{\text{trunc}} / (\text{MeV g}^{-1} \text{cm}^2)]$ distribution of low-pile-up minimum-bias charged-particle tracks in a momentum slice of $302 \text{ MeV} < p < 331 \text{ MeV}$ in the pseudorapidity range $|\eta| < 0.4$. Tracks are classified by OF_{IBL} . Triangle markers indicate identified MPVs corresponding to pions (red), kaons (yellow), protons (blue) and deuterons (green). The result of fitting a superposition of the $\langle dE/dx \rangle_{\text{trunc}}$ distributions of identified particles is also overlaid for each data series. (b) MPV values of $\langle dE/dx \rangle_{\text{trunc}}$ as a function of particle $\beta\gamma$ in $|\eta| < 0.4$, classified by OF_{IBL} . The data values are fitted by a function respecting the Bethe–Bloch formula. (c) The fraction of $\text{OF}_{\text{IBL}} = 1$ tracks as a function of particle $\beta\gamma$ in $|\eta| < 0.4$. The data values are fitted with an analytic function $y_0 + \frac{1 - y_0 - y_1}{1 + a [\log_{10}(\beta\gamma) - x_0]^n}$. In order to show all important features, a linear scale is used in the upper panel for the fraction above 0.14, while a logarithmic scale is used for the lower panel.

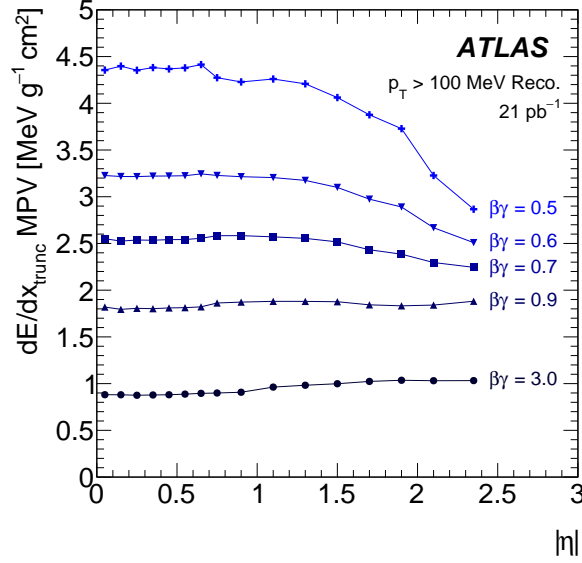


Figure 5: $|\eta|$ -dependence of the MPV of $\langle dE/dx \rangle_{\text{trunc}}$ for various charged-particle $\beta\gamma$ values before MPV equalisation over $|\eta|$ for the $\text{OF}_{\text{IBL}} = 0$ case. A value of $\beta\gamma = 3$ is approximately the MIP case. In the signal region of this search, $\langle dE/dx \rangle_{\text{trunc}}$ approximately corresponds to $\beta\gamma < 0.9$. A low-pile-up dataset recorded in 2017 (21 pb^{-1}) with $p_{\text{T}} > 100 \text{ MeV}$ track reconstruction is used to probe the dependence on $\beta\gamma$.

6 Selection of events, tracks and mass windows

In this section, criteria applied to events and tracks are described in detail. These selections except the mass windows described in Section 6.4 are summarised in Table 1.

6.1 Event selection

Events in the signal region are first selected with a trigger based on $E_{\text{T}}^{\text{miss}}$, which is calculated using energy measurements in the calorimeter with corrections for multiple pp interactions in each event [43]. The high-level $E_{\text{T}}^{\text{miss}}$ trigger threshold varies from 70 GeV to 110 GeV during the data-taking period. In the offline reconstruction of the recorded events, $E_{\text{T}}^{\text{miss}}$ is built from calibrated muons and electrons which pass baseline selections, and from calibrated jets reconstructed with the anti- k_r jet clustering algorithm [72, 73] with radius parameter $R = 0.4$, using clusters of energy depositions in the calorimeter as inputs. A term that includes soft tracks not associated with any other objects in the event [74] but consistent with the hard-scatter primary vertex (PV) (i.e. the vertex with the largest $\sum p_{\text{T}}^2$ for the associated tracks) is added to the $E_{\text{T}}^{\text{miss}}$ calculation. Events are required to have $E_{\text{T}}^{\text{miss}} > 170 \text{ GeV}$ to enhance the signal sensitivity and to ensure that the selected events are near the efficiency plateau of the trigger. To ensure a reliable calculation of $E_{\text{T}}^{\text{miss}}$, events are rejected if they contain a jet with $E_{\text{T}} > 20 \text{ GeV}$ that is consistent with detector noise or beam-induced background, as determined from shower shape information. Unlike in standard ATLAS selections for jet-cleaning [75], a requirement on the relationship between track and calorimeter measurements of p_{T} and a requirement on the fraction of jet energy deposited in the electromagnetic

Table 1: Summary of signal selection.

Category	Item	Description
Event topology	Trigger	Unprescaled lowest-threshold E_T^{miss} trigger
	E_T^{miss}	$E_T^{\text{miss}} > 170 \text{ GeV}$
	Primary vertex	The hard-scatter vertex must have at least two tracks
Events are required to have at least one track fulfilling <i>all</i> criteria listed below; tracks sorted in p_T descending order		
Track kinematics	Momentum	$p_T > 120 \text{ GeV}$
	Pseudorapidity	$ \eta < 1.8$
	$W^\pm \rightarrow \ell^\pm \nu$ veto	$m_T(\text{track}, \vec{p}_T^{\text{miss}}) > 130 \text{ GeV}$
Track quality	Impact parameters	Track matched to the hard-scatter vertex; $ d_0 < 2 \text{ mm}$ and $ \Delta z_0 \sin \theta < 3 \text{ mm}$
	Rel. momentum resolution	$\sigma_p < \max\left(10\%, -1\% + 90\% \times \frac{ p }{\text{TeV}}\right)$ and $\sigma_p < 200\%$
	Cluster requirement (1)	At least two clusters used for the $\langle dE/dx \rangle_{\text{trunc}}$ calculation
	Cluster requirement (2)	Must have a cluster in the IBL (if this is expected), or a cluster in the next-to-innermost pixel layer (if this is expected while a cluster is not expected in IBL)
	Cluster requirement (3)	No shared pixel clusters and no split pixel clusters
Veto	Cluster requirement (4)	Number of SCT clusters > 5
	Isolation	$\left(\sum_{\text{trk}} p_T\right) < 5 \text{ GeV}$ (cone size $\Delta R = 0.3$)
	Electron veto	EM fraction < 0.95
	Hadron and τ -lepton veto	$E_{\text{jet}}/p_{\text{track}} < 1$
	Muon requirement	SR- μ : MS track matched to ID track; SR-Trk: otherwise
Pixel dE/dx	Inclusive	Low: $dE/dx \in [1.8, 2.4] \text{ MeV g}^{-1}\text{cm}^2$ High: $dE/dx > 2.4 \text{ MeV g}^{-1}\text{cm}^2$
	Binned	IBL0_Low: $dE/dx \in [1.8, 2.4] \text{ MeV g}^{-1}\text{cm}^2$ and $\text{OF}_{\text{IBL}} = 0$ IBL0_High: $dE/dx > 2.4 \text{ MeV g}^{-1}\text{cm}^2$ and $\text{OF}_{\text{IBL}} = 0$ IBL1: $dE/dx > 1.8 \text{ MeV g}^{-1}\text{cm}^2$ and $\text{OF}_{\text{IBL}} = 1$

calorimeter are not applied, since they are found to be inefficient for signal events in which an LLP decays before or inside the calorimeters.

Events that pass the trigger and E_T^{miss} selections are required to have a PV built from at least two reconstructed tracks each with p_T above 500 MeV, and must contain at least one candidate track that passes the track-level selections detailed below.

6.2 Track selection

All the track parameters are derived using only ID information, including the TRT hits. This choice is justified by the desire to remain agnostic about the decay products of the LLPs. When combining an ID track and muon spectrometer track segments, it is assumed that the combined track has $\beta = 1$. Therefore, the addition of track information from the muon spectrometer would not improve the mass resolution of selected low- $\beta\gamma$ LLPs and would induce η -dependent effects related to the particle's time of flight.

In order to enrich the selected sample in potential signal events, candidate tracks are required to have $p_T > 120$ GeV and $|\eta| < 1.8$. To reject non-prompt background tracks and those inconsistent with the PV, the transverse impact parameter⁴ of candidate tracks, $|d_0|$, must be less than 2 mm, and the absolute value of the product of the longitudinal impact parameter relative to the z -position of the PV, Δz_0 , and $\sin \theta$ of the track, must satisfy $|\Delta z_0 \sin \theta| < 3$ mm. Reconstructed tracks must have at least six clusters across the SCT detectors,⁵ and to be considered a candidate, the track must have an associated cluster in the innermost active pixel detector module within the first two layers. Tracks are rejected if any pixel cluster is shared by two or more tracks (shared cluster), or if the shape of a pixel cluster is judged to be likely to arise from energy deposited by multiple particles (split cluster) by a neural-network algorithm applied to the pixel pattern of the cluster [48, 76]. To enhance the selection of isolated tracks, the scalar sum of the p_T of other tracks, with $p_T > 1$ GeV and consistent with the PV, in a cone of size $\Delta R = 0.3$ around the candidate track must be less than 5 GeV.

To reject tracks from leptonic W decays, the transverse mass, m_T ,⁶ associated with the candidate track must be greater than 130 GeV. Tracks from electrons are removed by considering any jets with $p_T > 20$ GeV that are within $\Delta R(\text{track, jet}) = 0.05$ of the candidate track,⁷ and rejecting the track if any such jet deposits at least 95% of its energy in the electromagnetic calorimeter. SM hadrons are removed by excluding tracks for which a nearby jet satisfying $\Delta R(\text{track, jet}) < 0.05$ has a calibrated energy larger than the track momentum.

At least two pixel clusters, after discarding the cluster (or the two clusters) with the highest ionisation, must be included in the calculation of dE/dx to ensure it is robust.

⁴ The transverse impact parameter (d_0) is defined as the distance of closest approach in the transverse plane between a track and the beam line. The longitudinal impact parameter (z_0) corresponds to the z -coordinate distance between the point along the track at which the transverse impact parameter is defined and the primary vertex.

⁵ In the SCT, clusters on each side of a double-sided strip module are individually counted as clusters; typically, two clusters are produced along a track in a module.

⁶ $m_T \equiv \sqrt{2p_T^{\text{track}} E_T^{\text{miss}} (1 - \cos \Delta\phi)}$, where $\Delta\phi$ is the azimuthal separation between the track and \vec{p}_T^{miss} .

⁷ The angular separation of two objects (i, j) is defined as $\Delta R(i, j) \equiv \sqrt{(\Delta\eta_{ij})^2 + (\Delta\phi_{ij})^2}$.

The relative uncertainty in the momentum measurement depends linearly on the momentum, and the uncertainty upper bound should lie between 10% and 200%, and must satisfy

$$\sigma_p < \max\left(10\%, \left(-1\% + 90\% \times \frac{|p|}{\text{TeV}}\right)\right) \text{ and } \sigma_p < 200\%$$

where $\sigma_p \equiv |\delta(p^{-1})/(p^{-1})|$ is the relative uncertainty of the inverse of the charge-signed track momentum. This selection was chosen so as to maximise the statistical significance of the signal over the full lifetime and mass range of the LLPs under study.

The dE/dx of the candidate track must be larger than $1.8 \text{ MeV g}^{-1}\text{cm}^2$, which corresponds to a selection of approximately 1% of the whole track set in data. This threshold value was used in all previous ATLAS searches based on dE/dx measurement in the pixel detector [37–40] and is related to the data-driven background generation method. The background extrapolation from a ‘below-threshold’ sample to the ‘above-threshold’ behaviour is driven by the sample size. The larger the available sample, the higher the threshold setting can be. The larger integrated luminosity available for this measurement allows a higher threshold setting. The threshold setting was optimised by maximising the statistical significance of the signal, and a specific-ionisation threshold of $2.4 \text{ MeV g}^{-1}\text{cm}^2$ was found to be the optimal choice (approximately 0.15% of the whole track set survives this cut). The interval $dE/dx \in [1.8, 2.4] \text{ MeV g}^{-1}\text{cm}^2$ below this threshold contains a sizeable fraction of the signal, approximately 25%–40% for particles with a hypothetical mass of 2.2–0.4 TeV respectively, but with less favourable statistical significance.

Two mutually exclusive intervals are considered: ‘Low’ for $dE/dx \in [1.8, 2.4] \text{ MeV g}^{-1}\text{cm}^2$ and ‘High’ for $dE/dx > 2.4 \text{ MeV g}^{-1}\text{cm}^2$. The latter has the higher sensitivity, but the former also contributes to the sensitivity, especially for smaller LLP masses.

Figure 6 illustrates the distribution of representative signal samples in the reconstructed p – dE/dx plane after the selection. While the Bethe–Bloch relation is clearly retained, a substantial amount of smearing is visible for higher LLP masses, reflecting the limited ID momentum resolution.

6.3 Event subsamples

A candidate track may be matched to a ‘combined muon’ object when a track reconstructed in the MS is consistent with the candidate track when using ‘combined fitting’ in the standard muon reconstruction algorithm [77, 78]. Depending on muon identification by ID–MS track matching using the ‘medium’ criteria [78], candidate tracks are categorised as either ‘muon tracks’ (SR–Mu) or ‘tracks’ (SR–Trk). This classification is useful because, as is described later, the SR–Mu category contains the majority of background tracks but only a limited fraction of the signal tracks, especially when the LLP’s average decay length $\beta\gamma c\tau$ is insufficient to traverse the MS. Indeed, even for the stable lifetime case, a substantial fraction of the signal tracks remain in the SR–Trk category, as can be seen in Figures 7–9. This is not only due to the intrinsic muon identification inefficiency, but also due to the fact that the standard ATLAS muon reconstruction algorithm assumes $\beta = 1$ muons, and a substantial fraction of the signal tracks arrive at the MS much later than SM muons. For R -hadron signal samples, there is additional complexity because R -hadrons have strong interactions with the calorimeter material, and generally the probability of muon identification is expected to be even smaller. For consistency, especially with the background estimation, the p_T of the track always refers to that of ID tracks, even for muon-identified candidates.

The presence of an IBL overflow cluster on a track can provide a useful way to discriminate signal from background. The data sample can then be split into two independent subsets according to the presence

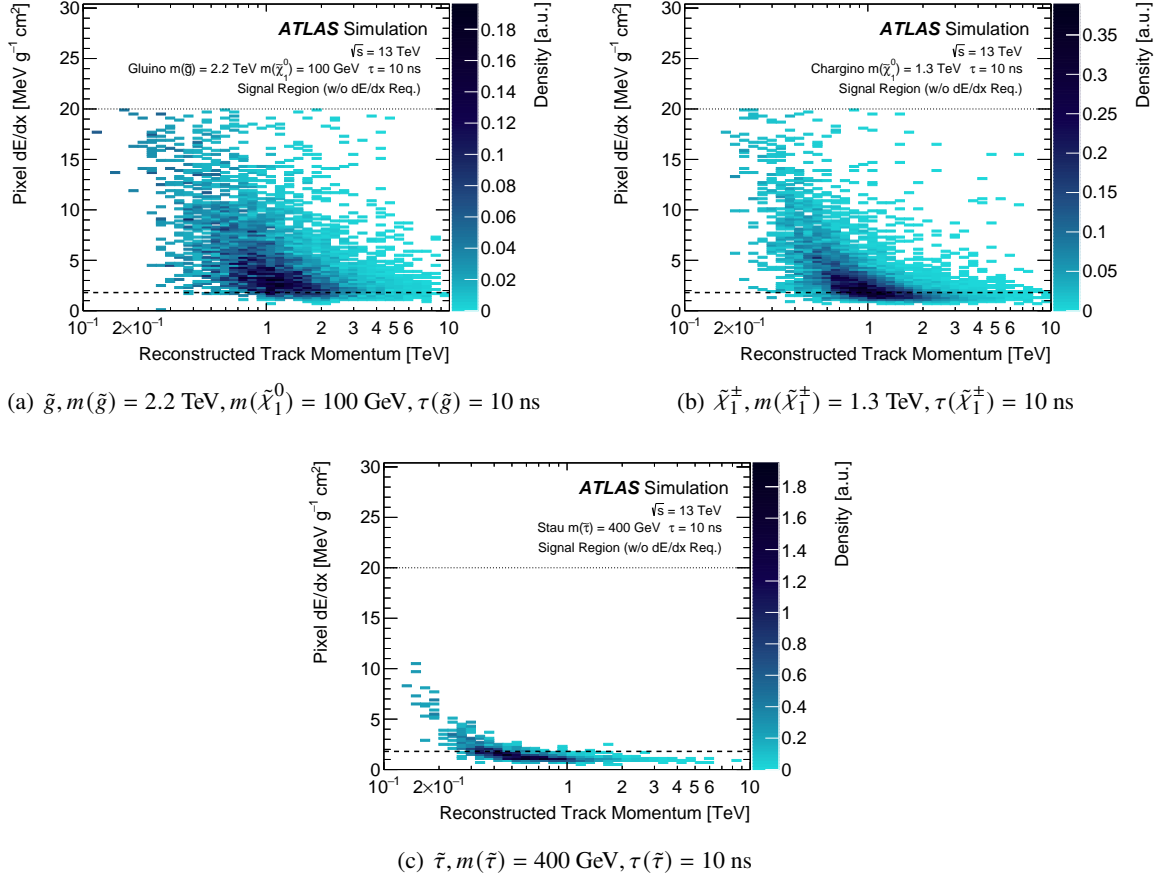


Figure 6: Simulated density distribution of representative signal tracks in the p - dE/dx plane after event selection except the dE/dx requirement. The region above the dashed horizontal line at $dE/dx = 1.8 \text{ MeV g}^{-1} \text{ cm}^2$ corresponds to the signal region. No events are expected above $dE/dx = 20 \text{ MeV g}^{-1} \text{ cm}^2$ because of the limited dynamic range of the pixel electronics. The data-driven dE/dx template technique described in Section 5 is used in the simulation of the dE/dx variable for these plots.

(IBL1) or absence (IBL0) of an IBL overflow cluster on the candidate track. These subsets are treated independently and their sensitivity is combined.

The analysis was therefore built to treat all the subsamples (IBL overflow yes/no, track identified as a muon yes/no) independently as well as all combined in a single sample, which is defined as the ‘Inclusive’ sample. All samples are split into Low and High dE/dx intervals, with the exception of the IBL1 events, where the tracks must satisfy the condition $dE/dx > 1.8 \text{ MeV g}^{-1} \text{ cm}^2$. This choice is justified by the small number of IBL1 tracks and by the better statistical significance expected in this sample.

In summary, the search is performed by splitting the data sample as illustrated in Table 2. If multiple tracks in an event are found in a single signal-region bin after all signal selections listed in Table 1, the track with the highest p_T is selected. However, more than one track can be selected from the same event if they enter different signal-region bins. The probability of this occurrence is negligibly small for the background events, while for the signal models, depending on the mass and lifetime parameters, the probability is as large as 10% when considering all events in the signal region. Figures 7–9 show how signal events are

Table 2: Table of signal-region bins, showing their purpose (discovery or limit setting) and properties.

SR name	Discovery	Limit setting	Track category	IBL overflow	dE/dx [MeV g ⁻¹ cm ²]
SR-Inclusive_Low	✓		inclusive	yes or no	[1.8, 2.4]
SR-Inclusive_High	✓				> 2.4
SR-Trk-IBL0_Low		✓	track	no	[1.8, 2.4]
SR-Trk-IBL0_High		✓		no	> 2.4
SR-Trk-IBL1		✓		yes	> 1.8
SR-Mu-IBL0_Low		✓	muon tracks	no	[1.8, 2.4]
SR-Mu-IBL0_High		✓		no	> 2.4
SR-Mu-IBL1		✓		yes	> 1.8

partitioned by this binning, depending on the LLP masses and lifetimes.

The two inclusive signal regions are less dependent on specific theory models and are therefore better suited to the search for an excess in the mass distribution. The six non-inclusive signal regions can be compared in detail to the LLP models considered in this analysis and are then used to derive limits directly related to these models.

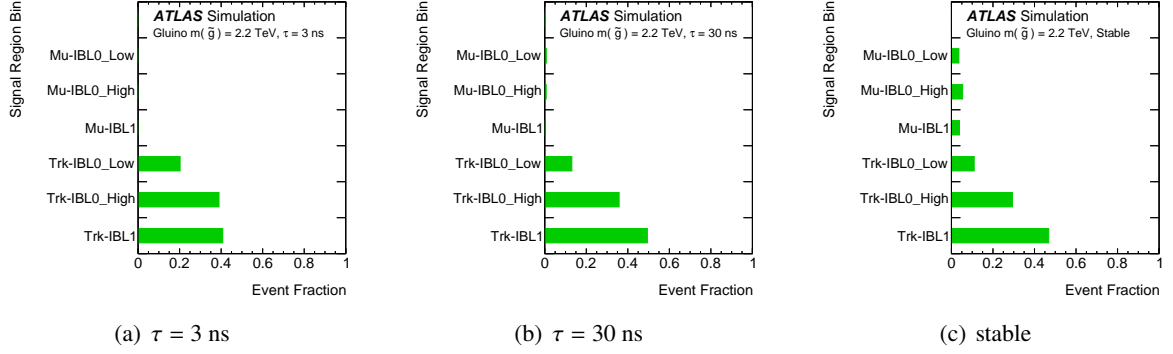


Figure 7: Relative fraction of events in the signal-region bins for gluino scenarios with $m(\tilde{g}) = 2.2$ TeV, $m(\tilde{\chi}_1^0) = 100$ GeV and different lifetime values. The fractions of events in muon-identified bins increase with the lifetime. The total probability to pass the event selection is 9.5% for $\tau = 3$ ns, 20.7% for $\tau = 30$ ns and 9.3% if the gluino is stable.

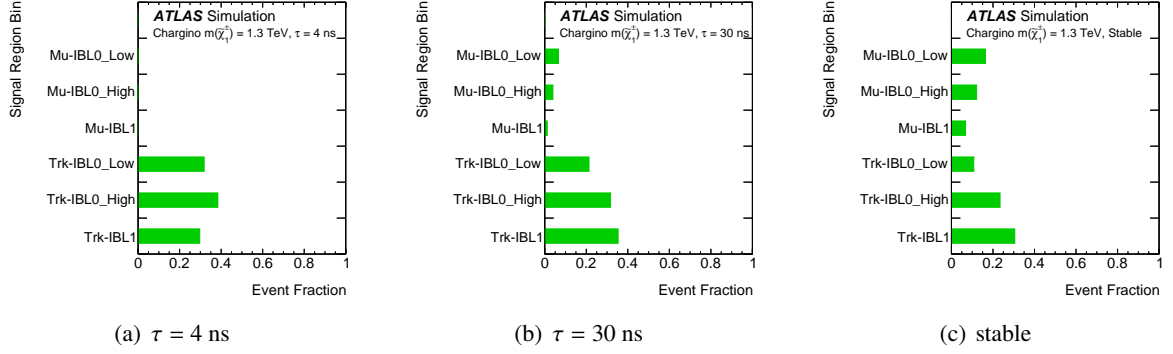


Figure 8: Relative fraction of events in the signal-region bins for chargino scenarios with $m(\tilde{\chi}_1^\pm) = 1.3$ TeV and different lifetime values. The fractions of events in muon-identified bins increase with the lifetime. The total probability to pass the event selection is 7.3% for $\tau = 4$ ns, 15.3% for $\tau = 30$ ns and 8.4% if the chargino is stable.

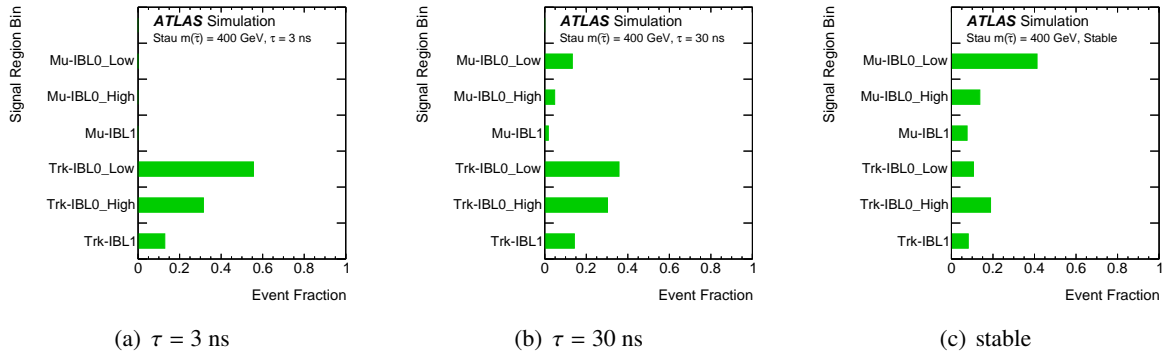


Figure 9: Relative fraction of events in the signal-region bins for stau scenarios with $m(\tilde{\tau}) = 400$ GeV and different lifetime values. The fractions of events in muon-identified bins increase with the lifetime. The total probability to pass the event selection is 3.4% for $\tau = 3$ ns, 4.0% for $\tau = 30$ ns and 1.4% if the stau is stable.

6.4 Mass windows

In the signal region, the expected background has a broad mass distribution which falls monotonically for $m \gtrsim 120$ GeV (see Section 7), while the signal forms a peak around its nominal mass. The signal mass resolution mainly reflects the momentum resolution of the tracks; the relative width of the core distribution is $\mathcal{O}(30\%) \times (m/\text{TeV})$, but it varies with the LLP’s decay length and therefore its lifetime. Therefore, a mass window is defined for each target mass, and for both the ‘short’ and ‘long’ lifetime regimes, targeting $\tau \leq 1$ ns and $\tau > 1$ ns, respectively. While the cross-sections span multiple orders of magnitude in the benchmarking models described in Section 4, the mass-spectrum shapes of these models are similar for a common target mass, reflecting the common kinematic nature of the $\beta\gamma$ spectrum of pair-produced particles. Therefore, the mass window for a given LLP mass is defined by taking the average of the normalised mass distributions of these models and finding the mass range that captures approximately 70% of the signal events in the signal region while excluding as much background as possible. Reflecting the steeply falling background distribution and the asymmetric long-tail mass distribution of the signal, especially at higher target masses, the window is asymmetric with respect to the target mass value and extends more to higher reconstructed masses. The lower boundary of the mass window is determined by maximising $1/\sqrt{B}$, where B is the expected background yield. Values of the window boundaries are tested in steps of 10 GeV ($m \leq 300$ GeV) or 50 GeV ($m > 300$ GeV). The range $m < 120$ GeV is not used for the window definition owing to signal selection cut-offs. The window is common to all signal-region bins (see Table 2) at a given target mass; minor acceptance differences for the various LLPs and the various lifetimes are taken care of in the sensitivity calculations. The windows cover the full range of target masses from 100 GeV to 3 TeV as shown in Figure 10. The ‘short’-lifetime regime has wider windows than the ‘long’-lifetime regime, reflecting poorer momentum resolution for shorter tracks. For consecutive target masses, the corresponding mass windows can largely overlap, and events common to such windows can be counted in each. The outcome of this search depends on the comparison of the data and background yields in each predefined mass window.

7 Background estimation

The mass distribution of SM tracks in the signal region is estimated using a data-driven technique. Two control regions per signal region, CR-kin and CR-dEdx, are defined adjacent in phase space to the signal region (see Table 3). CR-kin is defined by inverting the dE/dx requirement used in the signal region, and CR-dEdx is defined by inverting the E_T^{miss} requirement used in the signal region and removing the dE/dx requirement.⁸ Here, for a narrow $\Delta\eta$ slice, dE/dx and p_T are expected to be uncorrelated for minimum-ionising background tracks, and dE/dx and E_T^{miss} are similarly expected to be uncorrelated; therefore, for each $|\eta|$ slice, the $1/p_T$ distribution⁹ of tracks in CR-kin and the dE/dx distribution in CR-dEdx serve as the kinematic and dE/dx template distributions for the background mass prediction. The control-region distributions of tracks in the $1/p_T-|\eta|$ and $dE/dx-|\eta|$ planes are shown in Figure 11. In Figure 11(a) it is shown that the sample covers all kinematic space uniformly. Figure 11(b) indicates a slight dependence of the tails of the dE/dx distribution on $|\eta|$, which justifies slicing the background estimation in $|\eta|$. Because the mass of a track is defined by its momentum and $\beta\gamma$ (and therefore dE/dx), the background mass distribution can be constructed by sampling these two distributions.

⁸ the CR-dEdx will include all the ionization fluctuations (e.g. δ -ray effects) which may remain after the calculation of the truncated mean. Thus these are taken into account in the background generation.

⁹ Instead of p_T , $1/p_T$ is used here in order to partition the samples with a sufficient number of tracks in all bins.

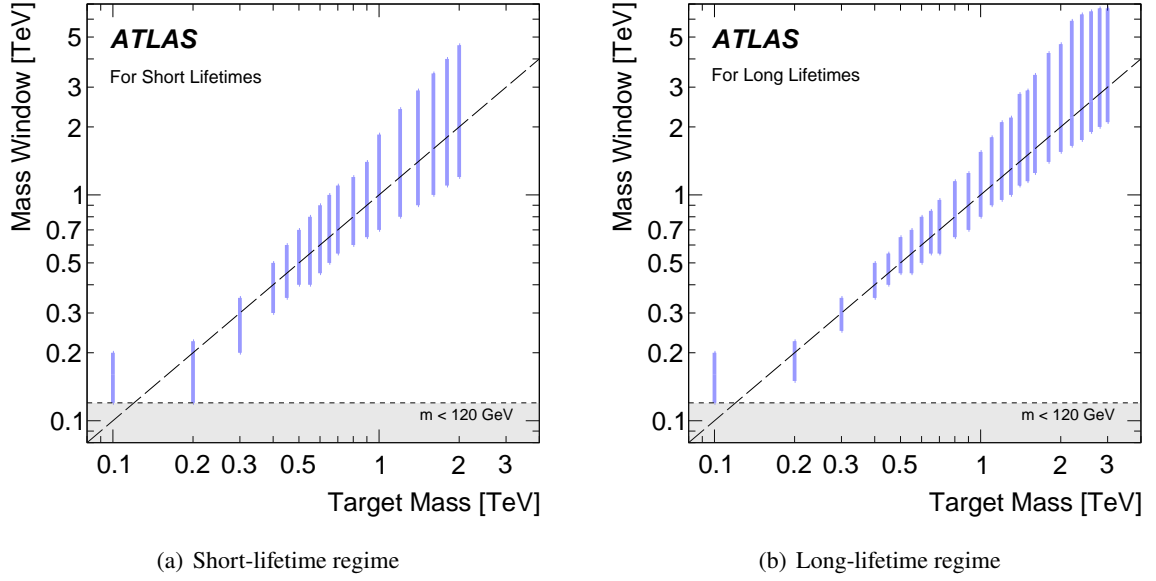


Figure 10: The mass windows for various LLP masses for (a) short lifetimes (i.e. ≤ 1 ns) and (b) long lifetimes. The range $m < 120$ GeV is not considered for mass-window boundaries due to the kinematical event selection.

Table 3: Definitions of the signal, control and validation regions.

Region	p_T [GeV]	$ \eta $	E_T^{miss} [GeV]	dE/dx [$\text{MeV g}^{-1}\text{cm}^2$]
SR			> 170	> 1.8
CR-kin	> 120	< 1.8	> 170	< 1.8
CR-dEdx			< 170	> 0
VR-LowPt			> 170	> 1.8
CR-LowPt-kin	[50, 110]	< 1.8	> 170	< 1.8
CR-LowPt-dEdx			< 170	> 0
VR-HiEta			> 170	> 1.6
CR-HiEta-kin	> 50	[1.8, 2.5]	> 170	< 1.6
CR-HiEta-dEdx			< 170	> 0

Although the dE/dx corrections described in Section 5 equalise the MPV of the dE/dx distribution as a function of $|\eta|$, any $|\eta|$ -dependent differences in the dE/dx tails remain after applying the corrections. As a result, the dE/dx template is sliced in bins of $|\eta|$. The event rate in CR-dEdx changes over time, reflecting adjustments to the E_T^{miss} trigger threshold during Run 2, while the event rate in CR-kin is stable since the E_T^{miss} requirement of 170 GeV is well above the trigger threshold. In order to compensate for this effect, events in the dE/dx template extracted from CR-dEdx are reweighted. The weight factor for the i -th run, w_i , is defined as $w_i \equiv R_{i_0}/R_i$ where the R_i is the ratio of the numbers of events in CR-LowPt-dEdx and CR-LowPt-kin for a given run i and i_0 is the reference run against which the events are calibrated. The weight factor differs from unity by up to $\pm 2\%$.

The CR-kin region, used to predict the background in signal regions requiring tracks to have a hit in the IBL overflow, is statistically sparse. To mitigate this, the kinematic template in the CR-kin region, requiring tracks have no hits in the IBL overflow, is used instead, with a weight factor $n(\text{OF}_{\text{IBL}} = 1)/n(\text{OF}_{\text{IBL}} = 0)$

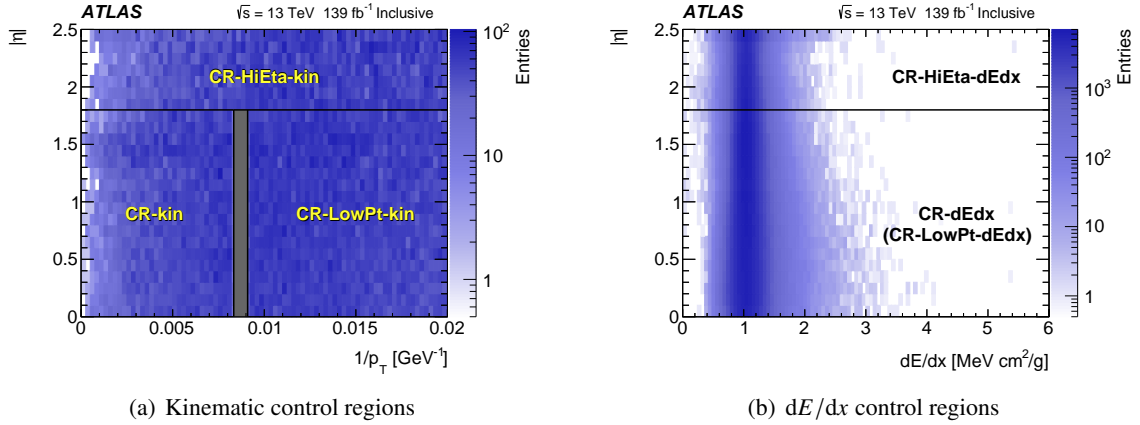


Figure 11: Event distributions of (a) kinematic control regions in the $1/p_T$ - $|\eta|$ plane and (b) dE/dx control regions in the dE/dx - $|\eta|$ plane for the inclusive sample.

applied to each $|\eta|$ slice.

To form a ‘toy’ background track, a pair of $1/p_T$ and $|\eta|$ values is sampled from the kinematic template. A dE/dx value is sampled from the corresponding $|\eta|$ bin of the dE/dx template. From these sampled values, the track mass, m , is calculated using the dE/dx - $\beta\gamma$ calibration. In total, 10 (40) million toy tracks are generated for the Low (High) dE/dx range so that the number of toy samples does not limit the accuracy of predictions in any mass range. Because there is no restriction on the range of dE/dx in sampling from CR-dEdx, these toy samples predict the background distribution in both of the signal regions and CR-kin simultaneously. Finally, the toy samples are normalised to data in a sub-region of CR-kin which is expected to be depleted in signal, with $m < 160$ GeV and $dE/dx < 1.8 \text{ MeV g}^{-1}\text{cm}^2$. After the normalisation, the mass distributions in the $m > 160$ GeV range of CR-kin are in good agreement with those derived from the toy samples.

The background estimation procedure is validated in two sets of validation regions: one set (VR-LowPt) selects tracks with lower p_T and the other set (VR-HiEta) selects tracks with higher $|\eta|$ and has a looser p_T requirement than in the signal regions. The definitions of these regions and the corresponding control regions used for the background estimation are shown in Table 3. The dE/dx requirement for the VR-HiEta region is loosened in order to probe a similar tail fraction of the narrower dE/dx distribution found at high $|\eta|$, and there is no subdivision of VR-HiEta into Low and High dE/dx ranges because of the limited sample size.

The expected and observed mass distributions for two of the individual validation regions, VR-LowPt-Inclusive_High (with $dE/dx > 2.4 \text{ MeV g}^{-1}\text{cm}^2$) and VR-HiEta-Inclusive (with $dE/dx > 1.6 \text{ MeV g}^{-1}\text{cm}^2$), are shown in Figure 12. The expected and observed distributions agree well across the lower mass range probed by VR-LowPt-Inclusive_High and the higher mass range probed by VR-HiEta-Inclusive.

The expected and observed yields in all of the validation-region bins are shown in Table 4, and the ratios of the observed to expected yields are shown in Figure 13. Good agreement is visible across all region bins except VR-LowPt-Trk-IBL0_Low, where the observed yield is approximately 35% lower than the prediction and unlikely to be a statistical fluctuation. In order to relieve this tension, an empirical systematic

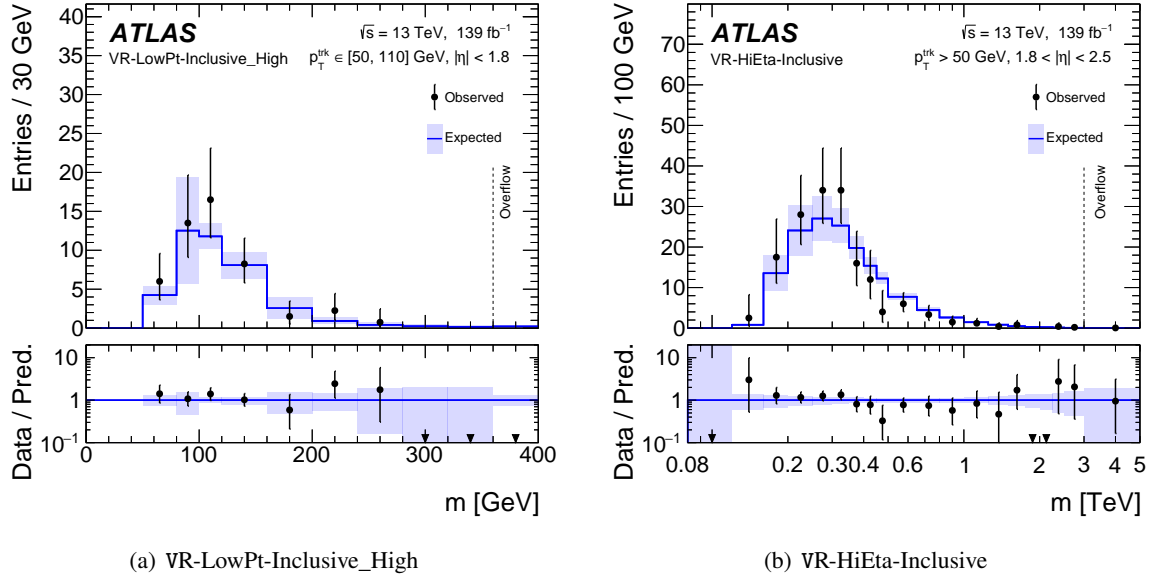


Figure 12: Comparison of the observed and expected mass distributions in (a) VR-LowPt-Inclusive_High and (b) VR-HiEta-Inclusive validation-region bins. The band on the expected background estimation indicates the total uncertainty of the estimation. Downward triangle markers at the bottom of the panels indicate there are no events observed in the corresponding bin.

scale uncertainty is added. The details of this treatment are described in Section 8. This additional uncertainty is already included in Figures 12 and 13 and in Table 4, combined with the rest of the systematic uncertainties.

8 Systematic uncertainties

The systematic uncertainties associated with the background estimate are evaluated for each mass window, as shown in Figure 14. The leading uncertainty at high masses is the template correlation uncertainty, labelled ‘Template corr.’, which estimates the effect of residual correlations between the template distributions used to generate the background. To test the assumption that the kinematic and dE/dx templates can be sampled separately to form a toy track, a pseudo signal region is defined in the CR- dE/dx region (the one based on inverting the E_T^{miss} requirement) by requiring $dE/dx > 1.8 \text{ MeV g}^{-1} \text{ cm}^2$. The background estimation procedure is then executed, extracting both the $(p_T^{-1}, |\eta|)$ pair and the dE/dx from the distributions in the CR- dE/dx region. The difference of the event counts in each mass window between the predicted and observed mass distributions in the pseudo signal regions is taken as a systematic uncertainty. The size of the uncertainty is evaluated for each signal-region bin separately. This uncertainty is the dominant uncertainty in the target mass above $\sim 1 \text{ TeV}$.

In the background estimation procedure, the dE/dx templates are sliced in $|\eta|$ due to the remaining $|\eta|$ -dependence of the dE/dx tails. To ensure that the background estimate is not heavily dependent on the choice of these bins, the background estimation is repeated with an alternative set of $|\eta|$ bins. The difference between the resulting mass distribution and the nominal one is taken as a systematic uncertainty,

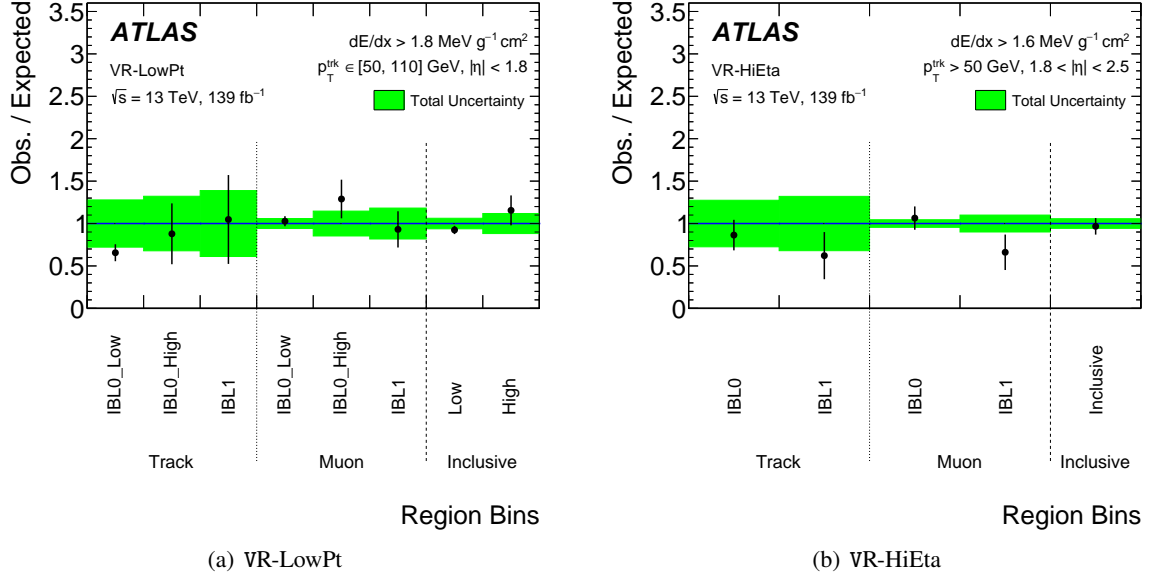


Figure 13: Comparison of the observed and expected event yields in (a) VR-LowPt and (b) VR-HiEta validation-region bins.

Table 4: Expected and observed event yields in the validation-region bins.

Region	Category	Bin	Expected	Observed
VR-LowPt	Trk	IBL0_Low	65.6 ± 18.3	43
		IBL0_High	6.8 ± 2.2	6
		IBL1	3.8 ± 1.5	4
	Mu	IBL0_Low	292 ± 17	300
		IBL0_High	24.8 ± 3.6	32
		IBL1	20.4 ± 3.7	19
	Inclusive	Low	391 ± 24	361
High		37.2 ± 4.4	43	
VR-HiEta	Trk	IBL0	26.6 ± 7.3	23
		IBL1	8.0 ± 2.6	5
	Mu	IBL0	56.4 ± 2.5	59
		IBL1	15.1 ± 1.5	10
	Inclusive	—	101 ± 6	97

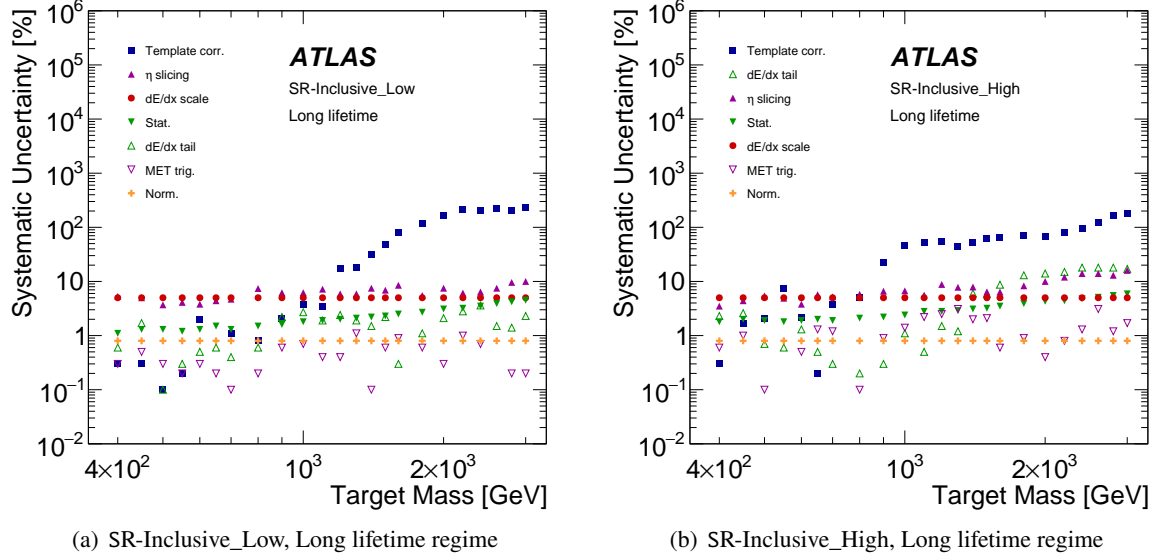


Figure 14: Systematic uncertainties in the background estimate for each mass window targeting long lifetimes in the (a) SR-Inclusive_Low region and (b) SR-Inclusive_High region.

labelled ‘ η slicing’. The $OF_{IBL} = 1$ region uses a reweighted version of the $OF_{IBL} = 0$ region’s kinematic template as explained in Section 7. An uncertainty is assigned to this method by generating an alternative background distribution using the original $OF_{IBL} = 1$ region’s kinematic template and comparing it with the background distribution generated by the reweighted kinematic template. This uncertainty only affects the IBL1 SR.

Since the E_T^{miss} trigger thresholds changed during Run 2, the dE/dx templates in the background estimation are reweighted to correct for any bias which may arise in the CR- $dEdx$ region, which is populated by events with low E_T^{miss} . An uncertainty labelled ‘MET trig.’, derived by comparing the predicted mass distributions with and without this reweighting, is applied to cover any deficiencies in the reweighting.

Uncertainties that account for the effect of statistical fluctuations in the control-region templates are also evaluated. The statistical uncertainties of the template histograms are derived by fluctuating each bin in the template histograms according to a Poisson distribution with a mean equal to the number of entries in the bin. The root-mean-square deviation of alternative mass distributions generated from the randomly fluctuated templates is taken as the uncertainty, which is labelled ‘Stat.’. To quantify the effect of statistical fluctuations in the tail of the dE/dx template distributions and assign an uncertainty, labelled ‘ dE/dx tail’, each tail is fitted with a Crystal Ball distribution, which is then used instead of the data in the dE/dx template to generate an alternative mass distribution. A statistical uncertainty, labelled ‘Norm.’, in the normalisation factor of the background prediction is also calculated and applied as a uniform uncertainty.

As described in the previous section, in validation-region bin VR-LowPt-Trk-IBL0_Low, a deficit of 35% relative to the prediction is observed in the range $m \lesssim 120$ GeV, which is significantly larger than the statistical uncertainty. In the other bins, no significant excesses or deficits are found. This deficit can be attributed to the difference between the dE/dx tail distributions for $dE/dx \in [1.8, 2.4]$ MeV $g^{-1}cm^2$ in the CR-LowPt- $dEdx$ and VR-LowPt samples. An empirical scale uncertainty in the number of events, labelled

‘ dE/dx scale’, is assigned based on the following considerations: the observed mismatch depends on the amount of pile-up, and for the `Mu` categories the dE/dx tail fraction is stable and the observed yield agrees with the prediction very well. The dE/dx response of well-isolated muon tracks is considered more robust against pile-up than that of other tracks. Therefore, different uncertainties are assigned to the `Trk` and `Mu` categories, and the uncertainty is correlated over all validation- and signal-region bins in the same category. With this global approach, a scale uncertainty of 27% (3%) is assigned to the `Trk` (`Mu`) category. For the `Inclusive` category, the combined scale uncertainty is found to be 5%, and this is consistent with the fact that the majority of the background tracks in the `Inclusive` category are identified as muons. The derived ‘ dE/dx scale’ uncertainty is assumed to be uniform over mass and is dominant, uniquely for the `Trk` category, below ~ 1.0 TeV.

Additional systematic uncertainties associated with the modelling and predicted yield of the signals in simulation are also considered when setting limits on specific models. An uncertainty of 1.7% applied to the dataset’s integrated luminosity is derived from x - y beam-separation scans [79]. Uncertainties in the QCD radiation modelling, which significantly impact the efficiency of triggering on signals with large initial-state radiation, are estimated using MC samples. These MC samples are generated identically to their corresponding signal MC samples but with variations in the factorisation, renormalisation, and merging scales, as well as in the parton showering tunes and radiation tunes. The differences between results from the nominal and alternative MC samples are then used as the systematic uncertainties. The majority of these uncertainties are found to be of order of 1%. The only exceptions are parton shower and radiation tuning uncertainties that can grow to be $\sim 10\%$ for some MC samples.

For the MC signal samples, the dE/dx distribution (and therefore the mass distribution), as well as the probability of a track to have $OF_{IBL} = 1$, is based on a template derived from a 2017 low-pile-up dataset. This dataset is also used to calibrate the dE/dx - $\beta\gamma$ relationship. Although the run-dependent corrections applied to the dE/dx measurement mitigate any time dependence of the most probable dE/dx measurement for a MIP-like particle, any remaining time dependence of the dE/dx distribution for particles with small $\beta\gamma$ in data is not accounted for in signal samples because the data-driven template is taken from a fixed point in time. To quantify the potential impact of this, the dE/dx - $\beta\gamma$ relationship was calibrated again, this time using a similar low-pile-up dataset taken in 2018. The probability of a track to have $OF_{IBL} = 1$ was also measured in this dataset. The difference between the two calibrations, quantified by comparing the resulting signal-region track masses, is negligible compared to the mass resolution and is less than $\sim 3\%$. The probability of a track to have $OF_{IBL} = 1$ was found to have increased significantly in 2018 due to a change in the IBL ToT front-end configuration. An associated uncertainty is therefore calculated by comparing the probabilities of a track to have $OF_{IBL} = 1$ in the 2017 and 2018 low-pile-up datasets and applied by using the $\beta\gamma$ -dependent ratio of these probabilities to reweight the events.

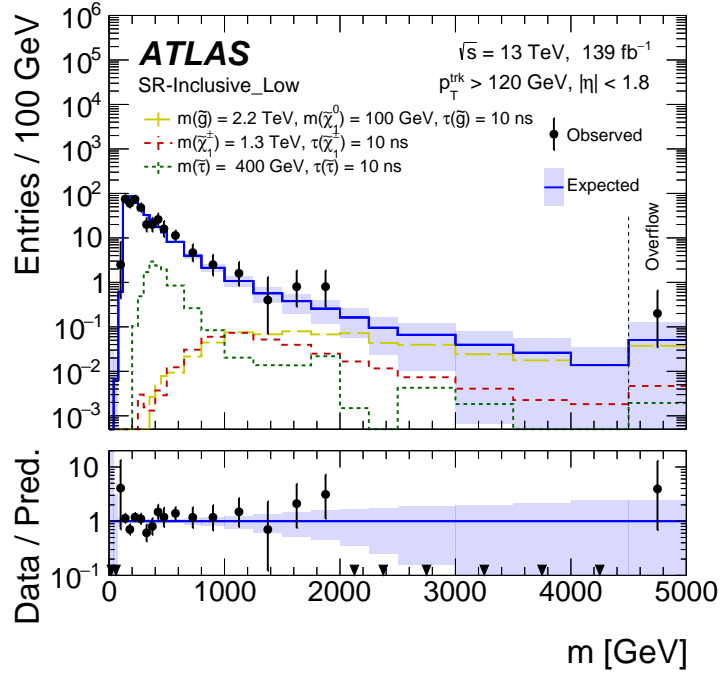
Other uncertainties associated with the simulation modelling include those related to the pile-up distribution, track-level quantities, muon identification, the E_T^{miss} trigger, and the offline E_T^{miss} calculation. The largest of these are the modelling uncertainties associated with track momentum measurement errors due to detector misalignments, the pile-up distribution, and the offline E_T^{miss} calculation.

9 Results

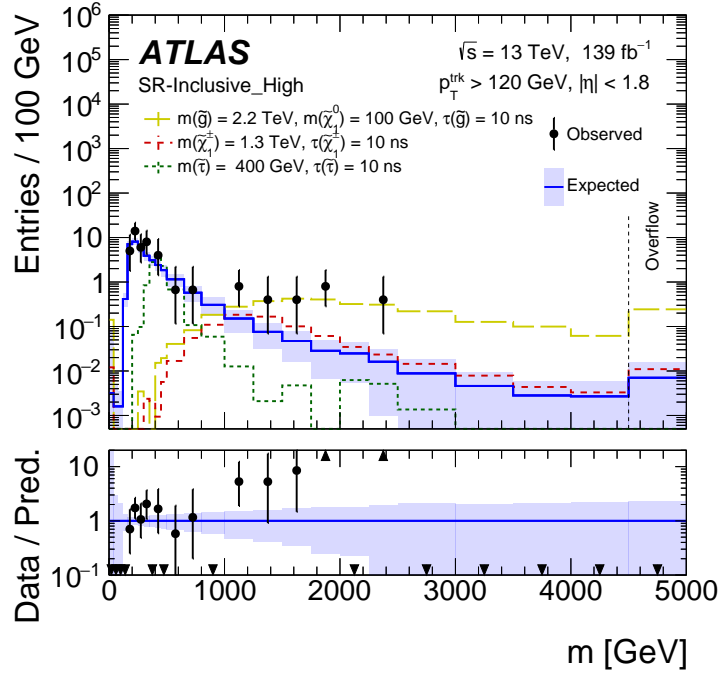
In total, 223 events are observed in the signal region combining all exclusive bins. The observation in each mass window (defined for each hypothetical particle mass) for the `Inclusive` signal-region bins is presented in Table 5, and in total 196 (27) events are observed in the `SR-Inclusive_Low` (`SR-Inclusive_High`)

Table 5: List of expected and observed numbers of events, p_0 -value (capped at 0.5) and the corresponding local Z significance, as well as the 95% CL_s upper limit on the expected and observed numbers of signal events (S_{exp}^{95} and S_{obs}^{95}) in each mass window for SR-Inclusive bins in the ‘short’ ($\tau \leq 1$ ns) and ‘long’ ($\tau > 1$ ns) lifetime regimes.

Target mass [GeV]	Mass window [GeV]	Signal region bin											
		SR-Inclusive_Low						SR-Inclusive_High					
		Exp.	Obs.	p_0	Z_{local}	S_{exp}^{95}	S_{obs}^{95}	Exp.	Obs.	p_0	Z_{local}	S_{exp}^{95}	S_{obs}^{95}
Short lifetime													
200	[120, 225]	81 ± 4	76	5.00×10^{-1}	0.0	21^{+8}_{-6}	18	5.6 ± 0.7	7	2.65×10^{-1}	0.6	$6.3^{+2.5}_{-1.7}$	7.8
300	[200, 350]	72 ± 4	72	4.72×10^{-1}	0.1	20^{+8}_{-6}	20	9.2 ± 0.8	14	7.11×10^{-2}	1.5	$7.6^{+3.0}_{-2.1}$	12.5
400	[300, 500]	45.6 ± 3.3	43	5.00×10^{-1}	0.0	16^{+6}_{-4}	14	5.8 ± 0.4	6	4.39×10^{-1}	0.1	$6.1^{+2.5}_{-1.8}$	6.5
450	[350, 600]	37.6 ± 2.7	44	1.72×10^{-1}	0.9	15^{+6}_{-4}	20	5.1 ± 0.4	3	5.00×10^{-1}	0.0	$6.0^{+2.2}_{-1.6}$	4.6
500	[400, 700]	30.6 ± 2.2	42	3.41×10^{-2}	1.8	13^{+5}_{-4}	24	4.3 ± 0.4	4	5.00×10^{-1}	0.0	$5.4^{+2.2}_{-1.3}$	5.2
550	[400, 800]	33.9 ± 2.5	45	4.74×10^{-2}	1.7	14^{+5}_{-4}	24	4.8 ± 0.4	4	5.00×10^{-1}	0.0	$5.8^{+2.5}_{-1.8}$	5.4
600	[450, 900]	27.5 ± 1.9	35	9.48×10^{-2}	1.3	$12.1^{+5.3}_{-3.5}$	19.3	3.91 ± 0.31	2	5.00×10^{-1}	0.0	$5.5^{+2.2}_{-1.6}$	4.0
650	[500, 1000]	22.5 ± 1.6	29	1.03×10^{-1}	1.3	$11.2^{+4.4}_{-2.8}$	17.2	3.22 ± 0.31	2	5.00×10^{-1}	0.0	$5.2^{+1.9}_{-1.6}$	4.4
700	[550, 1100]	18.7 ± 1.4	23	1.71×10^{-1}	0.9	$10.3^{+4.0}_{-2.7}$	14.3	2.64 ± 0.31	2	5.00×10^{-1}	0.0	$4.7^{+1.9}_{-1.0}$	4.3
800	[600, 1200]	15.6 ± 1.3	20	1.47×10^{-1}	1.1	$9.5^{+3.8}_{-2.9}$	13.7	2.22 ± 0.24	3	2.86×10^{-1}	0.6	$4.5^{+1.8}_{-1.0}$	5.5
900	[650, 1400]	13.8 ± 1.3	17	2.09×10^{-1}	0.8	$9.1^{+3.5}_{-2.5}$	11.9	2.0 ± 0.3	4	9.74×10^{-2}	1.3	$4.3^{+1.6}_{-0.9}$	6.8
1000	[700, 1850]	13.1 ± 1.3	17	1.54×10^{-1}	1.0	$8.8^{+3.6}_{-2.3}$	12.7	1.9 ± 0.5	4	9.01×10^{-2}	1.3	$4.1^{+1.9}_{-0.7}$	7.0
1200	[800, 2400]	11 ± 2	14	1.85×10^{-1}	0.9	$8.6^{+3.3}_{-2.5}$	11.9	1.5 ± 0.7	6	9.10×10^{-3}	2.4	$4.0^{+1.6}_{-0.8}$	10.0
1400	[900, 2900]	8.5 ± 2.1	11	2.37×10^{-1}	0.7	$8.1^{+3.1}_{-2.6}$	10.5	1.1 ± 0.7	7	2.08×10^{-3}	2.9	$4.0^{+1.4}_{-0.7}$	11.5
1600	[1000, 3450]	6.9 ± 2.4	9	2.57×10^{-1}	0.7	$7.8^{+3.0}_{-2.6}$	10.1	0.9 ± 0.5	7	6.03×10^{-4}	3.2	$3.6^{+1.5}_{-0.5}$	11.8
1800	[1100, 4000]	5.7 ± 2.6	8	2.35×10^{-1}	0.7	$7.3^{+2.8}_{-2.3}$	9.9	0.8 ± 0.6	7	8.87×10^{-4}	3.1	$3.5^{+1.1}_{-0.2}$	11.9
2000	[1200, 4600]	5 ± 4	6	3.03×10^{-1}	0.5	$7.3^{+3.0}_{-2.3}$	9.0	0.6 ± 0.5	5	4.92×10^{-3}	2.6	$3.1^{+1.1}_{-0.1}$	9.4
Long lifetime													
100	[120, 200]	68 ± 4	63	5.00×10^{-1}	0.0	19^{+7}_{-5}	16	3.9 ± 0.6	5	2.81×10^{-1}	0.6	$5.4^{+2.1}_{-1.0}$	6.7
200	[150, 225]	63 ± 4	54	5.00×10^{-1}	0.0	18^{+7}_{-4}	13	5.5 ± 0.6	7	2.61×10^{-1}	0.6	$6.1^{+2.6}_{-1.8}$	7.8
300	[250, 350]	40.9 ± 2.7	35	5.00×10^{-1}	0.0	15^{+6}_{-4}	11	5.1 ± 0.5	7	2.01×10^{-1}	0.8	$5.9^{+2.4}_{-1.4}$	8.0
400	[350, 500]	29.2 ± 2.2	33	2.54×10^{-1}	0.7	$12.6^{+5.3}_{-3.2}$	16.0	3.83 ± 0.26	2	5.00×10^{-1}	0.0	$5.4^{+1.9}_{-1.3}$	4.2
450	[400, 550]	21.5 ± 1.6	30	5.03×10^{-2}	1.6	$11.0^{+4.2}_{-2.9}$	19.4	3.00 ± 0.23	2	5.00×10^{-1}	0.0	$5.1^{+1.7}_{-1.3}$	4.3
500	[450, 650]	19.4 ± 1.2	27	5.62×10^{-2}	1.6	$10.3^{+4.3}_{-2.6}$	17.4	2.73 ± 0.22	1	5.00×10^{-1}	0.0	$4.7^{+1.9}_{-0.9}$	3.9
550	[450, 700]	21.8 ± 1.5	29	7.73×10^{-2}	1.4	$11.0^{+4.2}_{-3.2}$	17.8	3.06 ± 0.32	2	5.00×10^{-1}	0.0	$5.0^{+2.1}_{-1.5}$	4.2
600	[500, 800]	18.4 ± 1.3	24	1.12×10^{-1}	1.2	10^{+4}_{-3}	15	2.64 ± 0.19	2	5.00×10^{-1}	0.0	$4.4^{+2.2}_{-1.2}$	4.2
650	[550, 850]	15 ± 1	19	1.32×10^{-1}	1.1	$9.1^{+3.7}_{-2.7}$	13.4	2.07 ± 0.17	2	5.00×10^{-1}	0.0	$4.5^{+1.5}_{-1.2}$	4.6
700	[550, 950]	16.6 ± 1.2	21	1.52×10^{-1}	1.0	$9.7^{+3.8}_{-2.8}$	13.7	2.4 ± 0.2	2	5.00×10^{-1}	0.0	$4.5^{+2.0}_{-0.9}$	4.3
800	[650, 1150]	12.0 ± 1.1	14	2.86×10^{-1}	0.6	$8.4^{+3.5}_{-2.3}$	10.4	1.74 ± 0.16	3	1.79×10^{-1}	0.9	$4.1^{+1.8}_{-0.8}$	5.8
900	[700, 1250]	10.4 ± 0.9	13	2.17×10^{-1}	0.8	$8.1^{+3.0}_{-2.6}$	10.3	1.5 ± 0.4	3	1.35×10^{-1}	1.1	$3.9^{+1.8}_{-1.0}$	6.0
1000	[800, 1550]	8.6 ± 0.8	11	2.16×10^{-1}	0.8	$7.5^{+2.9}_{-2.5}$	9.6	1.2 ± 0.6	4	3.73×10^{-2}	1.8	$3.8^{+1.4}_{-0.8}$	7.5
1100	[900, 1800]	7.1 ± 0.7	10	1.46×10^{-1}	1.1	$7.0^{+2.5}_{-1.9}$	9.8	1.0 ± 0.5	4	2.13×10^{-2}	2.0	$3.7^{+1.2}_{-0.8}$	7.6
1200	[950, 2100]	6.7 ± 1.3	10	1.38×10^{-1}	1.1	$7.0^{+2.5}_{-2.3}$	10.2	0.9 ± 0.5	6	1.65×10^{-3}	2.9	$3.7^{+1.3}_{-0.6}$	10.4
1300	[1000, 2200]	6.1 ± 1.2	9	1.48×10^{-1}	1.0	$6.5^{+2.9}_{-1.4}$	9.7	0.8 ± 0.4	6	5.47×10^{-4}	3.3	$3.5^{+1.2}_{-0.5}$	10.3
1400	[1100, 2800]	5.2 ± 1.7	8	1.76×10^{-1}	0.9	$6.5^{+2.6}_{-2.0}$	9.6	0.7 ± 0.4	7	1.46×10^{-4}	3.6	$3.2^{+1.1}_{-0.1}$	11.9
1500	[1150, 2900]	4.9 ± 2.4	7	2.41×10^{-1}	0.7	$6.6^{+2.8}_{-1.9}$	9.3	0.6 ± 0.4	6	6.09×10^{-4}	3.2	$3.2^{+1.2}_{-0.1}$	10.7
1600	[1250, 3400]	4.2 ± 3.4	5	3.24×10^{-1}	0.5	$7.0^{+2.9}_{-2.2}$	8.4	0.54 ± 0.35	5	1.19×10^{-3}	3.0	$3.1^{+1.2}_{-0.1}$	9.5
1800	[1400, 4250]	3^{+4}_{-3}	4	2.74×10^{-1}	0.6	$7.2^{+2.4}_{-1.5}$	8.3	0.44 ± 0.32	4	3.36×10^{-3}	2.7	$3.2^{+1.0}_{-0.1}$	8.1
2000	[1550, 4650]	3^{+4}_{-3}	3	3.14×10^{-1}	0.5	$6.2^{+1.9}_{-2.1}$	6.9	0.36 ± 0.25	3	6.96×10^{-3}	2.5	$3.1^{+1.0}_{-0.1}$	6.8
2200	[1650, 5900]	2^{+5}_{-2}	4	2.18×10^{-1}	0.8	$6.0^{+2.4}_{-2.2}$	8.2	0.33 ± 0.28	3	8.85×10^{-3}	2.4	$3.0^{+1.1}_{-0.1}$	6.8
2400	[1750, 6300]	2^{+4}_{-2}	3	3.17×10^{-1}	0.5	$5.5^{+1.5}_{-1.5}$	6.7	0.29 ± 0.28	3	9.75×10^{-3}	2.3	$3.2^{+0.8}_{-0.0}$	6.9
2600	[1900, 6500]	2^{+4}_{-2}	1	5.00×10^{-1}	0.0	$4.9^{+2.0}_{-1.6}$	4.0	$0.25^{+0.31}_{-0.25}$	3	9.71×10^{-3}	2.3	$3.1^{+0.7}_{-0.0}$	6.9
2800	[2000, 6700]	$1.5^{+3.1}_{-1.5}$	1	5.00×10^{-1}	0.0	$4.5^{+2.1}_{-1.4}$	4.2	$0.2^{+0.4}_{-0.2}$	1	1.07×10^{-1}	1.2	$3.0^{+0.6}_{-0.0}$	4.0
3000	[2100, 6700]	$1.4^{+3.1}_{-1.4}$	1	5.00×10^{-1}	0.0	$4.4^{+1.4}_{-1.1}$	4.3	$0.2^{+0.4}_{-0.2}$	1	9.43×10^{-2}	1.3	$2.9^{+0.4}_{-0.0}$	4.1

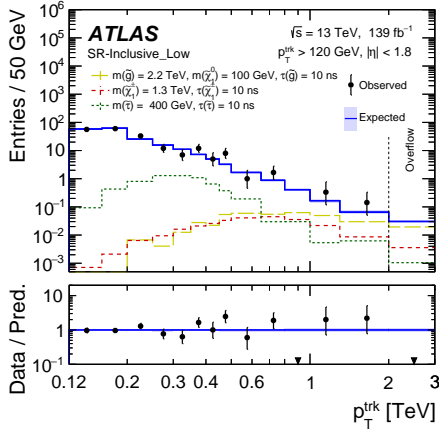


(a) SR-Inclusive_Low

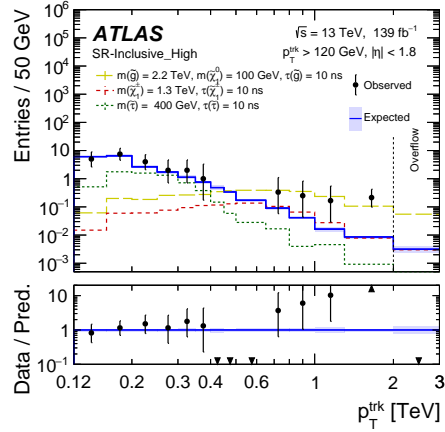


(b) SR-Inclusive_High

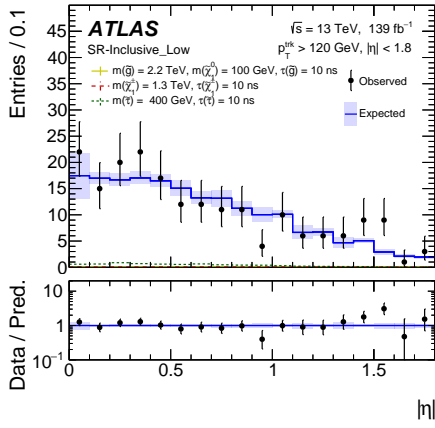
Figure 15: The observed mass distribution in the Inclusive signal-region bins. The band on the expected background indicates the total uncertainty of the estimation. Several representative signal models are overlaid. Events outside the shown range are accumulated in the rightmost bin indicated as ‘Overflow’. Downward triangle markers at the bottom of the panels indicate that no events are observed in the corresponding mass bin, while the upward triangle markers at the top of the lower panel in (b) indicate that the observed data is beyond the range. The excess of events seen in the lower panel is further discussed in the text.



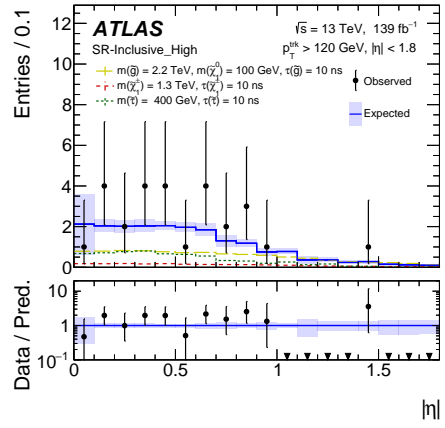
(a) SR-Inclusive_Low



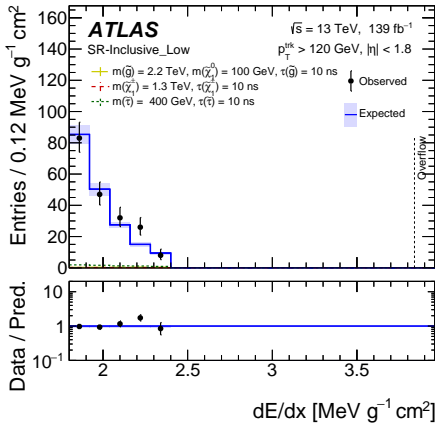
(b) SR-Inclusive_High



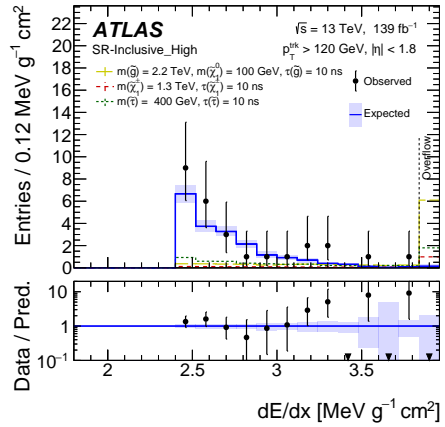
(c) SR-Inclusive_Low



(d) SR-Inclusive_High



(e) SR-Inclusive_Low



(f) SR-Inclusive_High

Figure 16: The observed p_T , $|\eta|$ and dE/dx distributions in the Inclusive signal-region bins. The band on the expected background indicates the total uncertainty of the estimation. Several representative signal models are overlaid. Events outside the shown range are accumulated in the rightmost bin indicated as ‘Overflow’. Downward triangle markers at the bottom of the panels indicate that no events are observed in the corresponding bin, while the upward triangle marker at the top of the lower panel in (b) indicates that the observed data is beyond the range.

bin over the full mass range (see Table 2). The mass, p_T , $|\eta|$ and dE/dx distributions in each of the SR-Inclusive_Low and SR-Inclusive_High bins are shown in Figures 15 and 16, compared with the expected background yields and several representative signal points. Overall, the observed event distribution agrees well with the expected background distribution in these variables within the estimated uncertainties, except in the SR-Inclusive_High bin in the high mass range.

The statistical analysis and likelihood construction were implemented in the `pyhf` software framework [80]. For each mass window, the likelihood of the background-only hypothesis given the observed data was constructed from the background prediction and the associated systematic uncertainties. The effect of the systematic uncertainties is incorporated through nuisance parameters which are constrained to be Gaussian-distributed. Using a profile-likelihood-based test statistic [81], independent p_0 -values quantifying the level of agreement between the observed data and the background prediction were calculated for each of these windows. The lowest p_0 -value of 1.46×10^{-4} is associated with the SR-Inclusive_High bin in the mass window of [1100, 2800] GeV, corresponding to a target mass of 1.4 TeV in the ‘long’ lifetime regime. In this window, 0.7 ± 0.4 events are expected and seven events are observed, and the p_0 -value corresponds to a local Z significance¹⁰ of 3.6. The mild excess reported in Ref. [40] at around 600 GeV is not confirmed in the dataset analysed here: the maximum local Z significance observed in that region is 1.8 for a target mass of 500 GeV in the SR-Inclusive_Low bin in the ‘short’ lifetime regime.

After taking into account the look-elsewhere effect [82, 83], the corresponding global Z significance for the 1.4 TeV target mass in the SR-Inclusive_High bin is evaluated to be approximately 3.3 by using pseudo-experiments, including all ‘long’ and ‘short’ lifetime windows. The pseudo-experiments generate event distributions in the signal-region bins according to the background estimate, assuming the systematic uncertainty is correlated over all masses. In total, one million pseudo-experiments were generated per signal-region bin to evaluate the global significance. Reflecting the relatively broad mass resolution above 1 TeV, the look-elsewhere effect is found to be mild, consistent with the relatively small difference between the local and global Z significances.

Events in the mass window with the lowest p_0 -value were examined individually. Out of these seven events, four are in the SR-Mu category and have no IBL overflow, two of the remaining three events are in the SR-Trk category and have an IBL overflow, and the last event is in the SR-Trk category and has no IBL overflow. One of the three events in the SR-Trk category has a matched muon which does not satisfy the identification criterion applied in this analysis. Detailed pixel cluster information was extracted, and no obvious pathologies or instrumental data-quality problems were found. In particular, no signatures of multiple densely clustered particles, which could lead to poor track reconstruction, were found around the candidate tracks. Candidate tracks are well isolated both at the track level and at the calorimeter cluster level, as required by the signal selection. For each of the four SR-Mu category events and the one SR-Trk event that has a matched muon, the track momentum when reconstructed as a muon using both the inner detector and the muon spectrometer was compared with the nominal momentum obtained using only the inner detector. Allowing for the momentum resolution, the two reconstructed momentum values are compatible with each other for all five events.

The event topology of these excess events typically contains a counterbalancing jet, opposite in ϕ to the candidate signal track. Such a ‘back-to-back’ topology is typical in the CR-kin region at high- p_T values above several hundred GeV. One event lacks a counterbalancing jet, but a balancing amount of E_T^{miss} is present. Overall, no obvious pathologies or instrumental issues were found.

¹⁰ By convention, the Z significance of a p_0 -value is defined as $Z \equiv \Phi^{-1}(1 - p_0)$ where Φ^{-1} is the inverse of the cumulative distribution for a unit Gaussian function.

The dE/dx values of the excess candidate tracks span 2.42–3.72 MeV g⁻¹cm², and they map to particle speeds of $\beta = 0.62$ – 0.52 according to the dE/dx – $\beta\gamma$ relationship in Eq. (1), which assumes the given dE/dx value is the MPV. This range of β should result in a significantly longer time-of-flight through the ATLAS detector than for $\beta = 1$ SM particles, and this is used as a consistency test. As in the searches for stable charged particles [37], two independent β values were examined: one is the β value measured by the muon spectrometer (β_{MS}) when fitting muon tracks with β as a free parameter; the other is the β value obtained from calorimeter cell hits associated with the candidate track (β_{calo}). In the latter case, β is derived from the average ToF weighted by the timing resolution of the cells, which depends on the size of the energy deposit. The probability distributions of these two β variables for the $\beta = 1$ SM particles are modelled from the CR-kin dataset. Both β probability distributions exhibit non-Gaussianity with approximately symmetric side-lobes. The FWHM of the peak divided by 2.35 for β_{MS} is 0.045, while it is 0.075 and 0.050 for β_{calo} in the CR-kin-Mu and CR-kin-Trk samples, respectively. The efficiency of obtaining a β_{MS} value from the CR-kin-Mu sample is 95%, while that of obtaining a β_{calo} value is 85% from the CR-kin-Mu sample and 95% for the CR-kin-Trk sample. Using MC signal samples, where particles have low β , it was found that the β values from the ToF observables and the β value deduced from the pixel dE/dx measurement agree within 6%.

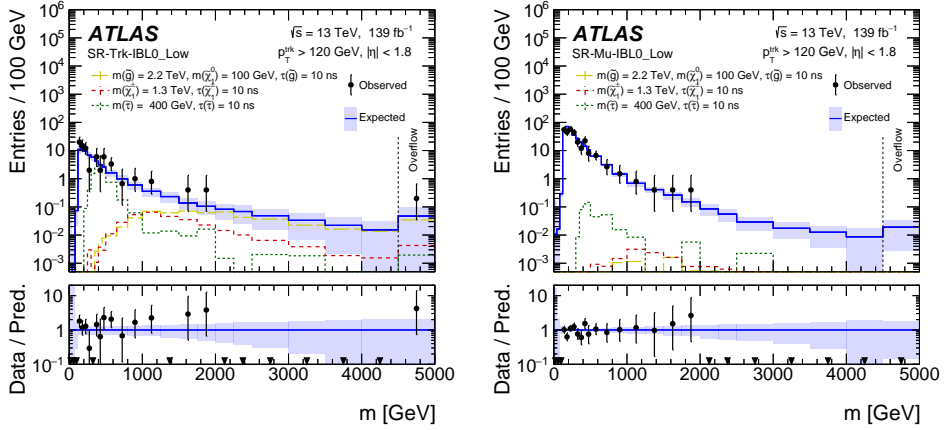
The β values measured by ToF of the seven candidate tracks were all found to be compatible with $\beta = 1$, with all the β_{MS} and β_{calo} values being well within the 95% confidence interval of the distribution. Therefore, the low particle speed suggested by the pixel dE/dx measurement for the seven candidate tracks in the excess was not confirmed by these ToF observables.

The results of this study are interpreted for the benchmark signal models considered, and the 95% CL upper limit on the cross-section is extracted using the CL_s prescription [42] for each signal mass and lifetime hypothesis, using a simultaneous fit of the six exclusive signal-region bins listed in Table 2. These six signal-region bins are exclusive at the track level. The cross-section limit is derived by combining the six track-based regions as independent observations, with the exception of correlations through systematic uncertainties. According to simulation, the probability of having multiple tracks from the same event entering different bins is small and its impact is insignificant compared to the experimental uncertainty. The mass spectra of these exclusive bins are presented in Figure 17. When both the ‘short’ and ‘long’ lifetime windows are available, the window which provides the better expected limit is selected.

To more accurately probe the sensitivity of the analysis to LLP lifetimes other than those used in the generation of the signal samples, the same samples are reinterpreted for intermediate lifetime values by reweighting the LLP particle decay spectra. Intermediate lifetimes are modelled by reweighting the closest longer-lifetime sample to shorter lifetimes, except for $\tau > 30$ ns. The choice of target lifetimes for $\tau > 30$ ns is limited by the reduced size of the reweighted sample.

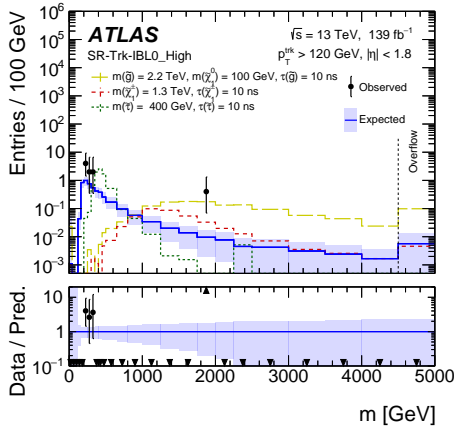
Figure 18 show the mass limits for gluino R -hadron pair production for both the $m(\tilde{\chi}_1^0) = 100$ GeV and $\Delta m(\tilde{g}, \tilde{\chi}_1^0) = 30$ GeV cases. The highest observed lower limit on the mass is 2.27 TeV (2.06 TeV) and is obtained at $\tau = 20$ ns ($\tau = 30$ ns) for $m(\tilde{\chi}_1^0) = 100$ GeV ($\Delta m(\tilde{g}, \tilde{\chi}_1^0) = 30$ GeV), while the corresponding expected limit is 2.35 TeV (2.14 TeV). Similarly, the limits in the chargino and stau scenarios are shown in Figure 19(a) and Figure 19(b), respectively. The highest observed mass limit of 1.07 TeV is obtained at $\tau = 30$ ns for the chargino production model, while the corresponding expected limit is 1.19 TeV. For the stau case, the mass range 220–360 GeV is excluded for $\tau = 10$ ns, while the corresponding expected exclusion is 200–470 GeV. Masses below the excluded mass range are not excluded by this search because of acceptance losses mainly due to the p_{T} selection. These results provide the most stringent limits on

these scenarios in the given lifetime range to date. Due to the observation of more events than expected at high masses, the observed limits are weaker than the expected limits for LLPs with mass $m \gtrsim 1$ TeV.



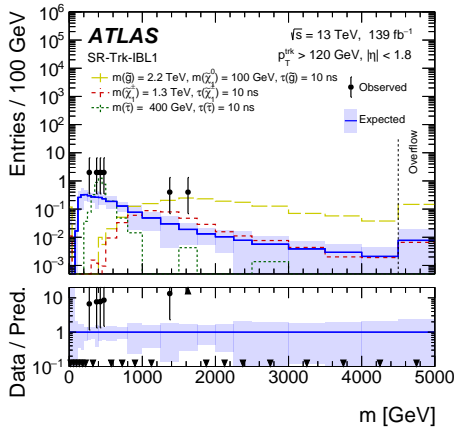
(a) SR-Trk_IBL0_Low

(b) SR-Mu_IBL0_Low



(c) SR-Trk_IBL0_High

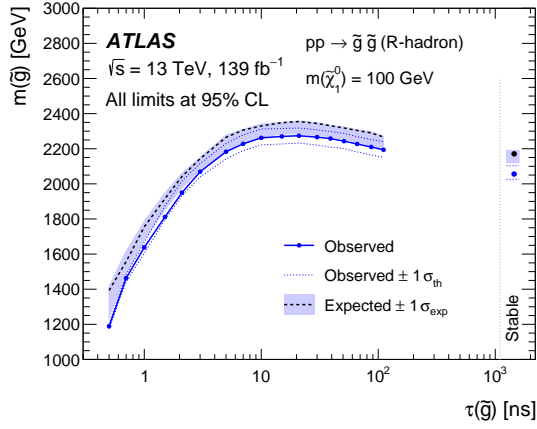
(d) SR-Mu_IBL0_High



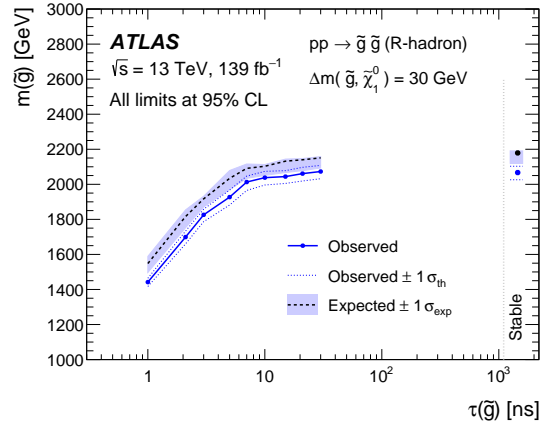
(e) SR-Trk_IBL1

(f) SR-Mu_IBL1

Figure 17: The observed mass distribution in the Trk and Mu signal-region bins. The band on the expected background indicates the total uncertainty of the estimation. Several representative signal models are overlaid. Events outside the shown range are accumulated in the rightmost bin indicated as ‘Overflow’. Downward triangle markers at the bottom of the panels indicate that no events are observed in the corresponding mass bin, while upward triangle markers in the lower panels indicate that the observed data is beyond the range.

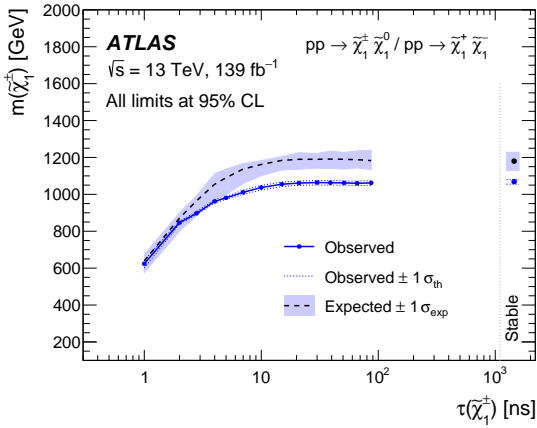


(a) R -hadron, $m(\tilde{\chi}_1^0) = 100$ GeV

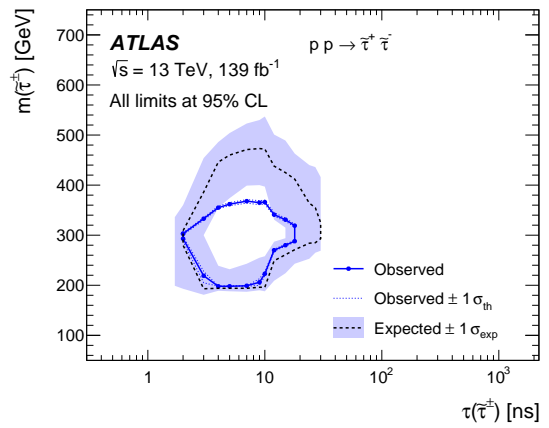


(b) R -hadron, $\Delta m(\tilde{g}, \tilde{\chi}_1^0) = 30$ GeV

Figure 18: Lower limits on the gluino mass, from gluino R -hadron pair production, as a function of gluino lifetime for two neutralino mass assumptions of (a) $m(\tilde{\chi}_1^0) = 100$ GeV and (b) $\Delta m(\tilde{g}, \tilde{\chi}_1^0) = 30$ GeV. The upper $1\sigma_{\text{exp}}$ expected bound is very close to the expected limit for some lifetime values due to the expected background getting very close to 0 events.



(a) Chargino



(b) Stau

Figure 19: (a) Lower limits on the chargino mass as a function of lifetime, and (b) the contours around the excluded mass–lifetime region for stau pair production.

10 Conclusion

A search is performed for heavy charged LLPs, with lifetimes sufficient ($\tau \gtrsim 1$ ns) to reconstruct inner-detector tracks, produced at the LHC in 139 fb^{-1} of pp collisions at $\sqrt{s} = 13$ TeV. The identification of LLPs is based on anomalously high specific ionisation measured by the ATLAS pixel detector for isolated high-momentum tracks in events with high $E_{\text{T}}^{\text{miss}}$. The considerable increase in sensitivity compared to previous ATLAS searches is not only due to the higher integrated luminosity, but also to several significant improvements in the analysis strategy. The most noticeable are the use of a higher dE/dx threshold, the separate treatment of the tracks with an IBL overflow flag and the use of a data-driven dE/dx -response template instead of a simulated one, as well as a more optimised definition of sub-regions in the signal region for exclusion interpretations. Evaluation of systematic uncertainties was also improved through the adoption of a high-momentum validation region and the implementation of a pseudo signal region to test the background generation method.

Observed yields and distributions agree with the SM background expectations, with the exception of an accumulation of events in the high- dE/dx and high-mass range. The local (global) significance of this excess is 3.6σ (3.3σ) in a sub-range of the signal region optimised for a target mass hypothesis of 1.4 TeV. The events in the excess region were examined in detail. Although no obvious pathologies were identified in the measurement of these events, the time-of-flight measurements in outer detector subsystems clearly indicate that none of the candidate tracks are from charged particles moving significantly slower than the speed of light.

Maximum sensitivity is reached for LLPs with lifetimes of around 10–30 ns. Masses smaller than 2.27 TeV are excluded at the 95% confidence level for gluino R -hadrons with a lifetime of 20 ns and $m(\tilde{\chi}_1^0) = 100$ GeV. The mass limit for compressed-scenario R -hadrons, with $\Delta m(\tilde{g}, \tilde{\chi}_1^0) = 30$ GeV and a lifetime of 30 ns, is 2.06 TeV. Masses below 1.07 TeV for charginos and in the range 220–360 GeV for staus are excluded for lifetimes of 30 ns and 10 ns, respectively. The limits in the mass–lifetime plane are the most stringent to date and provide further constraints on the R -hadron, chargino and stau production models considered.

Acknowledgements

We thank CERN for the very successful operation of the LHC, as well as the support staff from our institutions without whom ATLAS could not be operated efficiently.

We acknowledge the support of ANPCyT, Argentina; YerPhI, Armenia; ARC, Australia; BMWFW and FWF, Austria; ANAS, Azerbaijan; CNPq and FAPESP, Brazil; NSERC, NRC and CFI, Canada; CERN; ANID, Chile; CAS, MOST and NSFC, China; Minciencias, Colombia; MEYS CR, Czech Republic; DNRF and DNSRC, Denmark; IN2P3-CNRS and CEA-DRF/IRFU, France; SRNSFG, Georgia; BMBF, HGF and MPG, Germany; GSRI, Greece; RGC and Hong Kong SAR, China; ISF and Benoziyo Center, Israel; INFN, Italy; MEXT and JSPS, Japan; CNRST, Morocco; NWO, Netherlands; RCN, Norway; MEiN, Poland; FCT, Portugal; MNE/IFA, Romania; MESTD, Serbia; MSSR, Slovakia; ARRS and MIZŠ, Slovenia; DSI/NRF, South Africa; MICINN, Spain; SRC and Wallenberg Foundation, Sweden; SERI, SNSF and Cantons of Bern and Geneva, Switzerland; MOST, Taiwan; TENMAK, Türkiye; STFC, United Kingdom; DOE and NSF, United States of America. In addition, individual groups and members have received support from BCKDF, CANARIE, Compute Canada and CRC, Canada; PRIMUS 21/SCI/017 and UNCE SCI/013,

Czech Republic; COST, ERC, ERDF, Horizon 2020 and Marie Skłodowska-Curie Actions, European Union; Investissements d’Avenir Labex, Investissements d’Avenir IDEX and ANR, France; DFG and AvH Foundation, Germany; Herakleitos, Thales and Aristeia programmes co-financed by EU-ESF and the Greek NSRF, Greece; BSF-NSF and MINERVA, Israel; Norwegian Financial Mechanism 2014-2021, Norway; NCN and NAWA, Poland; La Caixa Banking Foundation, CERCA Programme Generalitat de Catalunya and PROMETEO and GenT Programmes Generalitat Valenciana, Spain; Göran Gustafssons Stiftelse, Sweden; The Royal Society and Leverhulme Trust, United Kingdom.

The crucial computing support from all WLCG partners is acknowledged gratefully, in particular from CERN, the ATLAS Tier-1 facilities at TRIUMF (Canada), NDGF (Denmark, Norway, Sweden), CC-IN2P3 (France), KIT/GridKA (Germany), INFN-CNAF (Italy), NL-T1 (Netherlands), PIC (Spain), ASGC (Taiwan), RAL (UK) and BNL (USA), the Tier-2 facilities worldwide and large non-WLCG resource providers. Major contributors of computing resources are listed in Ref. [84].

References

- [1] Y. Golfand and E. Likhtman, *Extension of the Algebra of Poincare Group Generators and Violation of P Invariance*, JETP Lett. **13** (1971) 323, [Pisma Zh. Eksp. Teor. Fiz. **13** (1971) 452].
- [2] D. Volkov and V. Akulov, *Is the neutrino a goldstone particle?*, Phys. Lett. B **46** (1973) 109.
- [3] J. Wess and B. Zumino, *Supergauge transformations in four dimensions*, Nucl. Phys. B **70** (1974) 39.
- [4] A. Salam and J. Strathdee, *Super-symmetry and non-Abelian gauges*, Phys. Lett. B **51** (1974) 353.
- [5] J. Wess and B. Zumino, *Supergauge invariant extension of quantum electrodynamics*, Nucl. Phys. B **78** (1974) 1.
- [6] S. Ferrara and B. Zumino, *Supergauge invariant Yang-Mills theories*, Nucl. Phys. B **79** (1974) 413.
- [7] P. Fayet, *Supersymmetry and weak, electromagnetic and strong interactions*, Phys. Lett. B **64** (1976) 159.
- [8] G. Giudice and A. Romanino, *Split supersymmetry*, Nucl. Phys. B **699** (2004) 65, arXiv: [hep-ph/0406088](https://arxiv.org/abs/hep-ph/0406088), Erratum: Nucl. Phys. B **706** (2005) 65.
- [9] N. Arkani-Hamed and S. Dimopoulos, *Supersymmetric unification without low energy supersymmetry and signatures for fine-tuning at the LHC*, JHEP **06** (2005) 073, arXiv: [hep-th/0405159](https://arxiv.org/abs/hep-th/0405159).
- [10] M. Fairbairn et al., *Stable massive particles at colliders*, Phys. Rep. **438** (2007) 1.
- [11] G. F. Giudice, M. A. Luty, H. Murayama and R. Rattazzi, *Gaugino mass without singlets*, JHEP **12** (1998) 027, arXiv: [hep-ph/9810442](https://arxiv.org/abs/hep-ph/9810442).
- [12] L. Randall and R. Sundrum, *Out of this world supersymmetry breaking*, Nucl. Phys. B **557** (1999) 79, arXiv: [hep-th/9810155](https://arxiv.org/abs/hep-th/9810155).
- [13] J. Alwall, M.-P. Le, M. Lisanti and J. G. Wacker, *Searching for directly decaying gluinos at the Tevatron*, Phys. Lett. B **666** (2008) 34, arXiv: [0803.0019 \[hep-ph\]](https://arxiv.org/abs/0803.0019).

- [14] J. Alwall, P. Schuster and N. Toro,
Simplified models for a first characterization of new physics at the LHC,
Phys. Rev. D **79** (2009) 075020, arXiv: [0810.3921 \[hep-ph\]](#).
- [15] D. Alves et al., *Simplified models for LHC new physics searches*, *J. Phys. G* **39** (2012) 105005,
arXiv: [1105.2838 \[hep-ph\]](#).
- [16] ATLAS Collaboration, *Search for long-lived, massive particles in events with displaced vertices and missing transverse momentum in $\sqrt{s} = 13$ TeV pp collisions with the ATLAS detector*,
Phys. Rev. D **97** (2018) 052012, arXiv: [1710.04901 \[hep-ex\]](#).
- [17] CMS Collaboration, *Search for long-lived particles decaying to jets with displaced vertices in proton–proton collisions at $\sqrt{s} = 13$ TeV*, *Phys. Rev. D* **104** (2021) 052011,
arXiv: [2104.13474 \[hep-ex\]](#).
- [18] CMS Collaboration,
Search for long-lived particles using displaced jets in proton–proton collisions at $\sqrt{s} = 13$ TeV,
Phys. Rev. D **104** (2020) 012015, arXiv: [2012.01581 \[hep-ex\]](#).
- [19] ATLAS Collaboration, *Search for heavy charged long-lived particles in the ATLAS detector in 36.1 fb^{-1} of proton–proton collision data at $\sqrt{s} = 13$ TeV*, *Phys. Rev. D* **99** (2019) 092007,
arXiv: [1902.01636 \[hep-ex\]](#).
- [20] ATLAS Collaboration, *Search for heavy long-lived charged R -hadrons with the ATLAS detector in 3.2 fb^{-1} of proton–proton collision data at $\sqrt{s} = 13$ TeV*, *Phys. Lett. B* **760** (2016) 647,
arXiv: [1606.05129 \[hep-ex\]](#).
- [21] CMS Collaboration,
Search for long-lived charged particles in proton–proton collisions at $\sqrt{s} = 13$ TeV,
Phys. Rev. D **94** (2016) 112004, arXiv: [1609.08382 \[hep-ex\]](#).
- [22] ATLAS Collaboration, *Searches for new phenomena in events with two leptons, jets, and missing transverse momentum in 139 fb^{-1} of $\sqrt{s} = 13$ TeV pp collisions with the ATLAS detector*, (2022),
arXiv: [2204.13072 \[hep-ex\]](#).
- [23] CMS Collaboration, *Search for decays of stopped exotic long-lived particles produced in proton–proton collisions at $\sqrt{s} = 13$ TeV*, *JHEP* **05** (2018) 127, arXiv: [1801.00359 \[hep-ex\]](#).
- [24] H. Fukuda, N. Nagata, H. Otono and S. Shirai,
Higgsino dark matter or not: Role of disappearing track searches at the LHC and future colliders,
Phys. Lett. B **781** (2018) 306.
- [25] ATLAS Collaboration, *Search for long-lived charginos based on a disappearing-track signature using 136 fb^{-1} of pp collisions at $\sqrt{s} = 13$ TeV with the ATLAS detector*,
Eur. Phys. J. C **82** (2022) 606, arXiv: [2201.02472 \[hep-ex\]](#).
- [26] ATLAS Collaboration, *Search for long-lived charginos based on a disappearing-track signature in pp collisions at $\sqrt{s} = 13$ TeV with the ATLAS detector*, *JHEP* **06** (2018) 022,
arXiv: [1712.02118 \[hep-ex\]](#).
- [27] CMS Collaboration,
Searches for physics beyond the standard model with the M_{T2} variable in hadronic final states with and without disappearing tracks in proton–proton collisions at $\sqrt{s} = 13$ TeV,
Eur. Phys. J. C **80** (2020) 3, arXiv: [1909.03460 \[hep-ex\]](#).
- [28] CMS Collaboration, *Search for disappearing tracks in proton–proton collisions at $\sqrt{s} = 13$ TeV*,
Phys. Lett. B **806** (2020) 135502, arXiv: [2004.05153 \[hep-ex\]](#).

- [29] CMS Collaboration, *Search for disappearing tracks as a signature of new long-lived particles in proton–proton collisions at $\sqrt{s} = 13$ TeV*, *JHEP* **08** (2018) 016, arXiv: 1804.07321 [hep-ex].
- [30] ATLAS Collaboration, *Search for displaced leptons in $\sqrt{s} = 13$ TeV pp collisions with the ATLAS detector*, *Phys. Rev. Lett.* **127** (2020) 051802, arXiv: 2011.07812 [hep-ex].
- [31] ATLAS Collaboration, *ATLAS Pixel Detector: Technical Design Report*, ATLAS-TDR-11; CERN-LHCC-98-013, 1998, URL: <https://cds.cern.ch/record/381263>.
- [32] ATLAS Collaboration, *ATLAS Insertable B-Layer: Technical Design Report*, ATLAS-TDR-19; CERN-LHCC-2010-013, 2010, URL: <https://cds.cern.ch/record/1291633>, Addendum: ATLAS-TDR-19-ADD-1; CERN-LHCC-2012-009, 2012, URL: <https://cds.cern.ch/record/1451888>.
- [33] B. Abbott et al., *Production and integration of the ATLAS Insertable B-Layer*, *JINST* **13** (2018) T05008, arXiv: 1803.00844 [physics.ins-det].
- [34] ATLAS Collaboration, *The ATLAS Experiment at the CERN Large Hadron Collider*, *JINST* **3** (2008) S08003.
- [35] ATLAS Collaboration, *ATLAS Liquid Argon Calorimeter: Technical Design Report*, ATLAS-TDR-2; CERN-LHCC-96-041, 1996, URL: <https://cds.cern.ch/record/331061>.
- [36] ATLAS Collaboration, *ATLAS Tile Calorimeter: Technical Design Report*, ATLAS-TDR-3; CERN-LHCC-96-042, 1996, URL: <https://cds.cern.ch/record/331062>.
- [37] ATLAS Collaboration, *Search for heavy long-lived charged particles with the ATLAS detector in pp collisions at $\sqrt{s} = 7$ TeV*, *Phys. Lett. B* **703** (2011) 428, arXiv: 1106.4495 [hep-ex].
- [38] ATLAS Collaboration, *Search for metastable heavy charged particles with large ionisation energy loss in pp collisions at $\sqrt{s} = 8$ TeV using the ATLAS experiment*, *Eur. Phys. J. C* **75** (2015) 407, arXiv: 1506.05332 [hep-ex].
- [39] ATLAS Collaboration, *Search for metastable heavy charged particles with large ionization energy loss in pp collisions at $\sqrt{s} = 13$ TeV using the ATLAS experiment*, *Phys. Rev. D* **93** (2016) 112015, arXiv: 1604.04520 [hep-ex].
- [40] ATLAS Collaboration, *Search for heavy charged long-lived particles in proton–proton collisions at $\sqrt{s} = 13$ TeV using an ionisation measurement with the ATLAS detector*, *Phys. Lett. B* **788** (2019) 96, arXiv: 1808.04095 [hep-ex].
- [41] CMS Collaboration, *Searches for long-lived charged particles in pp collisions at $\sqrt{s} = 7$ and 8 TeV*, *JHEP* **07** (2013) 122, arXiv: 1305.0491 [hep-ex].
- [42] A. L. Read, *Presentation of search results: the CL_S technique*, *J. Phys. G* **28** (2002) 2693.
- [43] ATLAS Collaboration, *Performance of the ATLAS trigger system in 2015*, *Eur. Phys. J. C* **77** (2017) 317, arXiv: 1611.09661 [hep-ex].
- [44] ATLAS Collaboration, *The ATLAS Collaboration Software and Firmware*, ATL-SOFT-PUB-2021-001, 2021, URL: <https://cds.cern.ch/record/2767187>.
- [45] ATLAS Collaboration, *Performance of the ATLAS Transition Radiation Tracker in Run 1 of the LHC: tracker properties*, *JINST* **12** (2017) P05002, arXiv: 1702.06473 [hep-ex].
- [46] ATLAS Collaboration, *Operation and performance of the ATLAS semiconductor tracker*, *JINST* **9** (2014) P08009, arXiv: 1404.7473 [hep-ex].

- [47] B. Aubert et al., *The BABAR Detector*, *Nucl. Instrum. Meth. A* **479** (2002) 1, arXiv: [hep-ex/0105044v1](https://arxiv.org/abs/hep-ex/0105044v1).
- [48] ATLAS Collaboration, *A neural network clustering algorithm for the ATLAS silicon pixel detector*, *JINST* **9** (2014) P09009, arXiv: [1406.7690](https://arxiv.org/abs/1406.7690) [[hep-ex](#)].
- [49] Particle Data Group et al., *Review of Particle Physics, section 34.2.8*, *Progress of Theoretical and Experimental Physics* **2020** (2020), 083C01, ISSN: 2050-3911, eprint: <https://academic.oup.com/ptep/article-pdf/2020/8/083C01/34673722/ptaa104.pdf>, URL: <https://doi.org/10.1093/ptep/ptaa104>.
- [50] ATLAS Collaboration, *Performance of the missing transverse momentum triggers for the ATLAS detector during Run-2 data taking*, *JHEP* **08** (2020) 080, arXiv: [2005.09554](https://arxiv.org/abs/2005.09554) [[hep-ex](#)].
- [51] ATLAS Collaboration, *Alignment of the ATLAS Inner Detector and its Performance in 2012*, ATLAS-CONF-2014-047, 2014, URL: <https://cds.cern.ch/record/1741021>.
- [52] ATLAS Collaboration, *ATLAS data quality operations and performance for 2015–2018 data-taking*, *JINST* **15** (2020) P04003, arXiv: [1911.04632](https://arxiv.org/abs/1911.04632) [[physics.ins-det](#)].
- [53] T. Sjöstrand et al., *An introduction to PYTHIA 8.2*, *Comput. Phys. Commun.* **191** (2015) 159, arXiv: [1410.3012](https://arxiv.org/abs/1410.3012) [[hep-ph](#)].
- [54] ATLAS Collaboration, *ATLAS Pythia 8 tunes to 7 TeV data*, ATL-PHYS-PUB-2014-021, 2014, URL: <https://cds.cern.ch/record/1966419>.
- [55] D. J. Lange, *The EvtGen particle decay simulation package*, *Nucl. Instrum. Meth. A* **462** (2001) 152.
- [56] S. Catani, F. Krauss, B. R. Webber and R. Kuhn, *QCD Matrix Elements + Parton Showers*, *JHEP* **11** (2001) 063, arXiv: [hep-ph/0109231](https://arxiv.org/abs/hep-ph/0109231).
- [57] S. Höche, F. Krauss, S. Schumann and F. Siegert, *QCD matrix elements and truncated showers*, *JHEP* **05** (2009) 053, arXiv: [0903.1219](https://arxiv.org/abs/0903.1219) [[hep-ph](#)].
- [58] ATLAS Collaboration, *Generation and Simulation of R-Hadrons in the ATLAS Experiment*, ATL-PHYS-PUB-2019-019, 2019, URL: <https://cds.cern.ch/record/2676309>.
- [59] C. Borschensky et al., *Squark and gluino production cross sections in pp collisions at $\sqrt{s} = 13, 14, 33$ and 100 TeV*, *Eur. Phys. J. C* **74** (2014) 3174, arXiv: [1407.5066](https://arxiv.org/abs/1407.5066) [[hep-ph](#)].
- [60] W. Beenakker, R. Höpker, M. Spira and P. Zerwas, *Squark and gluino production at hadron colliders*, *Nucl. Phys. B* **492** (1997) 51, arXiv: [hep-ph/9610490](https://arxiv.org/abs/hep-ph/9610490).
- [61] W. Beenakker et al., *Production of Charginos, Neutralinos, and Stopped Squarks at Hadron Colliders*, *Phys. Rev. Lett.* **83** (1999) 3780, arXiv: [hep-ph/9906298](https://arxiv.org/abs/hep-ph/9906298), Erratum: *Phys. Rev. Lett.* **100** (2008) 029901.
- [62] J. Debove, B. Fuks and M. Klasen, *Threshold resummation for gaugino pair production at hadron colliders*, *Nucl. Phys. B* **842** (2011) 51, arXiv: [1005.2909](https://arxiv.org/abs/1005.2909) [[hep-ph](#)].
- [63] B. Fuks, M. Klasen, D. R. Lamprea and M. Rothering, *Gaugino production in proton-proton collisions at a center-of-mass energy of 8 TeV*, *JHEP* **10** (2012) 081, arXiv: [1207.2159](https://arxiv.org/abs/1207.2159) [[hep-ph](#)].

- [64] B. Fuks, M. Klasen, D. R. Lamprea and M. Rothering, *Precision predictions for electroweak superpartner production at hadron colliders with RESUMMINO*, *Eur. Phys. J. C* **73** (2013) 2480, arXiv: [1304.0790 \[hep-ph\]](#).
- [65] J. Fiaschi and M. Klasen, *Neutralino-chargino pair production at NLO+NLL with resummation-improved parton density functions for LHC Run II*, *Phys. Rev. D* **98** (2018) 055014, arXiv: [1805.11322 \[hep-ph\]](#).
- [66] ATLAS Collaboration, *The Pythia 8 A3 tune description of ATLAS minimum bias and inelastic measurements incorporating the Donnachie–Landshoff diffractive model*, ATL-PHYS-PUB-2016-017, 2016, URL: <https://cds.cern.ch/record/2206965>.
- [67] ATLAS Collaboration, *The ATLAS Simulation Infrastructure*, *Eur. Phys. J. C* **70** (2010) 823, arXiv: [1005.4568 \[physics.ins-det\]](#).
- [68] S. Agostinelli et al., *GEANT4 – a simulation toolkit*, *Nucl. Instrum. Meth. A* **506** (2003) 250.
- [69] F. Wang, S. Dong, B. Nachman, M. Garcia-Sciveres and Q. Zeng, *The impact of incorporating shell-corrections to energy loss in silicon*, *Nucl. Instrum. Meth. A* **899** (2018) 1.
- [70] M. Oreglia, *A Study of the Reactions $\psi' \rightarrow \gamma\gamma\psi$* , SLAC-236, PhD thesis: Stanford University, 1980.
- [71] T. Skwarnicki, *A study of the radiative CASCADE transitions between the Upsilon-Prime and Upsilon resonances*, DESY-F31-86-02, PhD thesis: Cracow Institut of Nuclear Physics, 1986.
- [72] M. Cacciari, G. P. Salam and G. Soyez, *The anti- k_t jet clustering algorithm*, *JHEP* **04** (2008) 063.
- [73] M. Cacciari, G. P. Salam and G. Soyez, *FastJet user manual*, *Eur. Phys. J. C* **72** (2012) 1896, arXiv: [1111.6097 \[hep-ph\]](#).
- [74] ATLAS Collaboration, *Performance of algorithms that reconstruct missing transverse momentum in $\sqrt{s} = 8$ TeV proton–proton collisions in the ATLAS detector*, *Eur. Phys. J. C* **77** (2017) 241, arXiv: [1609.09324 \[hep-ex\]](#).
- [75] ATLAS Collaboration, *Selection of jets produced in 13 TeV proton–proton collisions with the ATLAS detector*, ATLAS-CONF-2015-029, 2015, URL: <https://cds.cern.ch/record/2037702>.
- [76] ATLAS Collaboration, *Performance of the ATLAS track reconstruction algorithms in dense environments in LHC Run 2*, *Eur. Phys. J. C* **77** (2017) 673, arXiv: [1704.07983 \[hep-ex\]](#).
- [77] ATLAS Collaboration, *Muon reconstruction and identification efficiency in ATLAS using the full Run 2 pp collision data set at $\sqrt{s} = 13$ TeV*, *Eur. Phys. J. C* **81** (2021) 578, arXiv: [2012.00578 \[hep-ex\]](#).
- [78] ATLAS Collaboration, *Muon reconstruction performance of the ATLAS detector in proton–proton collision data at $\sqrt{s} = 13$ TeV*, *Eur. Phys. J. C* **76** (2016) 292, arXiv: [1603.05598 \[hep-ex\]](#).
- [79] ATLAS Collaboration, *Luminosity determination in pp collisions at $\sqrt{s} = 13$ TeV using the ATLAS detector at the LHC*, ATLAS-CONF-2019-021, 2019, URL: <https://cds.cern.ch/record/2677054>.
- [80] L. Heinrich, M. Feickert and G. Stark, *pyhf: v0.6.1*, version 0.6.1, URL: <https://github.com/scikit-hep/pyhf>.

- [81] G. Cowan, K. Cranmer, E. Gross and O. Vitells,
Asymptotic formulae for likelihood-based tests of new physics,
[The European Physical Journal C 71 \(2011\)](#), ISSN: 1434-6052,
URL: <http://dx.doi.org/10.1140/epjc/s10052-011-1554-0>.
- [82] E. Gross and O. Vitells, *Trial factors for the look elsewhere effect in high energy physics*,
[The European Physical Journal C 7 \(2010\) 525](#), arXiv: [1005.1891 \[physics.data-an\]](#).
- [83] T. C. C. The ATLAS Collaboration and T. L. H. C. Group,
Procedure for the LHC Higgs boson search combination in summer 2011,
ATL-PHYS-PUB-2011-011, 2011, URL: <https://cds.cern.ch/record/1375842>.
- [84] ATLAS Collaboration, *ATLAS Computing Acknowledgements*, ATL-SOFT-PUB-2021-003, 2021,
URL: <https://cds.cern.ch/record/2776662>.

The ATLAS Collaboration

G. Aad ¹⁰⁰, B. Abbott ¹¹⁸, D.C. Abbott ¹⁰¹, A. Abed Abud ³⁵, K. Abeling ⁵⁴,
D.K. Abhayasinghe ⁹³, S.H. Abidi ²⁸, A. Aboulhorma ^{34e}, H. Abramowicz ¹⁴⁹, H. Abreu ¹⁴⁸,
Y. Abulaiti ¹¹⁵, A.C. Abusleme Hoffman ^{135a}, B.S. Acharya ^{67a,67b,o}, B. Achkar ⁵⁴, L. Adam ⁹⁸,
C. Adam Bourdarios ⁴, L. Adamczyk ^{83a}, L. Adamek ¹⁵³, S.V. Addepalli ²⁵, J. Adelman ¹¹³,
A. Adiguzel ^{11c,z}, S. Adorni ⁵⁵, T. Adye ¹³², A.A. Affolder ¹³⁴, Y. Afik ³⁵, C. Agapopoulou ⁶⁵,
M.N. Agaras ¹³, J. Agarwala ^{71a,71b}, A. Aggarwal ¹¹¹, C. Agheorghiesei ^{26c},
J.A. Aguilar-Saavedra ^{128f,128a,y}, A. Ahmad ³⁵, F. Ahmadov ^{37,w}, W.S. Ahmed ¹⁰², X. Ai ⁴⁷,
G. Aielli ^{74a,74b}, I. Aizenberg ¹⁶⁶, S. Akatsuka ⁸⁵, M. Akbiyik ⁹⁸, T.P.A. Åkesson ⁹⁶,
A.V. Akimov ³⁶, K. Al Khoury ⁴⁰, G.L. Alberghi ^{22b}, J. Albert ¹⁶², P. Albicocco ⁵²,
M.J. Alconada Verzini ⁸⁸, S. Alderweireldt ⁵¹, M. Aleksa ³⁵, I.N. Aleksandrov ³⁷, C. Alexa ^{26b},
T. Alexopoulos ⁹, A. Alfonsi ¹¹², F. Alfonsi ^{22b}, M. Alhroob ¹¹⁸, B. Ali ¹³⁰, S. Ali ¹⁴⁶,
M. Aliev ³⁶, G. Alimonti ^{69a}, C. Allaire ³⁵, B.M.M. Allbrooke ¹⁴⁴, P.P. Allport ²⁰,
A. Aloisio ^{70a,70b}, F. Alonso ⁸⁸, C. Alpigiani ¹³⁶, E. Alunno Camelia ^{74a,74b}, M. Alvarez Estevez ⁹⁷,
M.G. Alvigi ^{70a,70b}, Y. Amaral Coutinho ^{80b}, A. Ambler ¹⁰², L. Ambroz ¹²⁴, C. Amelung ³⁵,
D. Amidei ¹⁰⁴, S.P. Amor Dos Santos ^{128a}, S. Amoroso ⁴⁷, K.R. Amos ¹⁶⁰, C.S. Amrouche ⁵⁵,
V. Ananiev ¹²³, C. Anastopoulos ¹³⁷, N. Andari ¹³³, T. Andeen ¹⁰, J.K. Anders ¹⁹,
S.Y. Andrean ^{46a,46b}, A. Andreazza ^{69a,69b}, S. Angelidakis ⁸, A. Angerami ⁴⁰, A.V. Anisenkov ³⁶,
A. Annovi ^{72a}, C. Antel ⁵⁵, M.T. Anthony ¹³⁷, E. Antipov ¹¹⁹, M. Antonelli ⁵²,
D.J.A. Antrim ^{17a}, F. Anulli ^{73a}, M. Aoki ⁸¹, J.A. Aparisi Pozo ¹⁶⁰, M.A. Aparo ¹⁴⁴,
L. Aperio Bella ⁴⁷, N. Aranzabal ³⁵, V. Araujo Ferraz ^{80a}, C. Arcangeletti ⁵², A.T.H. Arce ⁵⁰,
E. Arena ⁹⁰, J-F. Arguin ¹⁰⁶, S. Argyropoulos ⁵³, J.-H. Arling ⁴⁷, A.J. Armbruster ³⁵,
A. Armstrong ¹⁵⁷, O. Arnaez ¹⁵³, H. Arnold ³⁵, Z.P. Arrubarrena Tame ¹⁰⁷, G. Artoni ^{73a,73b},
H. Asada ¹⁰⁹, K. Asai ¹¹⁶, S. Asai ¹⁵¹, N.A. Asbah ⁶⁰, E.M. Asimakopoulou ¹⁵⁸, L. Asquith ¹⁴⁴,
J. Assahsah ^{34d}, K. Assamagan ²⁸, R. Astalos ^{27a}, R.J. Atkin ^{32a}, M. Atkinson ¹⁵⁹, N.B. Atlay ¹⁸,
H. Atmani ^{61b}, P.A. Atlasiddha ¹⁰⁴, K. Augsten ¹³⁰, S. Auricchio ^{70a,70b}, V.A. Austrup ¹⁶⁸,
G. Avner ¹⁴⁸, G. Avolio ³⁵, M.K. Ayoub ^{14c}, G. Azuelos ^{106,ah}, D. Babal ^{27a}, H. Bachacou ¹³³,
K. Bachas ¹⁵⁰, A. Bachi ³³, F. Backman ^{46a,46b}, A. Badea ⁶⁰, P. Bagnaia ^{73a,73b}, M. Bahmani ¹⁸,
A.J. Bailey ¹⁶⁰, V.R. Bailey ¹⁵⁹, J.T. Baines ¹³², C. Bakalis ⁹, O.K. Baker ¹⁶⁹, P.J. Bakker ¹¹²,
E. Bakos ¹⁵, D. Bakshi Gupta ⁷, S. Balaji ¹⁴⁵, R. Balasubramanian ¹¹², E.M. Baldin ³⁶,
P. Balek ¹³¹, E. Ballabene ^{69a,69b}, F. Balli ¹³³, L.M. Baltes ^{62a}, W.K. Balunas ¹²⁴, J. Balz ⁹⁸,
E. Banas ⁸⁴, M. Bandieramonte ¹²⁷, A. Bandyopadhyay ²³, S. Bansal ²³, L. Barak ¹⁴⁹,
E.L. Barberio ¹⁰³, D. Barberis ^{56b,56a}, M. Barbero ¹⁰⁰, G. Barbour ⁹⁴, K.N. Barends ^{32a},
T. Barillari ¹⁰⁸, M-S. Barisits ³⁵, J. Barkeloo ¹²¹, T. Barklow ¹⁴¹, R.M. Barnett ^{17a}, P. Baron ¹²⁰,
A. Baroncelli ^{61a}, G. Barone ²⁸, A.J. Barr ¹²⁴, L. Barranco Navarro ^{46a,46b}, F. Barreiro ⁹⁷,
J. Barreiro Guimarães da Costa ^{14a}, U. Barron ¹⁴⁹, S. Barsov ³⁶, F. Bartels ^{62a}, R. Bartoldus ¹⁴¹,
G. Bartolini ¹⁰⁰, A.E. Barton ⁸⁹, P. Bartos ^{27a}, A. Basalae ⁴⁷, A. Basan ⁹⁸, M. Baselga ⁴⁷,
I. Bashta ^{75a,75b}, A. Bassalat ^{65,ad}, M.J. Basso ¹⁵³, C.R. Basson ⁹⁹, R.L. Bates ⁵⁸, S. Batlamous ^{34e},
J.R. Batley ³¹, B. Batool ¹³⁹, M. Battaglia ¹³⁴, M. Baucé ^{73a,73b}, F. Bauer ^{133,*}, P. Bauer ²³,
A. Bayirli ^{11c}, J.B. Beacham ⁵⁰, T. Beau ¹²⁵, P.H. Beauchemin ¹⁵⁶, F. Becherer ⁵³, P. Bechtel ²³,
H.P. Beck ^{19,q}, K. Becker ¹⁶⁴, C. Becot ⁴⁷, A.J. Beddall ^{11c}, V.A. Bednyakov ³⁷, C.P. Bee ¹⁴³,
T.A. Beermann ³⁵, M. Begalli ^{80b}, M. Begel ²⁸, A. Behera ¹⁴³, J.K. Behr ⁴⁷,
C. Beirao Da Cruz E Silva ³⁵, J.F. Beirer ^{54,35}, F. Beisiegel ²³, M. Belfkir ⁴, G. Bella ¹⁴⁹,
L. Bellagamba ^{22b}, A. Bellerive ³³, P. Bellos ²⁰, K. Beloborodov ³⁶, K. Belotskiy ³⁶,
N.L. Belyaev ³⁶, D. Benckekroun ^{34a}, Y. Benhammou ¹⁴⁹, D.P. Benjamin ²⁸, M. Benoit ²⁸,

J.R. Bensinger ²⁵, S. Bentvelsen ¹¹², L. Beresford ³⁵, M. Beretta ⁵², D. Berge ¹⁸,
 E. Bergeaas Kuutmann ¹⁵⁸, N. Berger ⁴, B. Bergmann ¹³⁰, L.J. Bergsten ²⁵, J. Beringer ^{17a},
 S. Berlendis ⁶, G. Bernardi ¹²⁵, C. Bernius ¹⁴¹, F.U. Bernlochner ²³, T. Berry ⁹³, P. Berta ¹³¹,
 A. Berthold ⁴⁹, I.A. Bertram ⁸⁹, O. Bessidskaia Bylund ¹⁶⁸, S. Bethke ¹⁰⁸, A. Betti ⁴³,
 A.J. Bevan ⁹², S. Bhatta ¹⁴³, D.S. Bhattacharya ¹⁶³, P. Bhattarai ²⁵, V.S. Bhopatkar ⁵, R. Bi ¹²⁷,
 R. Bi ²⁸, R.M. Bianchi ¹²⁷, O. Biebel ¹⁰⁷, R. Bielski ¹²¹, N.V. Biesuz ^{72a,72b}, M. Biglietti ^{75a},
 T.R.V. Billoud ¹³⁰, M. Bindi ⁵⁴, A. Bingul ^{11d}, C. Bini ^{73a,73b}, S. Biondi ^{22b,22a}, A. Biondini ⁹⁰,
 C.J. Birch-sykes ⁹⁹, G.A. Bird ^{20,132}, M. Birman ¹⁶⁶, T. Bisanz ³⁵, D. Biswas ^{167,k},
 A. Bitadze ⁹⁹, K. Bjørke ¹²³, I. Bloch ⁴⁷, C. Blocker ²⁵, A. Blue ⁵⁸, U. Blumenschein ⁹²,
 J. Blumenthal ⁹⁸, G.J. Bobbink ¹¹², V.S. Bobrovnikov ³⁶, M. Boehler ⁵³, D. Bogavac ¹³,
 A.G. Bogdanchikov ³⁶, C. Bohm ^{46a}, V. Boisvert ⁹³, P. Bokan ⁴⁷, T. Bold ^{83a}, M. Bomben ¹²⁵,
 M. Bona ⁹², M. Boonekamp ¹³³, C.D. Booth ⁹³, A.G. Borbély ⁵⁸, H.M. Borecka-Bielska ¹⁰⁶,
 L.S. Borgna ⁹⁴, G. Borissov ⁸⁹, D. Bortoletto ¹²⁴, D. Boscherini ^{22b}, M. Bosman ¹³,
 J.D. Bossio Sola ³⁵, K. Bouaouda ^{34a}, J. Boudreau ¹²⁷, E.V. Bouhova-Thacker ⁸⁹,
 D. Boumediene ³⁹, R. Bouquet ¹²⁵, A. Boveia ¹¹⁷, J. Boyd ³⁵, D. Boye ²⁸, I.R. Boyko ³⁷,
 A.J. Bozson ⁹³, J. Bracinik ²⁰, N. Brahimy ^{61d,61c}, G. Brandt ¹⁶⁸, O. Brandt ³¹, F. Braren ⁴⁷,
 B. Brau ¹⁰¹, J.E. Brau ¹²¹, W.D. Breaden Madden ⁵⁸, K. Brendlinger ⁴⁷, R. Brenner ¹⁶⁶,
 L. Brenner ³⁵, R. Brenner ¹⁵⁸, S. Bressler ¹⁶⁶, B. Brickwedde ⁹⁸, D. Britton ⁵⁸, D. Britzger ¹⁰⁸,
 I. Brock ²³, G. Brooijmans ⁴⁰, W.K. Brooks ^{135f}, E. Brost ²⁸, P.A. Bruckman de Renstrom ⁸⁴,
 B. Brüers ⁴⁷, D. Bruncko ^{27b,*}, A. Bruni ^{22b}, G. Bruni ^{22b}, M. Bruschi ^{22b}, N. Bruscinò ^{73a,73b},
 L. Bryngemark ¹⁴¹, T. Buanes ¹⁶, Q. Buat ¹³⁶, P. Buchholz ¹³⁹, A.G. Buckley ⁵⁸,
 I.A. Budagov ^{37,*}, M.K. Bugge ¹²³, O. Bulekov ³⁶, B.A. Bullard ⁶⁰, S. Burdin ⁹⁰,
 C.D. Burgard ⁴⁷, A.M. Burger ¹¹⁹, B. Burghgrave ⁷, J.T.P. Burr ³¹, C.D. Burton ¹⁰,
 J.C. Burzynski ¹⁴⁰, E.L. Busch ⁴⁰, V. Büscher ⁹⁸, P.J. Bussey ⁵⁸, J.M. Butler ²⁴, C.M. Buttar ⁵⁸,
 J.M. Butterworth ⁹⁴, W. Buttinger ¹³², C.J. Buxo Vazquez ¹⁰⁵, A.R. Buzykaev ³⁶, G. Cabras ^{22b},
 S. Cabrera Urbán ¹⁶⁰, D. Caforio ⁵⁷, H. Cai ¹²⁷, V.M.M. Cairo ¹⁴¹, O. Cakir ^{3a}, N. Calace ³⁵,
 P. Calafiura ^{17a}, G. Calderini ¹²⁵, P. Calfayan ⁶⁶, G. Callea ⁵⁸, L.P. Caloba ^{80b}, D. Calvet ³⁹,
 S. Calvet ³⁹, T.P. Calvet ¹⁰⁰, M. Calvetti ^{72a,72b}, R. Camacho Toro ¹²⁵, S. Camarda ³⁵,
 D. Camarero Munoz ⁹⁷, P. Camarri ^{74a,74b}, M.T. Camerlingo ^{75a,75b}, D. Cameron ¹²³,
 C. Camincher ¹⁶², M. Campanelli ⁹⁴, A. Camplani ⁴¹, V. Canale ^{70a,70b}, A. Canesse ¹⁰²,
 M. Cano Bret ⁷⁸, J. Cantero ⁹⁷, Y. Cao ¹⁵⁹, F. Capocasa ²⁵, M. Capua ^{42b,42a}, A. Carbone ^{69a,69b},
 R. Cardarelli ^{74a}, J.C.J. Cardenas ⁷, F. Cardillo ¹⁶⁰, T. Carli ³⁵, G. Carlino ^{70a}, B.T. Carlson ¹²⁷,
 E.M. Carlson ^{162,154a}, L. Carminati ^{69a,69b}, M. Carnesale ^{73a,73b}, S. Caron ¹¹¹, E. Carquin ^{135f},
 S. Carrá ⁴⁷, G. Carratta ^{22b,22a}, J.W.S. Carter ¹⁵³, T.M. Carter ⁵¹, D. Casadei ^{32c},
 M.P. Casado ^{13,h}, A.F. Casha ¹⁵³, E.G. Castiglia ¹⁶⁹, F.L. Castillo ^{62a}, L. Castillo Garcia ¹³,
 V. Castillo Gimenez ¹⁶⁰, N.F. Castro ^{128a,128e}, A. Catinaccio ³⁵, J.R. Catmore ¹²³, V. Cavaliere ²⁸,
 N. Cavalli ^{22b,22a}, V. Cavalinì ^{72a,72b}, E. Celebi ^{11c}, F. Celli ¹²⁴, M.S. Centonze ^{68a,68b},
 K. Cerny ¹²⁰, A.S. Cerqueira ^{80a}, A. Cerri ¹⁴⁴, L. Cerrito ^{74a,74b}, F. Cerutti ^{17a}, A. Cervelli ^{22b},
 S.A. Cetin ^{11c,aa}, Z. Chadi ^{34a}, D. Chakraborty ¹¹³, M. Chala ^{128f}, J. Chan ¹⁶⁷, W.S. Chan ¹¹²,
 W.Y. Chan ⁹⁰, J.D. Chapman ³¹, B. Chargeishvili ^{147b}, D.G. Charlton ²⁰, T.P. Charman ⁹²,
 M. Chatterjee ¹⁹, S. Chekanov ⁵, S.V. Chekulaev ^{154a}, G.A. Chelkov ^{37,a}, A. Chen ¹⁰⁴,
 B. Chen ¹⁴⁹, B. Chen ¹⁶², C. Chen ^{61a}, H. Chen ^{14c}, H. Chen ²⁸, J. Chen ^{61c}, J. Chen ²⁵,
 S. Chen ¹²⁶, S.J. Chen ^{14c}, X. Chen ^{61c}, X. Chen ^{14b,ag}, Y. Chen ^{61a}, C.L. Cheng ¹⁶⁷,
 H.C. Cheng ^{63a}, A. Cheplakov ³⁷, E. Cheremushkina ⁴⁷, E. Cherepanova ³⁷,
 R. Cherkaoui El Moursli ^{34e}, E. Cheu ⁶, K. Cheung ⁶⁴, L. Chevalier ¹³³, V. Chiarella ⁵²,
 G. Chiarelli ^{72a}, G. Chiodini ^{68a}, A.S. Chisholm ²⁰, A. Chitan ^{26b}, Y.H. Chiu ¹⁶²,
 M.V. Chizhov ³⁷, K. Choi ¹⁰, A.R. Chomont ^{73a,73b}, Y. Chou ¹⁰¹, E.Y.S. Chow ¹¹²,

T. Chowdhury [ID32f](#), L.D. Christopher [ID32f](#), M.C. Chu [ID63a](#), X. Chu [ID14a,14d](#), J. Chudoba [ID129](#),
 J.J. Chwastowski [ID84](#), D. Cieri [ID108](#), K.M. Ciesla [ID84](#), V. Cindro [ID91](#), I.A. Cioară [ID26b](#), A. Ciocio [ID17a](#),
 F. Cirotto [ID70a,70b](#), Z.H. Citron [ID166,1](#), M. Citterio [ID69a](#), D.A. Ciubotaru [ID26b](#), B.M. Ciungu [ID153](#),
 A. Clark [ID55](#), P.J. Clark [ID51](#), J.M. Clavijo Columbie [ID47](#), S.E. Clawson [ID99](#), C. Clement [ID46a,46b](#),
 L. Clissa [ID22b,22a](#), Y. Coadou [ID100](#), M. Cobal [ID67a,67c](#), A. Coccaro [ID56b](#), R.F. Coelho Barrue [ID128a](#),
 R. Coelho Lopes De Sa [ID101](#), S. Coelli [ID69a](#), H. Cohen [ID149](#), A.E.C. Coimbra [ID35](#), B. Cole [ID40](#),
 J. Collot [ID59](#), P. Conde Muiño [ID128a,128g](#), S.H. Connell [ID32c](#), I.A. Connelly [ID58](#), E.I. Conroy [ID124](#),
 F. Conventi [ID70a,ai](#), H.G. Cooke [ID20](#), A.M. Cooper-Sarkar [ID124](#), F. Cormier [ID161](#), L.D. Corpe [ID35](#),
 M. Corradi [ID73a,73b](#), E.E. Corrigan [ID96](#), F. Corriveau [ID102,v](#), M.J. Costa [ID160](#), F. Costanza [ID4](#),
 D. Costanzo [ID137](#), B.M. Cote [ID117](#), G. Cowan [ID93](#), J.W. Cowley [ID31](#), K. Cranmer [ID115](#),
 S. Crépe-Renaudin [ID59](#), F. Crescioli [ID125](#), M. Cristinziani [ID139](#), M. Cristoforetti [ID76a,76b,c](#), V. Croft [ID156](#),
 G. Crosetti [ID42b,42a](#), A. Cueto [ID35](#), T. Cuhadar Donszelmann [ID157](#), H. Cui [ID14a,14d](#), Z. Cui [ID6](#),
 A.R. Cukierman [ID141](#), W.R. Cunningham [ID58](#), F. Curcio [ID42b,42a](#), P. Czodrowski [ID35](#), M.M. Czurylo [ID62b](#),
 M.J. Da Cunha Sargedas De Sousa [ID61a](#), J.V. Da Fonseca Pinto [ID80b](#), C. Da Via [ID99](#), W. Dabrowski [ID83a](#),
 T. Dado [ID48](#), S. Dahbi [ID32f](#), T. Dai [ID104](#), C. Dallapiccola [ID101](#), M. Dam [ID41](#), G. D'amen [ID28](#),
 V. D'Amico [ID75a,75b](#), J. Damp [ID98](#), J.R. Dandoy [ID126](#), M.F. Daneri [ID29](#), M. Danninger [ID140](#), V. Dao [ID35](#),
 G. Darbo [ID56b](#), S. Darmora [ID5](#), A. Dattagupta [ID121](#), S. D'Auria [ID69a,69b](#), C. David [ID154b](#),
 T. Davidek [ID131](#), D.R. Davis [ID50](#), B. Davis-Purcell [ID33](#), I. Dawson [ID92](#), K. De [ID7](#), R. De Asmundis [ID70a](#),
 M. De Beurs [ID112](#), S. De Castro [ID22b,22a](#), N. De Groot [ID111](#), P. de Jong [ID112](#), H. De la Torre [ID105](#),
 A. De Maria [ID14c](#), A. De Salvo [ID73a](#), U. De Sanctis [ID74a,74b](#), M. De Santis [ID74a,74b](#), A. De Santo [ID144](#),
 J.B. De Vivie De Regie [ID59](#), D.V. Dedovich [ID37](#), J. Degens [ID112](#), A.M. Deiana [ID43](#), J. Del Peso [ID97](#),
 F. Del Rio [ID62a](#), F. Deliot [ID133](#), C.M. Delitzsch [ID6](#), M. Della Pietra [ID70a,70b](#), D. Della Volpe [ID55](#),
 A. Dell'Acqua [ID35](#), L. Dell'Asta [ID69a,69b](#), M. Delmastro [ID4](#), P.A. Delsart [ID59](#), S. Demers [ID169](#),
 M. Demichev [ID37](#), S.P. Denisov [ID36](#), L. D'Eramo [ID113](#), D. Derendarz [ID84](#), F. Derue [ID125](#), P. Dervan [ID90](#),
 K. Desch [ID23](#), K. Dette [ID153](#), C. Deutsch [ID23](#), P.O. Deviveiros [ID35](#), F.A. Di Bello [ID73a,73b](#),
 A. Di Ciaccio [ID74a,74b](#), L. Di Ciaccio [ID4](#), A. Di Domenico [ID73a,73b](#), C. Di Donato [ID70a,70b](#),
 A. Di Girolamo [ID35](#), G. Di Gregorio [ID72a,72b](#), A. Di Luca [ID76a,76b,c](#), B. Di Micco [ID75a,75b](#),
 R. Di Nardo [ID75a,75b](#), C. Diaconu [ID100](#), F.A. Dias [ID112](#), T. Dias Do Vale [ID128a](#), M.A. Diaz [ID135a,135b](#),
 F.G. Diaz Capriles [ID23](#), M. Didenko [ID160](#), E.B. Diehl [ID104](#), S. Díez Cornell [ID47](#), C. Diez Pardos [ID139](#),
 C. Dimitriadi [ID23,158](#), A. Dimitrievska [ID17a](#), W. Ding [ID14b](#), J. Dingfelder [ID23](#), I-M. Dinu [ID26b](#),
 S.J. Dittmeier [ID62b](#), F. Dittus [ID35](#), F. Djama [ID100](#), T. Djobava [ID147b](#), J.I. Djuvsland [ID16](#),
 M.A.B. Do Vale [ID80c](#), D. Dodsworth [ID25](#), C. Doglioni [ID96](#), J. Dolejsi [ID131](#), Z. Dolezal [ID131](#),
 M. Donadelli [ID80d](#), B. Dong [ID61c](#), J. Donini [ID39](#), A. D'Onofrio [ID14c](#), M. D'Onofrio [ID90](#), J. Dopke [ID132](#),
 A. Doria [ID70a](#), M.T. Dova [ID88](#), A.T. Doyle [ID58](#), E. Drechsler [ID140](#), E. Dreyer [ID166](#), A.S. Drobac [ID156](#),
 D. Du [ID61a](#), T.A. du Pree [ID112](#), F. Dubinin [ID36](#), M. Dubovsky [ID27a](#), E. Duchovni [ID166](#), G. Duckeck [ID107](#),
 O.A. Ducu [ID35,26b](#), D. Duda [ID108](#), A. Dudarev [ID35](#), M. D'uffizi [ID99](#), L. Duflost [ID65](#), M. Dührssen [ID35](#),
 C. Dülsen [ID168](#), A.E. Dumitriu [ID26b](#), M. Dunford [ID62a](#), S. Dungs [ID48](#), K. Dunne [ID46a,46b](#),
 A. Duperrin [ID100](#), H. Duran Yildiz [ID3a](#), M. Düren [ID57](#), A. Durglishvili [ID147b](#), B. Dutta [ID47](#),
 B.L. Dwyer [ID113](#), G.I. Dyckes [ID17a](#), M. Dyndal [ID83a](#), S. Dysch [ID99](#), B.S. Dziedzic [ID84](#), B. Eckerova [ID27a](#),
 M.G. Eggleston [ID50](#), E. Egidio Purcino De Souza [ID80b](#), L.F. Ehrke [ID55](#), G. Eigen [ID16](#), K. Einsweiler [ID17a](#),
 T. Ekelof [ID158](#), Y. El Ghazali [ID34b](#), H. El Jarrari [ID34e](#), A. El Moussaouy [ID34a](#), V. Ellajosyula [ID158](#),
 M. Ellert [ID158](#), F. Ellinghaus [ID168](#), A.A. Elliot [ID92](#), N. Ellis [ID35](#), J. Elmsheuser [ID28](#), M. Elsing [ID35](#),
 D. Emelianov [ID132](#), A. Emerman [ID40](#), Y. Enari [ID151](#), J. Erdmann [ID48](#), A. Ereditato [ID19](#), P.A. Erland [ID84](#),
 M. Errenst [ID168](#), M. Escalier [ID65](#), C. Escobar [ID160](#), O. Estrada Pastor [ID160](#), E. Etzion [ID149](#),
 G. Evans [ID128a](#), H. Evans [ID66](#), M.O. Evans [ID144](#), A. Ezhilov [ID36](#), S. Ezzarqtouni [ID34a](#), F. Fabbri [ID58](#),
 L. Fabbri [ID22b,22a](#), G. Facini [ID164](#), V. Fadeyev [ID134](#), R.M. Fakhruddinov [ID36](#), S. Falciano [ID73a](#),
 P.J. Falke [ID23](#), S. Falke [ID35](#), J. Faltova [ID131](#), Y. Fan [ID14a](#), Y. Fang [ID14a,14d](#), G. Fanourakis [ID45](#),

M. Fanti [ID](#)^{69a,69b}, M. Faraj [ID](#)^{61c}, A. Farbin [ID](#)⁷, A. Farilla [ID](#)^{75a}, E.M. Farina [ID](#)^{71a,71b}, T. Farooque [ID](#)¹⁰⁵,
S.M. Farrington [ID](#)⁵¹, F. Fassi [ID](#)^{34e}, D. Fassouliotis [ID](#)⁸, M. Faucci Giannelli [ID](#)^{74a,74b}, W.J. Fawcett [ID](#)³¹,
L. Fayard [ID](#)⁶⁵, O.L. Fedin [ID](#)^{36,a}, G. Fedotov [ID](#)³⁶, M. Feickert [ID](#)¹⁵⁹, L. Feligioni [ID](#)¹⁰⁰, A. Fell [ID](#)¹³⁷,
C. Feng [ID](#)^{61b}, M. Feng [ID](#)^{14b}, M.J. Fenton [ID](#)¹⁵⁷, A.B. Fenyuk [ID](#)³⁶, S.W. Ferguson [ID](#)⁴⁴, J. Ferrando [ID](#)⁴⁷,
A. Ferrari [ID](#)¹⁵⁸, P. Ferrari [ID](#)¹¹², R. Ferrari [ID](#)^{71a}, D. Ferrere [ID](#)⁵⁵, C. Ferretti [ID](#)¹⁰⁴, F. Fiedler [ID](#)⁹⁸,
A. Filipčič [ID](#)⁹¹, F. Filthaut [ID](#)¹¹¹, M.C.N. Fiolhais [ID](#)^{128a,128c,b}, L. Fiorini [ID](#)¹⁶⁰, F. Fischer [ID](#)¹³⁹,
W.C. Fisher [ID](#)¹⁰⁵, T. Fitschen [ID](#)²⁰, I. Fleck [ID](#)¹³⁹, P. Fleischmann [ID](#)¹⁰⁴, T. Flick [ID](#)¹⁶⁸, L. Flores [ID](#)¹²⁶,
M. Flores [ID](#)^{32d,ac}, L.R. Flores Castillo [ID](#)^{63a}, F.M. Follega [ID](#)^{76a,76b}, N. Fomin [ID](#)¹⁶, J.H. Foo [ID](#)¹⁵³,
B.C. Forland [ID](#)⁶⁶, A. Formica [ID](#)¹³³, F.A. Förster [ID](#)¹³, A.C. Forti [ID](#)⁹⁹, E. Fortin [ID](#)¹⁰⁰, A.W. Fortman [ID](#)⁶⁰,
M.G. Foti [ID](#)¹²⁴, L. Fountas [ID](#)^{8,i}, D. Fournier [ID](#)⁶⁵, H. Fox [ID](#)⁸⁹, P. Francavilla [ID](#)^{72a,72b}, S. Francescato [ID](#)⁶⁰,
M. Franchini [ID](#)^{22b,22a}, S. Franchino [ID](#)^{62a}, D. Francis [ID](#)³⁵, L. Franco [ID](#)⁴, L. Franconi [ID](#)¹⁹, M. Franklin [ID](#)⁶⁰,
G. Frattari [ID](#)^{73a,73b}, A.C. Freegard [ID](#)⁹², P.M. Freeman [ID](#)²⁰, W.S. Freund [ID](#)^{80b}, E.M. Freundlich [ID](#)⁴⁸,
D. Froidevaux [ID](#)³⁵, J.A. Frost [ID](#)¹²⁴, Y. Fu [ID](#)^{61a}, M. Fujimoto [ID](#)¹¹⁶, E. Fullana Torregrosa [ID](#)^{160,*},
J. Fuster [ID](#)¹⁶⁰, A. Gabrielli [ID](#)^{22b,22a}, A. Gabrielli [ID](#)³⁵, P. Gadow [ID](#)⁴⁷, G. Gagliardi [ID](#)^{56b,56a},
L.G. Gagnon [ID](#)^{17a}, G.E. Gallardo [ID](#)¹²⁴, E.J. Gallas [ID](#)¹²⁴, B.J. Gallop [ID](#)¹³², R. Gamboa Goni [ID](#)⁹²,
K.K. Gan [ID](#)¹¹⁷, S. Ganguly [ID](#)¹⁵¹, J. Gao [ID](#)^{61a}, Y. Gao [ID](#)⁵¹, F.M. Garay Walls [ID](#)^{135a}, C. García [ID](#)¹⁶⁰,
J.E. García Navarro [ID](#)¹⁶⁰, J.A. García Pascual [ID](#)^{14a}, M. Garcia-Sciveres [ID](#)^{17a}, R.W. Gardner [ID](#)³⁸,
D. Garg [ID](#)⁷⁸, R.B. Garg [ID](#)^{141,p}, S. Gargiulo [ID](#)⁵³, C.A. Garner [ID](#)¹⁵³, V. Garonne [ID](#)²⁸, S.J. Gasiorowski [ID](#)¹³⁶,
P. Gaspar [ID](#)^{80b}, G. Gaudio [ID](#)^{71a}, P. Gauzzi [ID](#)^{73a,73b}, I.L. Gavrilenko [ID](#)³⁶, A. Gavriyuk [ID](#)³⁶, C. Gay [ID](#)¹⁶¹,
G. Gaycken [ID](#)⁴⁷, E.N. Gazis [ID](#)⁹, A.A. Geanta [ID](#)^{26b}, C.M. Gee [ID](#)¹³⁴, J. Geisen [ID](#)⁹⁶, M. Geisen [ID](#)⁹⁸,
C. Gemme [ID](#)^{56b}, M.H. Genest [ID](#)⁵⁹, S. Gentile [ID](#)^{73a,73b}, S. George [ID](#)⁹³, W.F. George [ID](#)²⁰, T. Geralis [ID](#)⁴⁵,
L.O. Gerlach [ID](#)⁵⁴, P. Gessinger-Befurt [ID](#)³⁵, M. Ghasemi Bostanabad [ID](#)¹⁶², M. Ghneimat [ID](#)¹³⁹,
A. Ghosh [ID](#)¹⁵⁷, A. Ghosh [ID](#)⁶, B. Giacobbe [ID](#)^{22b}, S. Giagu [ID](#)^{73a,73b}, N. Giangiacomi [ID](#)¹⁵³,
P. Giannetti [ID](#)^{72a}, A. Giannini [ID](#)^{61a}, S.M. Gibson [ID](#)⁹³, M. Gignac [ID](#)¹³⁴, D.T. Gil [ID](#)^{83b}, B.J. Gilbert [ID](#)⁴⁰,
D. Gillberg [ID](#)³³, G. Gilles [ID](#)¹¹², N.E.K. Gillwald [ID](#)⁴⁷, D.M. Gingrich [ID](#)^{2,ah}, M.P. Giordani [ID](#)^{67a,67c},
P.F. Giraud [ID](#)¹³³, G. Giugliarelli [ID](#)^{67a,67c}, D. Giugni [ID](#)^{69a}, F. Giuli [ID](#)^{74a,74b}, I. Gkialas [ID](#)^{8,i},
P. Gkoutoumis [ID](#)⁹, L.K. Gladilin [ID](#)³⁶, C. Glasman [ID](#)⁹⁷, G.R. Gledhill [ID](#)¹²¹, M. Glisic [ID](#)¹²¹, I. Gnesi [ID](#)^{42b,e},
Y. Go [ID](#)²⁸, M. Goblirsch-Kolb [ID](#)²⁵, D. Godin [ID](#)¹⁰⁶, S. Goldfarb [ID](#)¹⁰³, T. Golling [ID](#)⁵⁵, D. Golubkov [ID](#)³⁶,
J.P. Gombas [ID](#)¹⁰⁵, A. Gomes [ID](#)^{128a,128b}, R. Goncalves Gama [ID](#)⁵⁴, R. Gonçalves [ID](#)^{128a,128c}, G. Gonella [ID](#)¹²¹,
L. Gonella [ID](#)²⁰, A. Gongadze [ID](#)³⁷, F. Gonnella [ID](#)²⁰, J.L. Gonski [ID](#)⁴⁰, R.Y. González Andana [ID](#)⁵¹,
S. González de la Hoz [ID](#)¹⁶⁰, S. Gonzalez Fernandez [ID](#)¹³, R. Gonzalez Lopez [ID](#)⁹⁰,
C. Gonzalez Renteria [ID](#)^{17a}, R. Gonzalez Suarez [ID](#)¹⁵⁸, S. Gonzalez-Sevilla [ID](#)⁵⁵,
G.R. Gonzalvo Rodriguez [ID](#)¹⁶⁰, L. Goossens [ID](#)³⁵, N.A. Gorasia [ID](#)²⁰, P.A. Gorbounov [ID](#)³⁶, B. Gorini [ID](#)³⁵,
E. Gorini [ID](#)^{68a,68b}, A. Gorišek [ID](#)⁹¹, A.T. Goshaw [ID](#)⁵⁰, M.I. Gostkin [ID](#)³⁷, C.A. Gottardo [ID](#)¹¹¹,
M. Goughri [ID](#)^{34b}, V. Goumarre [ID](#)⁴⁷, A.G. Goussiou [ID](#)¹³⁶, N. Govender [ID](#)^{32c}, C. Goy [ID](#)⁴,
I. Grabowska-Bold [ID](#)^{83a}, K. Graham [ID](#)³³, E. Gramstad [ID](#)¹²³, S. Grancagnolo [ID](#)¹⁸, M. Grandi [ID](#)¹⁴⁴,
V. Gratchev [ID](#)^{36,*}, P.M. Gravila [ID](#)^{26f}, F.G. Gravili [ID](#)^{68a,68b}, H.M. Gray [ID](#)^{17a}, C. Grefe [ID](#)²³, I.M. Gregor [ID](#)⁴⁷,
P. Grenier [ID](#)¹⁴¹, K. Grevtsov [ID](#)⁴⁷, C. Grieco [ID](#)¹³, N.A. Grieser [ID](#)¹¹⁸, A.A. Grillo [ID](#)¹³⁴, K. Grimm [ID](#)^{30,m},
S. Grinstein [ID](#)^{13,s}, J.-F. Grivaz [ID](#)⁶⁵, S. Groh [ID](#)⁹⁸, E. Gross [ID](#)¹⁶⁶, J. Grosse-Knetter [ID](#)⁵⁴, C. Grud [ID](#)¹⁰⁴,
A. Grummer [ID](#)¹¹⁰, J.C. Grundy [ID](#)¹²⁴, L. Guan [ID](#)¹⁰⁴, W. Guan [ID](#)¹⁶⁷, C. Gubbels [ID](#)¹⁶¹,
J.G.R. Guerrero Rojas [ID](#)¹⁶⁰, F. Guescini [ID](#)¹⁰⁸, R. Gugel [ID](#)⁹⁸, A. Guida [ID](#)⁴⁷, T. Guillemain [ID](#)⁴,
S. Guindon [ID](#)³⁵, F. Guo [ID](#)^{14a,14d}, J. Guo [ID](#)^{61c}, L. Guo [ID](#)⁶⁵, Y. Guo [ID](#)¹⁰⁴, R. Gupta [ID](#)⁴⁷, S. Gurbuz [ID](#)²³,
G. Gustavino [ID](#)³⁵, M. Guth [ID](#)⁵⁵, P. Gutierrez [ID](#)¹¹⁸, L.F. Gutierrez Zagazeta [ID](#)¹²⁶, C. Gutschow [ID](#)⁹⁴,
C. Guyot [ID](#)¹³³, C. Gwenlan [ID](#)¹²⁴, C.B. Gwilliam [ID](#)⁹⁰, E.S. Haaland [ID](#)¹²³, A. Haas [ID](#)¹¹⁵,
M. Habedank [ID](#)⁴⁷, C. Haber [ID](#)^{17a}, H.K. Hadavand [ID](#)⁷, A. Hadeef [ID](#)⁹⁸, S. Hadzic [ID](#)¹⁰⁸, M. Haleem [ID](#)¹⁶³,
J. Haley [ID](#)¹¹⁹, J.J. Hall [ID](#)¹³⁷, G.D. Hallewell [ID](#)¹⁰⁰, L. Halser [ID](#)¹⁹, K. Hamano [ID](#)¹⁶², H. Hamdaoui [ID](#)^{34e},
M. Hamer [ID](#)²³, G.N. Hamity [ID](#)⁵¹, K. Han [ID](#)^{61a}, L. Han [ID](#)^{14c}, L. Han [ID](#)^{61a}, S. Han [ID](#)^{17a}, Y.F. Han [ID](#)¹⁵³,

K. Hanagaki ⁸¹, M. Hance ¹³⁴, D.A. Hangal ⁴⁰, M.D. Hank ³⁸, R. Hankache ⁹⁹, E. Hansen ⁹⁶,
 J.B. Hansen ⁴¹, J.D. Hansen ⁴¹, P.H. Hansen ⁴¹, K. Hara ¹⁵⁵, T. Harenberg ¹⁶⁸, S. Harkusha ³⁶,
 Y.T. Harris ¹²⁴, P.F. Harrison ¹⁶⁴, N.M. Hartman ¹⁴¹, N.M. Hartmann ¹⁰⁷, Y. Hasegawa ¹³⁸,
 A. Hasib ⁵¹, S. Haug ¹⁹, R. Hauser ¹⁰⁵, M. Havranek ¹³⁰, C.M. Hawkes ²⁰, R.J. Hawkings ³⁵,
 S. Hayashida ¹⁰⁹, D. Hayden ¹⁰⁵, C. Hayes ¹⁰⁴, R.L. Hayes ¹⁶¹, C.P. Hays ¹²⁴, J.M. Hays ⁹²,
 H.S. Hayward ⁹⁰, F. He ^{61a}, Y. He ¹⁵², Y. He ¹²⁵, M.P. Heath ⁵¹, V. Hedberg ⁹⁶,
 A.L. Heggelund ¹²³, N.D. Hehir ⁹², C. Heidegger ⁵³, K.K. Heidegger ⁵³, W.D. Heidorn ⁷⁹,
 J. Heilmann ³³, S. Heim ⁴⁷, T. Heim ^{17a}, B. Heinemann ^{47,ae}, J.G. Heinlein ¹²⁶, J.J. Heinrich ¹²¹,
 L. Heinrich ³⁵, J. Hejbal ¹²⁹, L. Helary ⁴⁷, A. Held ¹¹⁵, S. Hellesund ¹²³, C.M. Helling ¹³⁴,
 S. Hellman ^{46a,46b}, C. Helsens ³⁵, R.C.W. Henderson ⁸⁹, L. Henkelmann ³¹,
 A.M. Henriques Correia ³⁵, H. Herde ¹⁴¹, Y. Hernández Jiménez ¹⁴³, H. Herr ⁹⁸, M.G. Herrmann ¹⁰⁷,
 T. Herrmann ⁴⁹, G. Herten ⁵³, R. Hertenberger ¹⁰⁷, L. Hervas ³⁵, N.P. Hessey ^{154a}, H. Hibi ⁸²,
 S. Higashino ⁸¹, E. Higón-Rodríguez ¹⁶⁰, S.J. Hillier ²⁰, I. Hinchliffe ^{17a}, F. Hinterkeuser ²³,
 M. Hirose ¹²², S. Hirose ¹⁵⁵, D. Hirschbuehl ¹⁶⁸, B. Hiti ⁹¹, O. Hladik ¹²⁹, J. Hobbs ¹⁴³,
 R. Hobincu ^{26e}, N. Hod ¹⁶⁶, M.C. Hodgkinson ¹³⁷, B.H. Hodgkinson ³¹, A. Hoecker ³⁵,
 J. Hofer ⁴⁷, D. Hohn ⁵³, T. Holm ²³, M. Holzbock ¹⁰⁸, L.B.A.H. Hommels ³¹, B.P. Honan ⁹⁹,
 J. Hong ^{61c}, T.M. Hong ¹²⁷, Y. Hong ⁵⁴, J.C. Honig ⁵³, A. Hönle ¹⁰⁸, B.H. Hooberman ¹⁵⁹,
 W.H. Hopkins ⁵, Y. Horii ¹⁰⁹, L.A. Horyn ³⁸, S. Hou ¹⁴⁶, J. Howarth ⁵⁸, J. Hoya ⁸⁸,
 M. Hrabovsky ¹²⁰, A. Hrynevich ³⁶, T. Hryn'ova ⁴, P.J. Hsu ⁶⁴, S.-C. Hsu ¹³⁶, Q. Hu ⁴⁰,
 S. Hu ^{61c}, Y.F. Hu ^{14a,14d,aj}, D.P. Huang ⁹⁴, X. Huang ^{14c}, Y. Huang ^{61a}, Y. Huang ^{14a},
 Z. Hubacek ¹³⁰, M. Huebner ²³, F. Huegging ²³, T.B. Huffman ¹²⁴, M. Huhtinen ³⁵,
 S.K. Huiberts ¹⁶, R. Hulsken ⁵⁹, N. Huseynov ^{12,a}, J. Huston ¹⁰⁵, J. Huth ⁶⁰, R. Hyneman ¹⁴¹,
 S. Hyrych ^{27a}, G. Iacobucci ⁵⁵, G. Iakovidis ²⁸, I. Ibragimov ¹³⁹, L. Iconomidou-Fayard ⁶⁵,
 P. Iengo ³⁵, R. Iguchi ¹⁵¹, T. Iizawa ⁵⁵, Y. Ikegami ⁸¹, A. Ilg ¹⁹, N. Ilic ¹⁵³, H. Imam ^{34a},
 T. Ingebretsen Carlson ^{46a,46b}, G. Introzzi ^{71a,71b}, M. Iodice ^{75a}, V. Ippolito ^{73a,73b}, M. Ishino ¹⁵¹,
 W. Islam ¹⁶⁷, C. Issever ^{18,47}, S. Istin ^{11c,ak}, H. Ito ¹⁶⁵, J.M. Iturbe Ponce ^{63a}, R. Iuppa ^{76a,76b},
 A. Ivina ¹⁶⁶, J.M. Izen ⁴⁴, V. Izzo ^{70a}, P. Jacka ^{129,130}, P. Jackson ¹, R.M. Jacobs ⁴⁷,
 B.P. Jaeger ¹⁴⁰, C.S. Jagfeld ¹⁰⁷, G. Jäkel ¹⁶⁸, K. Jakobs ⁵³, T. Jakoubek ¹⁶⁶, J. Jamieson ⁵⁸,
 K.W. Janas ^{83a}, G. Jarlskog ⁹⁶, A.E. Jaspán ⁹⁰, T. Javůrek ³⁵, M. Javurkova ¹⁰¹, F. Jeanneau ¹³³,
 L. Jeanty ¹²¹, J. Jejelava ^{147a,x}, P. Jenni ^{53,f}, S. Jézéquel ⁴, J. Jia ¹⁴³, Z. Jia ^{14c}, Y. Jiang ^{61a},
 S. Jiggins ⁵¹, J. Jimenez Pena ¹⁰⁸, S. Jin ^{14c}, A. Jinaru ^{26b}, O. Jinnouchi ¹⁵², H. Jivan ^{32f},
 P. Johansson ¹³⁷, K.A. Johns ⁶, C.A. Johnson ⁶⁶, D.M. Jones ³¹, E. Jones ¹⁶⁴, R.W.L. Jones ⁸⁹,
 T.J. Jones ⁹⁰, J. Jovicevic ¹⁵, X. Ju ^{17a}, J.J. Jungburth ³⁵, A. Juste Rozas ^{13,s}, S. Kabana ^{135e},
 A. Kaczmarzka ⁸⁴, M. Kado ^{73a,73b}, H. Kagan ¹¹⁷, M. Kagan ¹⁴¹, A. Kahn ⁴⁰, A. Kahn ¹²⁶,
 C. Kahra ⁹⁸, T. Kaji ¹⁶⁵, E. Kajomovitz ¹⁴⁸, N. Kakati ¹⁶⁶, C.W. Kalderon ²⁸,
 A. Kamenshchikov ³⁶, N.J. Kang ¹³⁴, Y. Kano ¹⁰⁹, D. Kar ^{32f}, K. Karava ¹²⁴, M.J. Kareem ^{154b},
 E. Karentzos ⁵³, I. Karkanas ¹⁵⁰, S.N. Karpov ³⁷, Z.M. Karpova ³⁷, V. Kartvelishvili ⁸⁹,
 A.N. Karyukhin ³⁶, E. Kasimi ¹⁵⁰, C. Kato ^{61d}, J. Katzy ⁴⁷, S. Kaur ³³, K. Kawade ¹³⁸,
 K. Kawagoe ⁸⁷, T. Kawaguchi ¹⁰⁹, T. Kawamoto ¹³³, G. Kawamura ⁵⁴, E.F. Kay ¹⁶², F.I. Kaya ¹⁵⁶,
 S. Kazakos ¹³, V.F. Kazanin ³⁶, Y. Ke ¹⁴³, J.M. Keaveney ^{32a}, R. Keeler ¹⁶², J.S. Keller ³³,
 A.S. Kelly ⁹⁴, D. Kelsey ¹⁴⁴, J.J. Kempster ²⁰, J. Kendrick ²⁰, K.E. Kennedy ⁴⁰, O. Kepka ¹²⁹,
 S. Kersten ¹⁶⁸, B.P. Kerševan ⁹¹, S. Ketabchi Haghighat ¹⁵³, M. Khandoga ¹²⁵, A. Khanov ¹¹⁹,
 A.G. Kharlamov ³⁶, T. Kharlamova ³⁶, E.E. Khoda ¹³⁶, T.J. Khoo ¹⁸, G. Khoriauli ¹⁶³,
 J. Khubua ^{147b}, M. Kiehn ³⁵, A. Kilgallon ¹²¹, E. Kim ¹⁵², Y.K. Kim ³⁸, N. Kimura ⁹⁴,
 A. Kirchhoff ⁵⁴, D. Kirchmeier ⁴⁹, C. Kirfel ²³, J. Kirk ¹³², A.E. Kiryunin ¹⁰⁸, T. Kishimoto ¹⁵¹,
 D.P. Kisliuk ¹⁵³, C. Kitsaki ⁹, O. Kivernyk ²³, M. Klassen ^{62a}, C. Klein ³³, L. Klein ¹⁶³,
 M.H. Klein ¹⁰⁴, M. Klein ⁹⁰, U. Klein ⁹⁰, P. Klimek ³⁵, A. Klimentov ²⁸, F. Klimpel ¹⁰⁸,

T. Klingl ²³, T. Klioutchnikova ³⁵, F.F. Klitzner ¹⁰⁷, P. Kluit ¹¹², S. Kluth ¹⁰⁸, E. Kneringer ⁷⁷, T.M. Knight ¹⁵³, A. Knue ⁵³, D. Kobayashi ⁸⁷, R. Kobayashi ⁸⁵, M. Kocian ¹⁴¹, T. Kodama ¹⁵¹, P. Kodyš ¹³¹, D.M. Koeck ¹⁴⁴, P.T. Koenig ²³, T. Koffas ³³, N.M. Köhler ³⁵, M. Kolb ¹³³, I. Koletsou ⁴, T. Komarek ¹²⁰, K. Köneke ⁵³, A.X.Y. Kong ¹, T. Kono ¹¹⁶, V. Konstantinides ⁹⁴, N. Konstantinidis ⁹⁴, B. Konya ⁹⁶, R. Kopeliansky ⁶⁶, S. Koperny ^{83a}, K. Korcyl ⁸⁴, K. Kordas ¹⁵⁰, G. Koren ¹⁴⁹, A. Korn ⁹⁴, S. Korn ⁵⁴, I. Korolkov ¹³, N. Korotkova ³⁶, B. Kortman ¹¹², O. Kortner ¹⁰⁸, S. Kortner ¹⁰⁸, W.H. Kostecka ¹¹³, V.V. Kostyukhin ^{139,36}, A. Kotsokechagia ⁶⁵, A. Kotwal ⁵⁰, A. Koulouris ³⁵, A. Kourkoumeli-Charalampidi ^{71a,71b}, C. Kourkoumelis ⁸, E. Kourlitis ⁵, O. Kovanda ¹⁴⁴, R. Kowalewski ¹⁶², W. Kozanecki ¹³³, A.S. Kozhin ³⁶, V.A. Kramarenko ³⁶, G. Kramberger ⁹¹, P. Kramer ⁹⁸, D. Krasnopevtsev ^{61a}, M.W. Krasny ¹²⁵, A. Krasznahorkay ³⁵, J.A. Kremer ⁹⁸, J. Kretschmar ⁹⁰, K. Kreul ¹⁸, P. Krieger ¹⁵³, F. Krieter ¹⁰⁷, S. Krishnamurthy ¹⁰¹, A. Krishnan ^{62b}, M. Krivos ¹³¹, K. Krizka ^{17a}, K. Kroeninger ⁴⁸, H. Kroha ¹⁰⁸, J. Kroll ¹²⁹, J. Kroll ¹²⁶, K.S. Krowpman ¹⁰⁵, U. Kruchonak ³⁷, H. Krüger ²³, N. Krumnack ⁷⁹, M.C. Kruse ⁵⁰, J.A. Krzysiak ⁸⁴, A. Kubota ¹⁵², O. Kuchinskaia ³⁶, S. Kудay ^{3a}, D. Kuechler ⁴⁷, J.T. Kuechler ⁴⁷, S. Kuehn ³⁵, T. Kuhl ⁴⁷, V. Kukhtin ³⁷, Y. Kulchitsky ^{36,a}, S. Kuleshov ^{135d}, M. Kumar ^{32f}, N. Kumari ¹⁰⁰, M. Kuna ⁵⁹, A. Kupco ¹²⁹, T. Kupfer ⁴⁸, O. Kuprash ⁵³, H. Kurashige ⁸², L.L. Kurchaninov ^{154a}, Y.A. Kurochkin ³⁶, A. Kurova ³⁶, E.S. Kuwertz ³⁵, M. Kuze ¹⁵², A.K. Kvam ¹³⁶, J. Kvita ¹²⁰, T. Kwan ¹⁰², K.W. Kwok ^{63a}, C. Lacasta ¹⁶⁰, F. Lacava ^{73a,73b}, H. Lacker ¹⁸, D. Lacour ¹²⁵, N.N. Lad ⁹⁴, E. Ladygin ³⁷, B. Laforge ¹²⁵, T. Lagouri ^{135e}, S. Lai ⁵⁴, I.K. Lakomic ^{83a}, N. Lalloue ⁵⁹, J.E. Lambert ¹¹⁸, S. Lammers ⁶⁶, W. Lampl ⁶, C. Lampoudis ¹⁵⁰, E. Lançon ²⁸, U. Landgraf ⁵³, M.P.J. Landon ⁹², V.S. Lang ⁵³, J.C. Lange ⁵⁴, R.J. Langenberg ¹⁰¹, A.J. Lankford ¹⁵⁷, F. Lanni ²⁸, K. Lantzsch ²³, A. Lanza ^{71a}, A. Lapertosa ^{56b,56a}, J.F. Laporte ¹³³, T. Lari ^{69a}, F. Lasagni Manghi ^{22b}, M. Lassnig ³⁵, V. Latonova ¹²⁹, T.S. Lau ^{63a}, A. Laudrain ⁹⁸, A. Laurier ³³, M. Lavorgna ^{70a,70b}, S.D. Lawlor ⁹³, Z. Lawrence ⁹⁹, M. Lazzaroni ^{69a,69b}, B. Le ⁹⁹, B. Leban ⁹¹, A. Lebedev ⁷⁹, M. LeBlanc ³⁵, T. LeCompte ⁵, F. Ledroit-Guillon ⁵⁹, A.C.A. Lee ⁹⁴, G.R. Lee ¹⁶, L. Lee ⁶⁰, S.C. Lee ¹⁴⁶, L.L. Leeuw ^{32c}, B. Lefebvre ^{154a}, H.P. Lefebvre ⁹³, M. Lefebvre ¹⁶², C. Leggett ^{17a}, K. Lehmann ¹⁴⁰, G. Lehmann Miotto ³⁵, W.A. Leight ⁴⁷, A. Leisos ^{150,r}, M.A.L. Leite ^{80d}, C.E. Leitgeb ⁴⁷, R. Leitner ¹³¹, K.J.C. Leney ⁴³, T. Lenz ²³, S. Leone ^{72a}, C. Leonidopoulos ⁵¹, A. Leopold ¹⁴², C. Leroy ¹⁰⁶, R. Les ¹⁰⁵, C.G. Lester ³¹, M. Levchenko ³⁶, J. Levêque ⁴, D. Levin ¹⁰⁴, L.J. Levinson ¹⁶⁶, D.J. Lewis ²⁰, B. Li ^{14b}, B. Li ^{61b}, C. Li ^{61a}, C-Q. Li ^{61c,61d}, H. Li ^{61a}, H. Li ^{61b}, H. Li ^{61b}, J. Li ^{61c}, K. Li ¹³⁶, L. Li ^{61c}, M. Li ^{14a,14d}, Q.Y. Li ^{61a}, S. Li ^{61d,61c,d}, T. Li ^{61b}, X. Li ⁴⁷, Z. Li ^{61b}, Z. Li ¹²⁴, Z. Li ¹⁰², Z. Li ⁹⁰, Z. Liang ^{14a}, M. Liberatore ⁴⁷, B. Liberti ^{74a}, K. Lie ^{63c}, J. Lieber Marin ^{80b}, K. Lin ¹⁰⁵, R.A. Linck ⁶⁶, R.E. Lindley ⁶, J.H. Lindon ², J. Ling ⁶⁰, A. Linss ⁴⁷, E. Lipeles ¹²⁶, A. Lipniacka ¹⁶, T.M. Liss ^{159,af}, A. Lister ¹⁶¹, J.D. Little ⁷, B. Liu ^{14a}, B.X. Liu ¹⁴⁰, D. Liu ^{61d,61c}, J.B. Liu ^{61a}, J.K.K. Liu ³⁸, K. Liu ^{61d,61c}, M. Liu ^{61a}, M.Y. Liu ^{61a}, P. Liu ^{14a}, Q. Liu ^{61d,136,61c}, X. Liu ^{61a}, Y. Liu ⁴⁷, Y. Liu ^{14c,14d}, Y.L. Liu ¹⁰⁴, Y.W. Liu ^{61a}, M. Livan ^{71a,71b}, J. Llorente Merino ¹⁴⁰, S.L. Lloyd ⁹², E.M. Lobodzinska ⁴⁷, P. Loch ⁶, S. Loffredo ^{74a,74b}, T. Lohse ¹⁸, K. Lohwasser ¹³⁷, M. Lokajicek ^{129,*}, J.D. Long ¹⁵⁹, I. Longarini ^{73a,73b}, L. Longo ³⁵, R. Longo ¹⁵⁹, I. Lopez Paz ³⁵, A. Lopez Solis ⁴⁷, J. Lorenz ¹⁰⁷, N. Lorenzo Martinez ⁴, A.M. Lory ¹⁰⁷, A. Lösle ⁵³, X. Lou ^{46a,46b}, X. Lou ^{14a,14d}, A. Lounis ⁶⁵, J. Love ⁵, P.A. Love ⁸⁹, J.J. Lozano Bahilo ¹⁶⁰, G. Lu ^{14a,14d}, M. Lu ^{61a}, S. Lu ¹²⁶, Y.J. Lu ⁶⁴, H.J. Lubatti ¹³⁶, C. Luci ^{73a,73b}, F.L. Lucio Alves ^{14c}, A. Lucotte ⁵⁹, F. Luehring ⁶⁶, I. Luise ¹⁴³, O. Lundberg ¹⁴², B. Lund-Jensen ¹⁴², N.A. Luongo ¹²¹, M.S. Lutz ¹⁴⁹, D. Lynn ²⁸, H. Lyons ⁹⁰, R. Lysak ¹²⁹, E. Lytken ⁹⁶, F. Lyu ^{14a}, V. Lyubushkin ³⁷, T. Lyubushkina ³⁷, H. Ma ²⁸,

L.L. Ma ^{61b}, Y. Ma ⁹⁴, D.M. Mac Donell ¹⁶², G. Maccarrone ⁵², C.M. Macdonald ¹³⁷,
 J.C. MacDonald ¹³⁷, R. Madar ³⁹, W.F. Mader ⁴⁹, J. Maeda ⁸², T. Maeno ²⁸, M. Maerker ⁴⁹,
 V. Magerl ⁵³, J. Magro ^{67a,67c}, D.J. Mahon ⁴⁰, C. Maidantchik ^{80b}, A. Maio ^{128a,128b,128d},
 K. Maj ^{83a}, O. Majersky ^{27a}, S. Majewski ¹²¹, N. Makovec ⁶⁵, V. Maksimovic ¹⁵,
 B. Malaescu ¹²⁵, Pa. Malecki ⁸⁴, V.P. Maleev ³⁶, F. Malek ⁵⁹, D. Malito ^{42b,42a}, U. Mallik ⁷⁸,
 C. Malone ³¹, S. Maltezos ⁹, S. Malyukov ³⁷, J. Mamuzic ¹⁶⁰, G. Mancini ⁵², J.P. Mandalia ⁹²,
 I. Mandić ⁹¹, L. Manhaes de Andrade Filho ^{80a}, I.M. Maniatis ¹⁵⁰, M. Manisha ¹³³,
 J. Manjarres Ramos ⁴⁹, D.C. Mankad ¹⁶⁶, K.H. Mankinen ⁹⁶, A. Mann ¹⁰⁷, A. Manousos ⁷⁷,
 B. Mansoulie ¹³³, S. Manzoni ³⁵, A. Marantis ^{150,r}, G. Marchiori ¹²⁵, M. Marcisovsky ¹²⁹,
 L. Marcoccia ^{74a,74b}, C. Marcon ⁹⁶, M. Marjanovic ¹¹⁸, Z. Marshall ^{17a}, S. Marti-Garcia ¹⁶⁰,
 T.A. Martin ¹⁶⁴, V.J. Martin ⁵¹, B. Martin dit Latour ¹⁶, L. Martinelli ^{73a,73b}, M. Martinez ^{13,s},
 P. Martinez Agullo ¹⁶⁰, V.I. Martinez Outschoorn ¹⁰¹, S. Martin-Haugh ¹³², V.S. Martoiu ^{26b},
 A.C. Martyniuk ⁹⁴, A. Marzin ³⁵, S.R. Maschek ¹⁰⁸, L. Masetti ⁹⁸, T. Mashimo ¹⁵¹, J. Masik ⁹⁹,
 A.L. Maslennikov ³⁶, L. Massa ^{22b}, P. Massarotti ^{70a,70b}, P. Mastrandrea ^{72a,72b},
 A. Mastroberardino ^{42b,42a}, T. Masubuchi ¹⁵¹, T. Mathisen ¹⁵⁸, A. Matic ¹⁰⁷, N. Matsuzawa ¹⁵¹,
 J. Maurer ^{26b}, B. Maček ⁹¹, D.A. Maximov ³⁶, R. Mazini ¹⁴⁶, I. Maznas ¹⁵⁰, S.M. Mazza ¹³⁴,
 C. Mc Ginn ²⁸, J.P. Mc Gowan ¹⁰², S.P. Mc Kee ¹⁰⁴, T.G. McCarthy ¹⁰⁸, W.P. McCormack ^{17a},
 E.F. McDonald ¹⁰³, A.E. McDougall ¹¹², J.A. Mcfayden ¹⁴⁴, G. Mchedlidze ^{147b}, M.A. McKay ⁴³,
 R.P. McKenzie ^{32f}, D.J. McLaughlin ⁹⁴, K.D. McLean ¹⁶², S.J. McMahon ¹³², P.C. McNamara ¹⁰³,
 R.A. McPherson ^{162,v}, J.E. Mdhluli ^{32f}, Z.A. Meadows ¹⁰¹, S. Meehan ³⁵, T. Megy ³⁹,
 S. Mehlhase ¹⁰⁷, A. Mehta ⁹⁰, B. Meirose ⁴⁴, D. Melini ¹⁴⁸, B.R. Mellado Garcia ^{32f},
 A.H. Melo ⁵⁴, F. Meloni ⁴⁷, A. Melzer ²³, E.D. Mendes Gouveia ^{128a},
 A.M. Mendes Jacques Da Costa ²⁰, H.Y. Meng ¹⁵³, L. Meng ⁸⁹, S. Menke ¹⁰⁸, M. Mentink ³⁵,
 E. Meoni ^{42b,42a}, C. Merlassino ¹²⁴, L. Merola ^{70a,70b}, C. Meroni ^{69a}, G. Merz ¹⁰⁴, O. Meshkov ³⁶,
 J.K.R. Meshreki ¹³⁹, J. Metcalfe ⁵, A.S. Mete ⁵, C. Meyer ⁶⁶, J-P. Meyer ¹³³, M. Michetti ¹⁸,
 R.P. Middleton ¹³², L. Mijović ⁵¹, G. Mikenberg ¹⁶⁶, M. Mikestikova ¹²⁹, M. Mikuž ⁹¹,
 H. Mildner ¹³⁷, A. Milic ¹⁵³, C.D. Milke ⁴³, D.W. Miller ³⁸, L.S. Miller ³³, A. Milov ¹⁶⁶,
 D.A. Milstead ^{46a,46b}, T. Min ^{14c}, A.A. Minaenko ³⁶, I.A. Minashvili ^{147b}, L. Mince ⁵⁸,
 A.I. Mincer ¹¹⁵, B. Mindur ^{83a}, M. Mineev ³⁷, Y. Minegishi ¹⁵¹, Y. Mino ⁸⁵, L.M. Mir ¹³,
 M. Miralles Lopez ¹⁶⁰, M. Mironova ¹²⁴, T. Mitani ¹⁶⁵, A. Mitra ¹⁶⁴, V.A. Mitsou ¹⁶⁰,
 O. Miu ¹⁵³, P.S. Miyagawa ⁹², Y. Miyazaki ⁸⁷, A. Mizukami ⁸¹, J.U. Mjörnmark ⁹⁶,
 T. Mkrtchyan ^{62a}, M. Mlynarikova ¹¹³, T. Moa ^{46a,46b}, S. Mobius ⁵⁴, K. Mochizuki ¹⁰⁶,
 P. Moder ⁴⁷, P. Mogg ¹⁰⁷, A.F. Mohammed ^{14a,14d}, S. Mohapatra ⁴⁰, G. Mokgatitwane ^{32f},
 B. Mondal ¹³⁹, S. Mondal ¹³⁰, K. Mönig ⁴⁷, E. Monnier ¹⁰⁰, L. Monsonis Romero ¹⁶⁰,
 J. Montejo Berlingen ³⁵, M. Montella ¹¹⁷, F. Monticelli ⁸⁸, N. Morange ⁶⁵,
 A.L. Moreira De Carvalho ^{128a}, M. Moreno Llácer ¹⁶⁰, C. Moreno Martinez ¹³, P. Morettini ^{56b},
 S. Morgenstern ¹⁶⁴, D. Mori ¹⁴⁰, M. Morii ⁶⁰, M. Morinaga ¹⁵¹, V. Morisbak ¹²³,
 A.K. Morley ³⁵, A.P. Morris ⁹⁴, L. Morvaj ³⁵, P. Moschovakos ³⁵, B. Moser ¹¹², M. Mosidze ^{147b},
 T. Moskalets ⁵³, P. Moskvitina ¹¹¹, J. Moss ^{30,n}, E.J.W. Moyse ¹⁰¹, S. Muanza ¹⁰⁰,
 J. Mueller ¹²⁷, D. Muenstermann ⁸⁹, R. Müller ¹⁹, G.A. Mullier ⁹⁶, J.J. Mullin ¹²⁶,
 D.P. Mungo ^{69a,69b}, J.L. Munoz Martinez ¹³, F.J. Munoz Sanchez ⁹⁹, M. Murin ⁹⁹, P. Murin ^{27b},
 W.J. Murray ^{164,132}, A. Murrone ^{69a,69b}, J.M. Muse ¹¹⁸, M. Muškinja ^{17a}, C. Mwewa ²⁸,
 A.G. Myagkov ^{36,a}, A.J. Myers ⁷, A.A. Myers ¹²⁷, G. Myers ⁶⁶, M. Myska ¹³⁰, B.P. Nachman ^{17a},
 O. Nackenhorst ⁴⁸, A. Nag ⁴⁹, K. Nagai ¹²⁴, K. Nagano ⁸¹, J.L. Nagle ²⁸, E. Nagy ¹⁰⁰,
 A.M. Nairz ³⁵, Y. Nakahama ⁸¹, K. Nakamura ⁸¹, H. Nanjo ¹²², F. Napolitano ^{62a},
 R. Narayan ⁴³, E.A. Narayanan ¹¹⁰, I. Naryshkin ³⁶, M. Naseri ³³, C. Nass ²³, G. Navarro ^{21a},
 J. Navarro-Gonzalez ¹⁶⁰, R. Nayak ¹⁴⁹, P.Y. Nechaeva ³⁶, F. Nechansky ⁴⁷, T.J. Neep ²⁰,

A. Negri [ID71a,71b](#), M. Negrini [ID22b](#), C. Nellist [ID111](#), C. Nelson [ID102](#), K. Nelson [ID104](#), S. Nemecek [ID129](#),
 M. Nessi [ID35.g](#), M.S. Neubauer [ID159](#), F. Neuhaus [ID98](#), J. Neundorf [ID47](#), R. Newhouse [ID161](#),
 P.R. Newman [ID20](#), C.W. Ng [ID127](#), Y.S. Ng [ID18](#), Y.W.Y. Ng [ID157](#), B. Ngair [ID34e](#), H.D.N. Nguyen [ID106](#),
 R.B. Nickerson [ID124](#), R. Nicolaidou [ID133](#), D.S. Nielsen [ID41](#), J. Nielsen [ID134](#), M. Niemeyer [ID54](#),
 N. Nikiforou [ID10](#), V. Nikolaenko [ID36.a](#), I. Nikolic-Audit [ID125](#), K. Nikolopoulos [ID20](#), P. Nilsson [ID28](#),
 H.R. Nindhito [ID55](#), A. Nisati [ID73a](#), N. Nishu [ID2](#), R. Nisius [ID108](#), T. Nitta [ID165](#), S.J. Noacco Rosende [ID88](#),
 T. Nobe [ID151](#), D.L. Noel [ID31](#), Y. Noguchi [ID85](#), I. Nomidis [ID125](#), M.A. Nomura [ID28](#), M.B. Norfolk [ID137](#),
 R.R.B. Norisam [ID94](#), J. Novak [ID91](#), T. Novak [ID47](#), O. Novgorodova [ID49](#), L. Novotny [ID130](#),
 R. Novotny [ID110](#), L. Nozka [ID120](#), K. Ntekas [ID157](#), E. Nurse [ID94](#), F.G. Oakham [ID33,ah](#), J. Ocariz [ID125](#),
 A. Ochi [ID82](#), I. Ochoa [ID128a](#), J.P. Ochoa-Ricoux [ID135a](#), S. Oda [ID87](#), S. Odaka [ID81](#), S. Oerdek [ID158](#),
 A. Ogrodnik [ID83a](#), A. Oh [ID99](#), C.C. Ohm [ID142](#), H. Oide [ID152](#), R. Oishi [ID151](#), M.L. Ojeda [ID47](#),
 Y. Okazaki [ID85](#), M.W. O'Keefe [ID90](#), Y. Okumura [ID151](#), A. Olariu [ID26b](#), L.F. Oleiro Seabra [ID128a](#),
 S.A. Olivares Pino [ID135e](#), D. Oliveira Damazio [ID28](#), D. Oliveira Goncalves [ID80a](#), J.L. Oliver [ID157](#),
 M.J.R. Olsson [ID157](#), A. Olszewski [ID84](#), J. Olszowska [ID84.*](#), Ö.O. Öncel [ID23](#), D.C. O'Neil [ID140](#),
 A.P. O'Neill [ID19](#), A. Onofre [ID128a,128e](#), P.U.E. Onyisi [ID10](#), R.G. Oreamuno Madriz [ID113](#), M.J. Oreglia [ID38](#),
 G.E. Orellana [ID88](#), D. Orestano [ID75a,75b](#), N. Orlando [ID13](#), R.S. Orr [ID153](#), V. O'Shea [ID58](#),
 R. Ospanov [ID61a](#), G. Otero y Garzon [ID29](#), H. Otono [ID87](#), P.S. Ott [ID62a](#), G.J. Ottino [ID17a](#), M. Ouchrif [ID34d](#),
 J. Ouellette [ID28](#), F. Ould-Saada [ID123](#), A. Ouraou [ID133.*](#), Q. Ouyang [ID14a](#), M. Owen [ID58](#), R.E. Owen [ID132](#),
 K.Y. Oyulmaz [ID11c](#), V.E. Ozcan [ID11c](#), N. Ozturk [ID7](#), S. Ozturk [ID11c,aa](#), J. Pacalt [ID120](#), H.A. Pacey [ID31](#),
 K. Pachal [ID50](#), A. Pacheco Pages [ID13](#), C. Padilla Aranda [ID13](#), S. Pagan Griso [ID17a](#), G. Palacino [ID66](#),
 S. Palazzo [ID51](#), S. Palestini [ID35](#), M. Palka [ID83b](#), J. Pan [ID169](#), D.K. Panchal [ID10](#), C.E. Pandini [ID55](#),
 J.G. Panduro Vazquez [ID93](#), P. Pani [ID47](#), G. Panizzo [ID67a,67c](#), L. Paolozzi [ID55](#), C. Papadatos [ID106](#),
 S. Parajuli [ID43](#), A. Paramonov [ID5](#), C. Paraskevopoulos [ID9](#), D. Paredes Hernandez [ID63b](#), B. Parida [ID166](#),
 T.H. Park [ID153](#), A.J. Parker [ID30](#), M.A. Parker [ID31](#), F. Parodi [ID56b,56a](#), E.W. Parrish [ID113](#), V.A. Parrish [ID51](#),
 J.A. Parsons [ID40](#), U. Parzefall [ID53](#), L. Pascual Dominguez [ID149](#), V.R. Pascuzzi [ID17a](#), F. Pasquali [ID112](#),
 E. Pasqualucci [ID73a](#), S. Passaggio [ID56b](#), F. Pastore [ID93](#), P. Pasuwan [ID46a,46b](#), J.R. Pater [ID99](#),
 A. Pathak [ID167](#), J. Patton [ID90](#), T. Pauly [ID35](#), J. Pearkes [ID141](#), M. Pedersen [ID123](#), R. Pedro [ID128a](#),
 S.V. Peleganchuk [ID36](#), O. Penc [ID129](#), C. Peng [ID63b](#), H. Peng [ID61a](#), M. Penzin [ID36](#), B.S. Peralva [ID80a](#),
 A.P. Pereira Peixoto [ID128a](#), L. Pereira Sanchez [ID46a,46b](#), D.V. Perepelitsa [ID28](#), E. Perez Codina [ID154a](#),
 M. Perganti [ID9](#), L. Perini [ID69a,69b.*](#), H. Pernegger [ID35](#), S. Perrella [ID35](#), A. Perrevoort [ID111](#), K. Peters [ID47](#),
 R.F.Y. Peters [ID99](#), B.A. Petersen [ID35](#), T.C. Petersen [ID41](#), E. Petit [ID100](#), V. Petousis [ID130](#), C. Petridou [ID150](#),
 A. Petrukhin [ID139](#), M. Pettee [ID17a](#), N.E. Pettersson [ID35](#), K. Petukhova [ID131](#), A. Peyaud [ID133](#),
 R. Pezoa [ID135f](#), L. Pezzotti [ID35](#), G. Pezzullo [ID169](#), T. Pham [ID103](#), P.W. Phillips [ID132](#), M.W. Phipps [ID159](#),
 G. Piacquadio [ID143](#), E. Pianori [ID17a](#), F. Piazza [ID69a,69b](#), R. Piegaia [ID29](#), D. Pietreanu [ID26b](#),
 A.D. Pilkington [ID99](#), M. Pinamonti [ID67a,67c](#), J.L. Pinfeld [ID2](#), C. Pitman Donaldson [ID94](#), D.A. Pizzi [ID33](#),
 L. Pizzimento [ID74a,74b](#), A. Pizzini [ID112](#), M.-A. Pleier [ID28](#), V. Plesanovs [ID53](#), V. Pleskot [ID131](#),
 E. Plotnikova [ID37](#), R. Poettgen [ID96](#), R. Poggi [ID55](#), L. Poggioli [ID125](#), I. Pogrebnyak [ID105](#), D. Pohl [ID23](#),
 I. Pokharel [ID54](#), G. Polesello [ID71a](#), A. Poley [ID140,154a](#), R. Polifka [ID130](#), A. Polini [ID22b](#), C.S. Pollard [ID124](#),
 Z.B. Pollock [ID117](#), V. Polychronakos [ID28](#), D. Ponomarenko [ID36](#), L. Pontecorvo [ID35](#), S. Popa [ID26a](#),
 G.A. Popeneciu [ID26d](#), L. Portales [ID4](#), D.M. Portillo Quintero [ID154a](#), S. Pospisil [ID130](#), P. Postolache [ID26c](#),
 K. Potamianos [ID124](#), I.N. Potrap [ID37](#), C.J. Potter [ID31](#), H. Potti [ID1](#), T. Poulsen [ID47](#), J. Poveda [ID160](#),
 T.D. Powell [ID137](#), G. Pownall [ID47](#), M.E. Pozo Astigarraga [ID35](#), A. Prades Ibanez [ID160](#), P. Pralavorio [ID100](#),
 M.M. Prapa [ID45](#), J. Pretel [ID53](#), D. Price [ID99](#), M. Primavera [ID68a](#), M.A. Principe Martin [ID97](#),
 M.L. Proffitt [ID136](#), N. Proklova [ID36](#), K. Prokofiev [ID63c](#), G. Proto [ID74a,74b](#), S. Protopopescu [ID28](#),
 J. Proudfoot [ID5](#), M. Przybycien [ID83a](#), D. Pudzha [ID36](#), P. Puzo [ID65](#), D. Pyatiizbyantseva [ID36](#), J. Qian [ID104](#),
 Y. Qin [ID99](#), T. Qiu [ID92](#), A. Quadt [ID54](#), M. Queitsch-Maitland [ID35](#), G. Rabanal Bolanos [ID60](#),
 D. Rafanoharana [ID53](#), F. Ragusa [ID69a,69b](#), J.A. Raine [ID55](#), S. Rajagopalan [ID28](#), K. Ran [ID14a,14d](#),

D.F. Rassloff [ID62a](#), S. Rave [ID98](#), B. Ravina [ID58](#), I. Ravinovich [ID166](#), M. Raymond [ID35](#), A.L. Read [ID123](#),
 N.P. Readioff [ID137](#), D.M. Rebuzzi [ID71a,71b](#), G. Redlinger [ID28](#), K. Reeves [ID44](#), D. Reikher [ID149](#), A. Reiss⁹⁸,
 A. Rej [ID139](#), C. Rembser [ID35](#), A. Renardi [ID47](#), M. Renda [ID26b](#), M.B. Rendel¹⁰⁸, A.G. Rennie [ID58](#),
 S. Resconi [ID69a](#), M. Ressegotti [ID56b,56a](#), E.D. Resseguie [ID17a](#), S. Rettie [ID94](#), B. Reynolds¹¹⁷,
 E. Reynolds [ID17a](#), M. Rezaei Estabragh [ID168](#), O.L. Rezanova [ID36](#), P. Reznicek [ID131](#), E. Ricci [ID76a,76b](#),
 R. Richter [ID108](#), S. Richter [ID47](#), E. Richter-Was [ID83b](#), M. Ridel [ID125](#), P. Rieck [ID115](#), P. Riedler [ID35](#),
 M. Rijssenbeek [ID143](#), A. Rimoldi [ID71a,71b](#), M. Rimoldi [ID47](#), L. Rinaldi [ID22b,22a](#), T.T. Rinn [ID159](#),
 M.P. Rinnagel [ID107](#), G. Ripellino [ID142](#), I. Riu [ID13](#), P. Rivadeneira [ID47](#), J.C. Rivera Vergara [ID162](#),
 F. Rizatdinova [ID119](#), E. Rizvi [ID92](#), C. Rizzi [ID55](#), B.A. Roberts [ID164](#), B.R. Roberts [ID17a](#),
 S.H. Robertson [ID102,v](#), M. Robin [ID47](#), D. Robinson [ID31](#), C.M. Robles Gajardo^{135f},
 M. Robles Manzano [ID98](#), A. Robson [ID58](#), A. Rocchi [ID74a,74b](#), C. Roda [ID72a,72b](#), S. Rodriguez Bosca [ID62a](#),
 Y. Rodriguez Garcia [ID21a](#), A. Rodriguez Rodriguez [ID53](#), A.M. Rodríguez Vera [ID154b](#), S. Roe³⁵,
 A.R. Roepe-Gier [ID118](#), J. Roggel [ID168](#), O. Røhne [ID123](#), R.A. Rojas [ID162](#), B. Roland [ID53](#),
 C.P.A. Roland [ID66](#), J. Roloff [ID28](#), A. Romaniouk [ID36](#), M. Romano [ID22b](#), A.C. Romero Hernandez [ID159](#),
 N. Rompotis [ID90](#), M. Ronzani [ID115](#), L. Roos [ID125](#), S. Rosati [ID73a](#), B.J. Rosser [ID126](#), E. Rossi [ID153](#),
 E. Rossi [ID4](#), E. Rossi [ID70a,70b](#), L.P. Rossi [ID56b](#), L. Rossini [ID47](#), R. Rosten [ID117](#), M. Rotaru [ID26b](#),
 B. Rottler [ID53](#), D. Rousseau [ID65](#), D. Rouso [ID31](#), G. Rovelli [ID71a,71b](#), A. Roy [ID10](#), A. Rozanov [ID100](#),
 Y. Rozen [ID148](#), X. Ruan [ID32f](#), A.J. Ruby [ID90](#), T.A. Ruggeri [ID1](#), F. Rühr [ID53](#), A. Ruiz-Martinez [ID160](#),
 A. Rummler [ID35](#), Z. Rurikova [ID53](#), N.A. Rusakovich [ID37](#), H.L. Russell [ID162](#), L. Rustige [ID39](#),
 J.P. Rutherford [ID6](#), E.M. Rüttinger [ID137](#), K. Rybacki⁸⁹, M. Rybar [ID131](#), E.B. Rye [ID123](#), A. Ryzhov [ID36](#),
 J.A. Sabater Iglesias [ID55](#), P. Sabatini [ID160](#), L. Sabetta [ID73a,73b](#), H.F-W. Sadrozinski [ID134](#),
 F. Safai Tehrani [ID73a](#), B. Safarzadeh Samani [ID144](#), M. Safdari [ID141](#), S. Saha [ID102](#), M. Sahinsoy [ID108](#),
 A. Sahu [ID168](#), M. Saimpert [ID133](#), M. Saito [ID151](#), T. Saito [ID151](#), D. Salamani [ID35](#), G. Salamanna [ID75a,75b](#),
 A. Salnikov [ID141](#), J. Salt [ID160](#), A. Salvador Salas [ID13](#), D. Salvatore [ID42b,42a](#), F. Salvatore [ID144](#),
 A. Salzburger [ID35](#), D. Sammel [ID53](#), D. Sampsonidis [ID150](#), D. Sampsonidou [ID61d,61c](#), J. Sánchez [ID160](#),
 A. Sanchez Pineda [ID4](#), V. Sanchez Sebastian [ID160](#), H. Sandaker [ID123](#), C.O. Sander [ID47](#),
 I.G. Sanderswood [ID89](#), J.A. Sandesara [ID101](#), M. Sandhoff [ID168](#), C. Sandoval [ID21b](#), D.P.C. Sankey [ID132](#),
 A. Sansoni [ID52](#), C. Santoni [ID39](#), H. Santos [ID128a,128b](#), S.N. Santpur [ID17a](#), A. Santra [ID166](#),
 K.A. Saoucha [ID137](#), J.G. Saraiva [ID128a,128d](#), J. Sardain [ID100](#), O. Sasaki [ID81](#), K. Sato [ID155](#), C. Sauer^{62b},
 F. Sauerburger [ID53](#), E. Sauvan [ID4](#), P. Savard [ID153,ah](#), R. Sawada [ID151](#), C. Sawyer [ID132](#), L. Sawyer [ID95](#),
 I. Sayago Galvan¹⁶⁰, C. Sbarra [ID22b](#), A. Sbrizzi [ID22b,22a](#), T. Scanlon [ID94](#), J. Schaarschmidt [ID136](#),
 P. Schacht [ID108](#), D. Schaefer [ID38](#), U. Schäfer [ID98](#), A.C. Schaffer [ID65](#), D. Schaile [ID107](#),
 R.D. Schamberger [ID143](#), E. Schanet [ID107](#), C. Scharf [ID18](#), N. Scharmberg [ID99](#), V.A. Schegelsky [ID36](#),
 D. Scheirich [ID131](#), F. Schenck [ID18](#), M. Schernau [ID157](#), C. Schiavi [ID56b,56a](#), Z.M. Schillaci [ID25](#),
 E.J. Schioppa [ID68a,68b](#), M. Schioppa [ID42b,42a](#), B. Schlag [ID98](#), K.E. Schleicher [ID53](#), S. Schlenker [ID35](#),
 K. Schmieden [ID98](#), C. Schmitt [ID98](#), S. Schmitt [ID47](#), L. Schoeffel [ID133](#), A. Schoening [ID62b](#),
 P.G. Scholer [ID53](#), E. Schopf [ID124](#), M. Schott [ID98](#), J. Schovancova [ID35](#), S. Schramm [ID55](#),
 F. Schroeder [ID168](#), H-C. Schultz-Coulon [ID62a](#), M. Schumacher [ID53](#), B.A. Schumm [ID134](#), Ph. Schune [ID133](#),
 A. Schwartzman [ID141](#), T.A. Schwarz [ID104](#), Ph. Schwemling [ID133](#), R. Schwienhorst [ID105](#), A. Sciandra [ID134](#),
 G. Sciolla [ID25](#), F. Scuri [ID72a](#), F. Scutti¹⁰³, C.D. Sebastiani [ID90](#), K. Sedlaczek [ID48](#), P. Seema [ID18](#),
 S.C. Seidel [ID110](#), A. Seiden [ID134](#), B.D. Seidlitz [ID28](#), T. Seiss [ID38](#), C. Seitz [ID47](#), J.M. Seixas [ID80b](#),
 G. Sekhniaidze [ID70a](#), S.J. Sekula [ID43](#), L. Selem [ID4](#), N. Semprini-Cesari [ID22b,22a](#), S. Sen [ID50](#), L. Serin [ID65](#),
 L. Serkin [ID67a,67b](#), M. Sessa [ID75a,75b](#), H. Severini [ID118](#), S. Sevova [ID141](#), F. Sforza [ID56b,56a](#), A. Sfyrla [ID55](#),
 E. Shabalina [ID54](#), R. Shaheen [ID142](#), J.D. Shahinian [ID126](#), N.W. Shaikh [ID46a,46b](#), D. Shaked Renous [ID166](#),
 L.Y. Shan [ID14a](#), M. Shapiro [ID17a](#), A. Sharma [ID35](#), A.S. Sharma [ID1](#), S. Sharma [ID47](#), P.B. Shatalov [ID36](#),
 K. Shaw [ID144](#), S.M. Shaw [ID99](#), P. Sherwood [ID94](#), L. Shi [ID94](#), C.O. Shimmin [ID169](#), Y. Shimogama [ID165](#),
 J.D. Shinner [ID93](#), I.P.J. Shipsey [ID124](#), S. Shirabe [ID55](#), M. Shiyakova [ID37,u](#), J. Shlomi [ID166](#),

M.J. Shochet ¹³⁸, J. Shojaii ¹⁰³, D.R. Shope ¹⁴², S. Shrestha ¹¹⁷, E.M. Shrif ^{32f}, M.J. Shroff ¹⁶²,
E. Shulga ¹⁶⁶, P. Sicho ¹²⁹, A.M. Sickles ¹⁵⁹, E. Sideras Haddad ^{32f}, O. Sidiropoulou ³⁵,
A. Sidoti ^{22b}, F. Siegert ⁴⁹, Dj. Sijacki ¹⁵, F. Sili ⁸⁸, J.M. Silva ²⁰, M.V. Silva Oliveira ³⁵,
S.B. Silverstein ^{46a}, S. Simion ⁶⁵, R. Simoniello ³⁵, N.D. Simpson ⁹⁶, S. Simsek ^{11c}, S. Sindhu ⁵⁴,
P. Sinervo ¹⁵³, V. Sinetckii ³⁶, S. Singh ¹⁴⁰, S. Singh ¹⁵³, S. Sinha ⁴⁷, S. Sinha ^{32f},
M. Sioli ^{22b,22a}, I. Siral ¹²¹, S.Yu. Sivoklov ^{36,*}, J. Sjölin ^{46a,46b}, A. Skaf ⁵⁴, E. Skorda ⁹⁶,
P. Skubic ¹¹⁸, M. Slawinska ⁸⁴, V. Smakhtin ¹⁶⁶, B.H. Smart ¹³², J. Smiesko ¹³¹, S.Yu. Smirnov ³⁶,
Y. Smirnov ³⁶, L.N. Smirnova ^{36,a}, O. Smirnova ⁹⁶, E.A. Smith ³⁸, H.A. Smith ¹²⁴,
M. Smizanska ⁸⁹, K. Smolek ¹³⁰, A. Smykiewicz ⁸⁴, A.A. Snesarev ³⁶, H.L. Snoek ¹¹²,
S. Snyder ²⁸, R. Sobie ^{162,v}, A. Soffer ¹⁴⁹, C.A. Solans Sanchez ³⁵, E.Yu. Soldatov ³⁶,
U. Soldevila ¹⁶⁰, A.A. Solodkov ³⁶, S. Solomon ⁵³, A. Soloshenko ³⁷, K. Solovieva ⁵³,
O.V. Solovyanov ³⁶, V. Solovyev ³⁶, P. Sommer ¹³⁷, H. Son ¹⁵⁶, A. Sonay ¹³, W.Y. Song ^{154b},
A. Sopczak ¹³⁰, A.L. Sopio ⁹⁴, F. Sopkova ^{27b}, S. Sottocornola ^{71a,71b}, R. Soualah ^{114c},
Z. Soumami ^{34e}, D. South ⁴⁷, S. Spagnolo ^{68a,68b}, M. Spalla ¹⁰⁸, M. Spangenberg ¹⁶⁴,
F. Spanò ⁹³, D. Sperlich ⁵³, G. Spigo ³⁵, M. Spina ¹⁴⁴, S. Spinali ⁸⁹, D.P. Spiteri ⁵⁸,
M. Spousta ¹³¹, A. Stabile ^{69a,69b}, R. Stamen ^{62a}, M. Stamenkovic ¹¹², A. Stampekis ²⁰,
M. Standke ²³, E. Stanecka ⁸⁴, B. Stanislaus ^{17a}, M.M. Stanitzki ⁴⁷, M. Stankaityte ¹²⁴,
B. Stapf ⁴⁷, E.A. Starchenko ³⁶, G.H. Stark ¹³⁴, J. Stark ^{100,ab}, D.M. Starko ^{154b}, P. Staroba ¹²⁹,
P. Starovoitov ^{62a}, S. Stärz ¹⁰², R. Staszewski ⁸⁴, G. Stavropoulos ⁴⁵, P. Steinberg ²⁸,
A.L. Steinhebel ¹²¹, B. Stelzer ^{140,154a}, H.J. Stelzer ¹²⁷, O. Stelzer-Chilton ^{154a}, H. Stenzel ⁵⁷,
T.J. Stevenson ¹⁴⁴, G.A. Stewart ³⁵, M.C. Stockton ³⁵, G. Stoicea ^{26b}, M. Stolarski ^{128a},
S. Stonjek ¹⁰⁸, A. Straessner ⁴⁹, J. Strandberg ¹⁴², S. Strandberg ^{46a,46b}, M. Strauss ¹¹⁸,
T. Strebler ¹⁰⁰, P. Strizenec ^{27b}, R. Ströhmer ¹⁶³, D.M. Strom ¹²¹, L.R. Strom ⁴⁷,
R. Stroynowski ⁴³, A. Strubig ^{46a,46b}, S.A. Stucci ²⁸, B. Stugu ¹⁶, J. Stupak ¹¹⁸, N.A. Styles ⁴⁷,
D. Su ¹⁴¹, S. Su ^{61a}, W. Su ^{61d,136,61c}, X. Su ^{61a}, K. Sugizaki ¹⁵¹, V.V. Sulin ³⁶,
M.J. Sullivan ⁹⁰, D.M.S. Sultan ^{76a,76b}, L. Sultanaliyeva ³⁶, S. Sultansoy ^{3c}, T. Sumida ⁸⁵,
S. Sun ¹⁰⁴, S. Sun ¹⁶⁷, O. Sunneborn Gudnadottir ¹⁵⁸, M.R. Sutton ¹⁴⁴, M. Svatos ¹²⁹,
M. Swiatlowski ^{154a}, T. Swirski ¹⁶³, I. Sykora ^{27a}, M. Sykora ¹³¹, T. Sykora ¹³¹, D. Ta ⁹⁸,
K. Tackmann ^{47,t}, A. Taffard ¹⁵⁷, R. Tafirout ^{154a}, R.H.M. Taibah ¹²⁵, R. Takashima ⁸⁶,
K. Takeda ⁸², E.P. Takeva ⁵¹, Y. Takubo ⁸¹, M. Talby ¹⁰⁰, A.A. Talyshv ³⁶, K.C. Tam ^{63b},
N.M. Tamir ¹⁴⁹, A. Tanaka ¹⁵¹, J. Tanaka ¹⁵¹, R. Tanaka ⁶⁵, J. Tang ^{61c}, Z. Tao ¹⁶¹,
S. Tapia Araya ⁷⁹, S. Tapprogge ⁹⁸, A. Tarek Abouelfadl Mohamed ¹⁰⁵, S. Tarem ¹⁴⁸,
K. Tariq ^{61b}, G. Tarna ^{26b}, G.F. Tartarelli ^{69a}, P. Tas ¹³¹, M. Tasevsky ¹²⁹, E. Tassi ^{42b,42a},
G. Tateno ¹⁵¹, Y. Tayalati ^{34e}, G.N. Taylor ¹⁰³, W. Taylor ^{154b}, H. Teagle ⁹⁰, A.S. Tee ¹⁶⁷,
R. Teixeira De Lima ¹⁴¹, P. Teixeira-Dias ⁹³, J.J. Teoh ¹¹², K. Terashi ¹⁵¹, J. Terron ⁹⁷,
S. Terzo ¹³, M. Testa ⁵², R.J. Teuscher ^{153,v}, N. Themistokleous ⁵¹, T. Theveneaux-Pelzer ¹⁸,
O. Thielmann ¹⁶⁸, D.W. Thomas ⁹³, J.P. Thomas ²⁰, E.A. Thompson ⁴⁷, P.D. Thompson ²⁰,
E. Thomson ¹²⁶, E.J. Thorpe ⁹², Y. Tian ⁵⁴, V. Tikhomirov ^{36,a}, Yu.A. Tikhonov ³⁶,
S. Timoshenko ³⁶, E.X.L. Ting ¹, P. Tipton ¹⁶⁹, S. Tisserant ¹⁰⁰, S.H. Tlou ^{32f}, A. Tmourji ³⁹,
K. Todome ^{22b,22a}, S. Todorova-Nova ¹³¹, S. Todt ⁴⁹, M. Togawa ⁸¹, J. Tojo ⁸⁷, S. Tokár ^{27a},
K. Tokushuku ⁸¹, R. Tombs ³¹, M. Tomoto ^{81,109}, L. Tompkins ^{141,p}, P. Tornambe ¹⁰¹,
E. Torrence ¹²¹, H. Torres ⁴⁹, E. Torró Pastor ¹⁶⁰, M. Toscani ²⁹, C. Tosciri ³⁸, D.R. Tovey ¹³⁷,
A. Traeet ¹⁶, I.S. Trandafir ^{26b}, C.J. Treado ¹¹⁵, T. Trefzger ¹⁶³, A. Tricoli ²⁸, I.M. Trigger ^{154a},
S. Trincaz-Duvoid ¹²⁵, D.A. Trischuk ¹⁶¹, B. Trocme ⁵⁹, A. Trofymov ⁶⁵, C. Troncon ^{69a},
F. Trovato ¹⁴⁴, L. Truong ^{32c}, M. Trzebinski ⁸⁴, A. Trzuppek ⁸⁴, F. Tsai ¹⁴³, M. Tsai ¹⁰⁴,
A. Tsiamis ¹⁵⁰, P.V. Tsiareshka ³⁶, A. Tsirigotis ^{150,r}, V. Tsiskaridze ¹⁴³, E.G. Tskhadadze ^{147a},
M. Tsopoulou ¹⁵⁰, Y. Tsujikawa ⁸⁵, I.I. Tsukerman ³⁶, V. Tsulaia ^{17a}, S. Tsuno ⁸¹, O. Tsur ¹⁴⁸,

D. Tsybychev ¹⁴³, Y. Tu ^{63b}, A. Tudorache ^{26b}, V. Tudorache ^{26b}, A.N. Tuna ³⁵, S. Turchikhin ³⁷,
 I. Turk Cakir ^{3a}, R. Turra ^{69a}, P.M. Tuts ⁴⁰, S. Tzamarias ¹⁵⁰, P. Tzanis ⁹, E. Tzovara ⁹⁸,
 K. Uchida ¹⁵¹, F. Ukegawa ¹⁵⁵, P.A. Ulloa Poblete ^{135c}, G. Unal ³⁵, M. Unal ¹⁰, A. Undrus ²⁸,
 G. Unel ¹⁵⁷, K. Uno ¹⁵¹, J. Urban ^{27b}, P. Urquijo ¹⁰³, G. Usai ⁷, R. Ushioda ¹⁵²,
 M. Usman ¹⁰⁶, Z. Uysal ^{11d}, V. Vacek ¹³⁰, B. Vachon ¹⁰², K.O.H. Vadla ¹²³, T. Vafeiadis ³⁵,
 C. Valderanis ¹⁰⁷, E. Valdes Santurio ^{46a,46b}, M. Valente ^{154a}, S. Valentinetti ^{22b,22a}, A. Valero ¹⁶⁰,
 A. Vallier ^{100,ab}, J.A. Valls Ferrer ¹⁶⁰, T.R. Van Daalen ¹³⁶, P. Van Gemmeren ⁵, S. Van Stroud ⁹⁴,
 I. Van Vulpen ¹¹², M. Vanadia ^{74a,74b}, W. Vandelli ³⁵, M. Vandenbroucke ¹³³, E.R. Vandewall ¹¹⁹,
 D. Vannicola ¹⁴⁹, L. Vannoli ^{56b,56a}, R. Vari ^{73a}, E.W. Varnes ⁶, C. Varni ^{17a}, T. Varol ¹⁴⁶,
 D. Varouchas ⁶⁵, K.E. Varvell ¹⁴⁵, M.E. Vasile ^{26b}, L. Vaslin ³⁹, G.A. Vasquez ¹⁶², F. Vazeille ³⁹,
 D. Vazquez Furelos ¹³, T. Vazquez Schroeder ³⁵, J. Veatch ⁵⁴, V. Vecchio ⁹⁹, M.J. Veen ¹¹²,
 I. Veliscek ¹²⁴, L.M. Veloce ¹⁵³, F. Veloso ^{128a,128c}, S. Veneziano ^{73a}, A. Ventura ^{68a,68b},
 A. Verbytskyi ¹⁰⁸, M. Verducci ^{72a,72b}, C. Vergis ²³, M. Verissimo De Araujo ^{80b},
 W. Verkerke ¹¹², J.C. Vermeulen ¹¹², C. Vernieri ¹⁴¹, P.J. Verschuuren ⁹³, M. Vessella ¹⁰¹,
 M.L. Vesterbacka ¹¹⁵, M.C. Vetterli ^{140,ah}, A. Vgenopoulos ¹⁵⁰, N. Viaux Maira ^{135f},
 T. Vickey ¹³⁷, O.E. Vickey Boeriu ¹³⁷, G.H.A. Viehhauser ¹²⁴, L. Vigani ^{62b}, M. Villa ^{22b,22a},
 M. Villaplana Perez ¹⁶⁰, E.M. Villhauer ⁵¹, E. Vilucchi ⁵², M.G. Vincter ³³, G.S. Virdee ²⁰,
 A. Vishwakarma ⁵¹, C. Vittori ^{22b,22a}, I. Vivarelli ¹⁴⁴, V. Vladimirov ¹⁶⁴, E. Voevodina ¹⁰⁸,
 M. Vogel ¹⁶⁸, P. Vokac ¹³⁰, J. Von Ahnen ⁴⁷, E. Von Toerne ²³, B. Vormwald ³⁵, V. Vorobel ¹³¹,
 K. Vorobev ³⁶, M. Vos ¹⁶⁰, J.H. Vosseveld ⁹⁰, M. Vozak ⁹⁹, L. Vozdecky ⁹², N. Vranjes ¹⁵,
 M. Vranjes Milosavljevic ¹⁵, V. Vrba ^{130,*}, M. Vreeswijk ¹¹², R. Vuillermet ³⁵, O. Vujanovic ⁹⁸,
 I. Vukotic ³⁸, S. Wada ¹⁵⁵, C. Wagner ¹⁰¹, W. Wagner ¹⁶⁸, S. Wahdan ¹⁶⁸, H. Wahlberg ⁸⁸,
 R. Wakasa ¹⁵⁵, M. Wakida ¹⁰⁹, V.M. Walbrecht ¹⁰⁸, J. Walder ¹³², R. Walker ¹⁰⁷, S.D. Walker ⁹³,
 W. Walkowiak ¹³⁹, A.M. Wang ⁶⁰, A.Z. Wang ¹⁶⁷, C. Wang ^{61a}, C. Wang ^{61c}, H. Wang ^{17a},
 J. Wang ^{63a}, P. Wang ⁴³, R.-J. Wang ⁹⁸, R. Wang ⁶⁰, R. Wang ⁵, S.M. Wang ¹⁴⁶, S. Wang ^{61b},
 T. Wang ^{61a}, W.T. Wang ⁷⁸, W.X. Wang ^{61a}, X. Wang ^{14c}, X. Wang ¹⁵⁹, X. Wang ^{61c},
 Y. Wang ^{61a}, Z. Wang ¹⁰⁴, Z. Wang ^{61d,50,61c}, Z. Wang ¹⁰⁴, A. Warburton ¹⁰², R.J. Ward ²⁰,
 N. Warrack ⁵⁸, A.T. Watson ²⁰, M.F. Watson ²⁰, G. Watts ¹³⁶, B.M. Waugh ⁹⁴, A.F. Webb ¹⁰,
 C. Weber ²⁸, M.S. Weber ¹⁹, S.A. Weber ³³, S.M. Weber ^{62a}, C. Wei ^{61a}, Y. Wei ¹²⁴,
 A.R. Weidberg ¹²⁴, J. Weingarten ⁴⁸, M. Weirich ⁹⁸, C. Weiser ⁵³, T. Wenaus ²⁸,
 B. Wendland ⁴⁸, T. Wengler ³⁵, N. Wermes ²³, M. Wessels ^{62a}, K. Whalen ¹²¹,
 A.M. Wharton ⁸⁹, A.S. White ⁶⁰, A. White ⁷, M.J. White ¹, D. Whiteson ¹⁵⁷,
 L. Wickremasinghe ¹²², W. Wiedenmann ¹⁶⁷, C. Wiel ⁴⁹, M. Wielers ¹³², N. Wieseotte ⁹⁸,
 C. Wiglesworth ⁴¹, L.A.M. Wiik-Fuchs ⁵³, D.J. Wilbern ¹¹⁸, H.G. Wilkens ³⁵, L.J. Wilkins ⁹³,
 D.M. Williams ⁴⁰, H.H. Williams ¹²⁶, S. Williams ³¹, S. Willocq ¹⁰¹, P.J. Windischhofer ¹²⁴,
 F. Winklmeier ¹²¹, B.T. Winter ⁵³, M. Wittgen ¹⁴¹, M. Wobisch ⁹⁵, A. Wolf ⁹⁸, R. Wölker ¹²⁴,
 J. Wollrath ¹⁵⁷, M.W. Wolter ⁸⁴, H. Wolters ^{128a,128c}, V.W.S. Wong ¹⁶¹, A.F. Wongel ⁴⁷,
 S.D. Worm ⁴⁷, B.K. Wosiek ⁸⁴, K.W. Woźniak ⁸⁴, K. Wraight ⁵⁸, J. Wu ^{14a,14d}, S.L. Wu ¹⁶⁷,
 X. Wu ⁵⁵, Y. Wu ^{61a}, Z. Wu ^{133,61a}, J. Wuerzinger ¹²⁴, T.R. Wyatt ⁹⁹, B.M. Wynne ⁵¹,
 S. Xella ⁴¹, L. Xia ^{14c}, M. Xia ^{14b}, J. Xiang ^{63c}, X. Xiao ¹⁰⁴, M. Xie ^{61a}, X. Xie ^{61a},
 I. Xiotidis ¹⁴⁴, D. Xu ^{14a}, H. Xu ^{61a}, H. Xu ^{61a}, L. Xu ^{61a}, R. Xu ¹²⁶, T. Xu ^{61a}, W. Xu ¹⁰⁴,
 Y. Xu ^{14b}, Z. Xu ^{61b}, Z. Xu ¹⁴¹, B. Yabsley ¹⁴⁵, S. Yacoob ^{32a}, N. Yamaguchi ⁸⁷,
 Y. Yamaguchi ¹⁵², H. Yamauchi ¹⁵⁵, T. Yamazaki ^{17a}, Y. Yamazaki ⁸², J. Yan ^{61c}, S. Yan ¹²⁴,
 Z. Yan ²⁴, H.J. Yang ^{61c,61d}, H.T. Yang ^{17a}, S. Yang ^{61a}, T. Yang ^{63c}, X. Yang ^{61a}, X. Yang ^{14a},
 Y. Yang ¹⁵¹, Z. Yang ^{61a,104}, W.-M. Yao ^{17a}, Y.C. Yap ⁴⁷, H. Ye ^{14c}, J. Ye ⁴³, S. Ye ²⁸,
 I. Yeletsikh ³⁷, M.R. Yexley ⁸⁹, P. Yin ⁴⁰, K. Yorita ¹⁶⁵, C.J.S. Young ⁵³, C. Young ¹⁴¹,
 M. Yuan ¹⁰⁴, R. Yuan ^{61b,j}, X. Yue ^{62a}, M. Zaazoua ^{34e}, B. Zabinski ⁸⁴, G. Zacharis ⁹, E. Zaid ⁵¹,

T. Zakareishvili ^{147b}, N. Zakharchuk ³³, S. Zambito ³⁵, D. Zanzi ⁵³, O. Zaplatilek ¹³⁰, S.V. Zeißner ⁴⁸, C. Zeitnitz ¹⁶⁸, J.C. Zeng ¹⁵⁹, D.T. Zenger Jr ²⁵, O. Zenin ³⁶, T. Ženiš ^{27a}, S. Zenz ⁹², S. Zerradi ^{34a}, D. Zerwas ⁶⁵, B. Zhang ^{14c}, D.F. Zhang ¹³⁷, G. Zhang ^{14b}, J. Zhang ⁵, K. Zhang ^{14a,14d}, L. Zhang ^{14c}, M. Zhang ¹⁵⁹, R. Zhang ¹⁶⁷, S. Zhang ¹⁰⁴, X. Zhang ^{61c}, X. Zhang ^{61b}, Z. Zhang ⁶⁵, H. Zhao ¹³⁶, P. Zhao ⁵⁰, T. Zhao ^{61b}, Y. Zhao ¹³⁴, Z. Zhao ^{61a}, A. Zhemchugov ³⁷, Z. Zheng ¹⁴¹, D. Zhong ¹⁵⁹, B. Zhou¹⁰⁴, C. Zhou ¹⁶⁷, H. Zhou ⁶, N. Zhou ^{61c}, Y. Zhou⁶, C.G. Zhu ^{61b}, C. Zhu ^{14a,14d}, H.L. Zhu ^{61a}, H. Zhu ^{14a}, J. Zhu ¹⁰⁴, Y. Zhu ^{61a}, X. Zhuang ^{14a}, K. Zhukov ³⁶, V. Zhulanov ³⁶, D. Zieminska ⁶⁶, N.I. Zimine ³⁷, S. Zimmermann ^{53,*}, J. Zinsser ^{62b}, M. Ziolkowski ¹³⁹, L. Živković ¹⁵, A. Zoccoli ^{22b,22a}, K. Zoch ⁵⁵, T.G. Zorbas ¹³⁷, O. Zormpa ⁴⁵, W. Zou ⁴⁰, L. Zwalinski ³⁵.

¹Department of Physics, University of Adelaide, Adelaide; Australia.

²Department of Physics, University of Alberta, Edmonton AB; Canada.

³(^a)Department of Physics, Ankara University, Ankara; (^b)Istanbul Aydin University, Application and Research Center for Advanced Studies, Istanbul; (^c)Division of Physics, TOBB University of Economics and Technology, Ankara; Türkiye.

⁴LAPP, Université Savoie Mont Blanc, CNRS/IN2P3, Annecy; France.

⁵High Energy Physics Division, Argonne National Laboratory, Argonne IL; United States of America.

⁶Department of Physics, University of Arizona, Tucson AZ; United States of America.

⁷Department of Physics, University of Texas at Arlington, Arlington TX; United States of America.

⁸Physics Department, National and Kapodistrian University of Athens, Athens; Greece.

⁹Physics Department, National Technical University of Athens, Zografou; Greece.

¹⁰Department of Physics, University of Texas at Austin, Austin TX; United States of America.

¹¹(^a)Bahcesehir University, Faculty of Engineering and Natural Sciences, Istanbul; (^b)Istanbul Bilgi University, Faculty of Engineering and Natural Sciences, Istanbul; (^c)Department of Physics, Bogazici University, Istanbul; (^d)Department of Physics Engineering, Gaziantep University, Gaziantep; Türkiye.

¹²Institute of Physics, Azerbaijan Academy of Sciences, Baku; Azerbaijan.

¹³Institut de Física d'Altes Energies (IFAE), Barcelona Institute of Science and Technology, Barcelona; Spain.

¹⁴(^a)Institute of High Energy Physics, Chinese Academy of Sciences, Beijing; (^b)Physics Department, Tsinghua University, Beijing; (^c)Department of Physics, Nanjing University, Nanjing; (^d)University of Chinese Academy of Science (UCAS), Beijing; China.

¹⁵Institute of Physics, University of Belgrade, Belgrade; Serbia.

¹⁶Department for Physics and Technology, University of Bergen, Bergen; Norway.

¹⁷(^a)Physics Division, Lawrence Berkeley National Laboratory, Berkeley CA; (^b)University of California, Berkeley CA; United States of America.

¹⁸Institut für Physik, Humboldt Universität zu Berlin, Berlin; Germany.

¹⁹Albert Einstein Center for Fundamental Physics and Laboratory for High Energy Physics, University of Bern, Bern; Switzerland.

²⁰School of Physics and Astronomy, University of Birmingham, Birmingham; United Kingdom.

²¹(^a)Facultad de Ciencias y Centro de Investigaciones, Universidad Antonio Nariño,

Bogotá; (^b)Departamento de Física, Universidad Nacional de Colombia, Bogotá; Colombia.

²²(^a)Dipartimento di Fisica e Astronomia A. Righi, Università di Bologna, Bologna; (^b)INFN Sezione di Bologna; Italy.

²³Physikalisches Institut, Universität Bonn, Bonn; Germany.

²⁴Department of Physics, Boston University, Boston MA; United States of America.

²⁵Department of Physics, Brandeis University, Waltham MA; United States of America.

- ^{26(a)}Transilvania University of Brasov, Brasov;^(b)Horia Hulubei National Institute of Physics and Nuclear Engineering, Bucharest;^(c)Department of Physics, Alexandru Ioan Cuza University of Iasi, Iasi;^(d)National Institute for Research and Development of Isotopic and Molecular Technologies, Physics Department, Cluj-Napoca;^(e)University Politehnica Bucharest, Bucharest;^(f)West University in Timisoara, Timisoara; Romania.
- ^{27(a)}Faculty of Mathematics, Physics and Informatics, Comenius University, Bratislava;^(b)Department of Subnuclear Physics, Institute of Experimental Physics of the Slovak Academy of Sciences, Kosice; Slovak Republic.
- ²⁸Physics Department, Brookhaven National Laboratory, Upton NY; United States of America.
- ²⁹Universidad de Buenos Aires, Facultad de Ciencias Exactas y Naturales, Departamento de Física, y CONICET, Instituto de Física de Buenos Aires (IFIBA), Buenos Aires; Argentina.
- ³⁰California State University, CA; United States of America.
- ³¹Cavendish Laboratory, University of Cambridge, Cambridge; United Kingdom.
- ^{32(a)}Department of Physics, University of Cape Town, Cape Town;^(b)iThemba Labs, Western Cape;^(c)Department of Mechanical Engineering Science, University of Johannesburg, Johannesburg;^(d)National Institute of Physics, University of the Philippines Diliman (Philippines);^(e)University of South Africa, Department of Physics, Pretoria;^(f)School of Physics, University of the Witwatersrand, Johannesburg; South Africa.
- ³³Department of Physics, Carleton University, Ottawa ON; Canada.
- ^{34(a)}Faculté des Sciences Ain Chock, Réseau Universitaire de Physique des Hautes Energies - Université Hassan II, Casablanca;^(b)Faculté des Sciences, Université Ibn-Tofail, Kénitra;^(c)Faculté des Sciences Semlalia, Université Cadi Ayyad, LPHEA-Marrakech;^(d)LPMR, Faculté des Sciences, Université Mohamed Premier, Oujda;^(e)Faculté des sciences, Université Mohammed V, Rabat;^(f)Institute of Applied Physics, Mohammed VI Polytechnic University, Ben Guerir; Morocco.
- ³⁵CERN, Geneva; Switzerland.
- ³⁶Affiliated with an institute covered by a cooperation agreement with CERN.
- ³⁷Affiliated with an international laboratory covered by a cooperation agreement with CERN.
- ³⁸Enrico Fermi Institute, University of Chicago, Chicago IL; United States of America.
- ³⁹LPC, Université Clermont Auvergne, CNRS/IN2P3, Clermont-Ferrand; France.
- ⁴⁰Nevis Laboratory, Columbia University, Irvington NY; United States of America.
- ⁴¹Niels Bohr Institute, University of Copenhagen, Copenhagen; Denmark.
- ^{42(a)}Dipartimento di Fisica, Università della Calabria, Rende;^(b)INFN Gruppo Collegato di Cosenza, Laboratori Nazionali di Frascati; Italy.
- ⁴³Physics Department, Southern Methodist University, Dallas TX; United States of America.
- ⁴⁴Physics Department, University of Texas at Dallas, Richardson TX; United States of America.
- ⁴⁵National Centre for Scientific Research "Demokritos", Agia Paraskevi; Greece.
- ^{46(a)}Department of Physics, Stockholm University;^(b)Oskar Klein Centre, Stockholm; Sweden.
- ⁴⁷Deutsches Elektronen-Synchrotron DESY, Hamburg and Zeuthen; Germany.
- ⁴⁸Fakultät Physik, Technische Universität Dortmund, Dortmund; Germany.
- ⁴⁹Institut für Kern- und Teilchenphysik, Technische Universität Dresden, Dresden; Germany.
- ⁵⁰Department of Physics, Duke University, Durham NC; United States of America.
- ⁵¹SUPA - School of Physics and Astronomy, University of Edinburgh, Edinburgh; United Kingdom.
- ⁵²INFN e Laboratori Nazionali di Frascati, Frascati; Italy.
- ⁵³Physikalisches Institut, Albert-Ludwigs-Universität Freiburg, Freiburg; Germany.
- ⁵⁴II. Physikalisches Institut, Georg-August-Universität Göttingen, Göttingen; Germany.
- ⁵⁵Département de Physique Nucléaire et Corpusculaire, Université de Genève, Genève; Switzerland.
- ^{56(a)}Dipartimento di Fisica, Università di Genova, Genova;^(b)INFN Sezione di Genova; Italy.

- ⁵⁷II. Physikalisches Institut, Justus-Liebig-Universität Giessen, Giessen; Germany.
- ⁵⁸SUPA - School of Physics and Astronomy, University of Glasgow, Glasgow; United Kingdom.
- ⁵⁹LPSC, Université Grenoble Alpes, CNRS/IN2P3, Grenoble INP, Grenoble; France.
- ⁶⁰Laboratory for Particle Physics and Cosmology, Harvard University, Cambridge MA; United States of America.
- ⁶¹(^a) Department of Modern Physics and State Key Laboratory of Particle Detection and Electronics, University of Science and Technology of China, Hefei; (^b) Institute of Frontier and Interdisciplinary Science and Key Laboratory of Particle Physics and Particle Irradiation (MOE), Shandong University, Qingdao; (^c) School of Physics and Astronomy, Shanghai Jiao Tong University, Key Laboratory for Particle Astrophysics and Cosmology (MOE), SKLPPC, Shanghai; (^d) Tsung-Dao Lee Institute, Shanghai; China.
- ⁶²(^a) Kirchhoff-Institut für Physik, Ruprecht-Karls-Universität Heidelberg, Heidelberg; (^b) Physikalisches Institut, Ruprecht-Karls-Universität Heidelberg, Heidelberg; Germany.
- ⁶³(^a) Department of Physics, Chinese University of Hong Kong, Shatin, N.T., Hong Kong; (^b) Department of Physics, University of Hong Kong, Hong Kong; (^c) Department of Physics and Institute for Advanced Study, Hong Kong University of Science and Technology, Clear Water Bay, Kowloon, Hong Kong; China.
- ⁶⁴Department of Physics, National Tsing Hua University, Hsinchu; Taiwan.
- ⁶⁵IJCLab, Université Paris-Saclay, CNRS/IN2P3, 91405, Orsay; France.
- ⁶⁶Department of Physics, Indiana University, Bloomington IN; United States of America.
- ⁶⁷(^a) INFN Gruppo Collegato di Udine, Sezione di Trieste, Udine; (^b) ICTP, Trieste; (^c) Dipartimento Politecnico di Ingegneria e Architettura, Università di Udine, Udine; Italy.
- ⁶⁸(^a) INFN Sezione di Lecce; (^b) Dipartimento di Matematica e Fisica, Università del Salento, Lecce; Italy.
- ⁶⁹(^a) INFN Sezione di Milano; (^b) Dipartimento di Fisica, Università di Milano, Milano; Italy.
- ⁷⁰(^a) INFN Sezione di Napoli; (^b) Dipartimento di Fisica, Università di Napoli, Napoli; Italy.
- ⁷¹(^a) INFN Sezione di Pavia; (^b) Dipartimento di Fisica, Università di Pavia, Pavia; Italy.
- ⁷²(^a) INFN Sezione di Pisa; (^b) Dipartimento di Fisica E. Fermi, Università di Pisa, Pisa; Italy.
- ⁷³(^a) INFN Sezione di Roma; (^b) Dipartimento di Fisica, Sapienza Università di Roma, Roma; Italy.
- ⁷⁴(^a) INFN Sezione di Roma Tor Vergata; (^b) Dipartimento di Fisica, Università di Roma Tor Vergata, Roma; Italy.
- ⁷⁵(^a) INFN Sezione di Roma Tre; (^b) Dipartimento di Matematica e Fisica, Università Roma Tre, Roma; Italy.
- ⁷⁶(^a) INFN-TIFPA; (^b) Università degli Studi di Trento, Trento; Italy.
- ⁷⁷Universität Innsbruck, Department of Astro and Particle Physics, Innsbruck; Austria.
- ⁷⁸University of Iowa, Iowa City IA; United States of America.
- ⁷⁹Department of Physics and Astronomy, Iowa State University, Ames IA; United States of America.
- ⁸⁰(^a) Departamento de Engenharia Elétrica, Universidade Federal de Juiz de Fora (UFJF), Juiz de Fora; (^b) Universidade Federal do Rio De Janeiro COPPE/EE/IF, Rio de Janeiro; (^c) Universidade Federal de São João del Rei (UFSJ), São João del Rei; (^d) Instituto de Física, Universidade de São Paulo, São Paulo; Brazil.
- ⁸¹KEK, High Energy Accelerator Research Organization, Tsukuba; Japan.
- ⁸²Graduate School of Science, Kobe University, Kobe; Japan.
- ⁸³(^a) AGH University of Krakow, Faculty of Physics and Applied Computer Science, Krakow; (^b) Marian Smoluchowski Institute of Physics, Jagiellonian University, Krakow; Poland.
- ⁸⁴Institute of Nuclear Physics Polish Academy of Sciences, Krakow; Poland.
- ⁸⁵Faculty of Science, Kyoto University, Kyoto; Japan.
- ⁸⁶Kyoto University of Education, Kyoto; Japan.
- ⁸⁷Research Center for Advanced Particle Physics and Department of Physics, Kyushu University, Fukuoka ; Japan.

- ⁸⁸Instituto de Física La Plata, Universidad Nacional de La Plata and CONICET, La Plata; Argentina.
- ⁸⁹Physics Department, Lancaster University, Lancaster; United Kingdom.
- ⁹⁰Oliver Lodge Laboratory, University of Liverpool, Liverpool; United Kingdom.
- ⁹¹Department of Experimental Particle Physics, Jožef Stefan Institute and Department of Physics, University of Ljubljana, Ljubljana; Slovenia.
- ⁹²School of Physics and Astronomy, Queen Mary University of London, London; United Kingdom.
- ⁹³Department of Physics, Royal Holloway University of London, Egham; United Kingdom.
- ⁹⁴Department of Physics and Astronomy, University College London, London; United Kingdom.
- ⁹⁵Louisiana Tech University, Ruston LA; United States of America.
- ⁹⁶Fysiska institutionen, Lunds universitet, Lund; Sweden.
- ⁹⁷Departamento de Física Teórica C-15 and CIAFF, Universidad Autónoma de Madrid, Madrid; Spain.
- ⁹⁸Institut für Physik, Universität Mainz, Mainz; Germany.
- ⁹⁹School of Physics and Astronomy, University of Manchester, Manchester; United Kingdom.
- ¹⁰⁰CPPM, Aix-Marseille Université, CNRS/IN2P3, Marseille; France.
- ¹⁰¹Department of Physics, University of Massachusetts, Amherst MA; United States of America.
- ¹⁰²Department of Physics, McGill University, Montreal QC; Canada.
- ¹⁰³School of Physics, University of Melbourne, Victoria; Australia.
- ¹⁰⁴Department of Physics, University of Michigan, Ann Arbor MI; United States of America.
- ¹⁰⁵Department of Physics and Astronomy, Michigan State University, East Lansing MI; United States of America.
- ¹⁰⁶Group of Particle Physics, University of Montreal, Montreal QC; Canada.
- ¹⁰⁷Fakultät für Physik, Ludwig-Maximilians-Universität München, München; Germany.
- ¹⁰⁸Max-Planck-Institut für Physik (Werner-Heisenberg-Institut), München; Germany.
- ¹⁰⁹Graduate School of Science and Kobayashi-Maskawa Institute, Nagoya University, Nagoya; Japan.
- ¹¹⁰Department of Physics and Astronomy, University of New Mexico, Albuquerque NM; United States of America.
- ¹¹¹Institute for Mathematics, Astrophysics and Particle Physics, Radboud University/Nikhef, Nijmegen; Netherlands.
- ¹¹²Nikhef National Institute for Subatomic Physics and University of Amsterdam, Amsterdam; Netherlands.
- ¹¹³Department of Physics, Northern Illinois University, DeKalb IL; United States of America.
- ¹¹⁴(^a) New York University Abu Dhabi, Abu Dhabi; (^b) United Arab Emirates University, Al Ain; (^c) University of Sharjah, Sharjah; United Arab Emirates.
- ¹¹⁵Department of Physics, New York University, New York NY; United States of America.
- ¹¹⁶Ochanomizu University, Otsuka, Bunkyo-ku, Tokyo; Japan.
- ¹¹⁷Ohio State University, Columbus OH; United States of America.
- ¹¹⁸Homer L. Dodge Department of Physics and Astronomy, University of Oklahoma, Norman OK; United States of America.
- ¹¹⁹Department of Physics, Oklahoma State University, Stillwater OK; United States of America.
- ¹²⁰Palacký University, Joint Laboratory of Optics, Olomouc; Czech Republic.
- ¹²¹Institute for Fundamental Science, University of Oregon, Eugene, OR; United States of America.
- ¹²²Graduate School of Science, Osaka University, Osaka; Japan.
- ¹²³Department of Physics, University of Oslo, Oslo; Norway.
- ¹²⁴Department of Physics, Oxford University, Oxford; United Kingdom.
- ¹²⁵LPNHE, Sorbonne Université, Université Paris Cité, CNRS/IN2P3, Paris; France.
- ¹²⁶Department of Physics, University of Pennsylvania, Philadelphia PA; United States of America.
- ¹²⁷Department of Physics and Astronomy, University of Pittsburgh, Pittsburgh PA; United States of America.

America.

¹²⁸(*a*) Laboratório de Instrumentação e Física Experimental de Partículas - LIP, Lisboa; (*b*) Departamento de Física, Faculdade de Ciências, Universidade de Lisboa, Lisboa; (*c*) Departamento de Física, Universidade de Coimbra, Coimbra; (*d*) Centro de Física Nuclear da Universidade de Lisboa, Lisboa; (*e*) Departamento de Física, Universidade do Minho, Braga; (*f*) Departamento de Física Teórica y del Cosmos, Universidad de Granada, Granada (Spain); (*g*) Departamento de Física, Instituto Superior Técnico, Universidade de Lisboa, Lisboa; Portugal.

¹²⁹Institute of Physics of the Czech Academy of Sciences, Prague; Czech Republic.

¹³⁰Czech Technical University in Prague, Prague; Czech Republic.

¹³¹Charles University, Faculty of Mathematics and Physics, Prague; Czech Republic.

¹³²Particle Physics Department, Rutherford Appleton Laboratory, Didcot; United Kingdom.

¹³³IRFU, CEA, Université Paris-Saclay, Gif-sur-Yvette; France.

¹³⁴Santa Cruz Institute for Particle Physics, University of California Santa Cruz, Santa Cruz CA; United States of America.

¹³⁵(*a*) Departamento de Física, Pontificia Universidad Católica de Chile, Santiago; (*b*) Millennium Institute for Subatomic physics at high energy frontier (SAPHIR), Santiago; (*c*) Instituto de Investigación Multidisciplinario en Ciencia y Tecnología, y Departamento de Física, Universidad de La Serena; (*d*) Universidad Andres Bello, Department of Physics, Santiago; (*e*) Instituto de Alta Investigación, Universidad de Tarapacá, Arica; (*f*) Departamento de Física, Universidad Técnica Federico Santa María, Valparaíso; Chile.

¹³⁶Department of Physics, University of Washington, Seattle WA; United States of America.

¹³⁷Department of Physics and Astronomy, University of Sheffield, Sheffield; United Kingdom.

¹³⁸Department of Physics, Shinshu University, Nagano; Japan.

¹³⁹Department Physik, Universität Siegen, Siegen; Germany.

¹⁴⁰Department of Physics, Simon Fraser University, Burnaby BC; Canada.

¹⁴¹SLAC National Accelerator Laboratory, Stanford CA; United States of America.

¹⁴²Department of Physics, Royal Institute of Technology, Stockholm; Sweden.

¹⁴³Departments of Physics and Astronomy, Stony Brook University, Stony Brook NY; United States of America.

¹⁴⁴Department of Physics and Astronomy, University of Sussex, Brighton; United Kingdom.

¹⁴⁵School of Physics, University of Sydney, Sydney; Australia.

¹⁴⁶Institute of Physics, Academia Sinica, Taipei; Taiwan.

¹⁴⁷(*a*) E. Andronikashvili Institute of Physics, Iv. Javakhishvili Tbilisi State University, Tbilisi; (*b*) High Energy Physics Institute, Tbilisi State University, Tbilisi; (*c*) University of Georgia, Tbilisi; Georgia.

¹⁴⁸Department of Physics, Technion, Israel Institute of Technology, Haifa; Israel.

¹⁴⁹Raymond and Beverly Sackler School of Physics and Astronomy, Tel Aviv University, Tel Aviv; Israel.

¹⁵⁰Department of Physics, Aristotle University of Thessaloniki, Thessaloniki; Greece.

¹⁵¹International Center for Elementary Particle Physics and Department of Physics, University of Tokyo, Tokyo; Japan.

¹⁵²Department of Physics, Tokyo Institute of Technology, Tokyo; Japan.

¹⁵³Department of Physics, University of Toronto, Toronto ON; Canada.

¹⁵⁴(*a*) TRIUMF, Vancouver BC; (*b*) Department of Physics and Astronomy, York University, Toronto ON; Canada.

¹⁵⁵Division of Physics and Tomonaga Center for the History of the Universe, Faculty of Pure and Applied Sciences, University of Tsukuba, Tsukuba; Japan.

¹⁵⁶Department of Physics and Astronomy, Tufts University, Medford MA; United States of America.

¹⁵⁷Department of Physics and Astronomy, University of California Irvine, Irvine CA; United States of

America.

¹⁵⁸Department of Physics and Astronomy, University of Uppsala, Uppsala; Sweden.

¹⁵⁹Department of Physics, University of Illinois, Urbana IL; United States of America.

¹⁶⁰Instituto de Física Corpuscular (IFIC), Centro Mixto Universidad de Valencia - CSIC, Valencia; Spain.

¹⁶¹Department of Physics, University of British Columbia, Vancouver BC; Canada.

¹⁶²Department of Physics and Astronomy, University of Victoria, Victoria BC; Canada.

¹⁶³Fakultät für Physik und Astronomie, Julius-Maximilians-Universität Würzburg, Würzburg; Germany.

¹⁶⁴Department of Physics, University of Warwick, Coventry; United Kingdom.

¹⁶⁵Waseda University, Tokyo; Japan.

¹⁶⁶Department of Particle Physics and Astrophysics, Weizmann Institute of Science, Rehovot; Israel.

¹⁶⁷Department of Physics, University of Wisconsin, Madison WI; United States of America.

¹⁶⁸Fakultät für Mathematik und Naturwissenschaften, Fachgruppe Physik, Bergische Universität Wuppertal, Wuppertal; Germany.

¹⁶⁹Department of Physics, Yale University, New Haven CT; United States of America.

^a Also Affiliated with an institute covered by a cooperation agreement with CERN.

^b Also at Borough of Manhattan Community College, City University of New York, New York NY; United States of America.

^c Also at Bruno Kessler Foundation, Trento; Italy.

^d Also at Center for High Energy Physics, Peking University; China.

^e Also at Centro Studi e Ricerche Enrico Fermi; Italy.

^f Also at CERN, Geneva; Switzerland.

^g Also at Département de Physique Nucléaire et Corpusculaire, Université de Genève, Genève; Switzerland.

^h Also at Departament de Física de la Universitat Autònoma de Barcelona, Barcelona; Spain.

ⁱ Also at Department of Financial and Management Engineering, University of the Aegean, Chios; Greece.

^j Also at Department of Physics and Astronomy, Michigan State University, East Lansing MI; United States of America.

^k Also at Department of Physics and Astronomy, University of Louisville, Louisville, KY; United States of America.

^l Also at Department of Physics, Ben Gurion University of the Negev, Beer Sheva; Israel.

^m Also at Department of Physics, California State University, East Bay; United States of America.

ⁿ Also at Department of Physics, California State University, Sacramento; United States of America.

^o Also at Department of Physics, King's College London, London; United Kingdom.

^p Also at Department of Physics, Stanford University, Stanford CA; United States of America.

^q Also at Department of Physics, University of Fribourg, Fribourg; Switzerland.

^r Also at Hellenic Open University, Patras; Greece.

^s Also at Institutio Catalana de Recerca i Estudis Avancats, ICREA, Barcelona; Spain.

^t Also at Institut für Experimentalphysik, Universität Hamburg, Hamburg; Germany.

^u Also at Institute for Nuclear Research and Nuclear Energy (INRNE) of the Bulgarian Academy of Sciences, Sofia; Bulgaria.

^v Also at Institute of Particle Physics (IPP); Canada.

^w Also at Institute of Physics, Azerbaijan Academy of Sciences, Baku; Azerbaijan.

^x Also at Institute of Theoretical Physics, Ilia State University, Tbilisi; Georgia.

^y Also at Instituto de Física Teórica, IFT-UAM/CSIC, Madrid; Spain.

^z Also at Istanbul University, Dept. of Physics, Istanbul; Türkiye.

^{aa} Also at Istinye University, Istanbul; Türkiye.

^{ab} Also at L2IT, Université de Toulouse, CNRS/IN2P3, UPS, Toulouse; France.

- ac* Also at National Institute of Physics, University of the Philippines Diliman (Philippines); Philippines.
- ad* Also at Physics Department, An-Najah National University, Nablus; Palestine.
- ae* Also at Physikalisches Institut, Albert-Ludwigs-Universität Freiburg, Freiburg; Germany.
- af* Also at The City College of New York, New York NY; United States of America.
- ag* Also at The Collaborative Innovation Center of Quantum Matter (CICQM), Beijing; China.
- ah* Also at TRIUMF, Vancouver BC; Canada.
- ai* Also at Università di Napoli Parthenope, Napoli; Italy.
- aj* Also at University of Chinese Academy of Sciences (UCAS), Beijing; China.
- ak* Also at Yeditepe University, Physics Department, Istanbul; Türkiye.
- * Deceased